
OPTIMIZING BIOMANUFACTURING HARVESTING DECISIONS UNDER LIMITED HISTORICAL DATA

Bo Wang¹, Wei Xie^{*1}, Tugce Martagan², Alp Akcay², and Bram van Ravenstein³

¹Northeastern University, Boston, MA 02115

²Eindhoven University of Technology, 5612 AZ Eindhoven, The Netherlands

³MSD Animal Health, 5831 AN Boxmeer, The Netherlands

ABSTRACT

In biopharmaceutical manufacturing, fermentation processes play a critical role in productivity and profit. A fermentation process uses living cells with complex biological mechanisms, and this leads to high variability in the process outputs, namely, the protein and impurity levels. By building on the biological mechanisms of protein and impurity growth, we introduce a stochastic model to characterize the accumulation of the protein and impurity levels in the fermentation process. However, a common challenge in the industry is the availability of only a very limited amount of data, especially in the development and early stage of production. This adds an additional layer of uncertainty, referred to as model risk, due to the difficulty of estimating the model parameters with limited data. In this paper, we study the harvesting decision for a fermentation process under model risk (i.e., when to stop the fermentation and collect the production reward). We adopt a Bayesian approach to update the unknown parameters of the growth-rate distributions, and use the resulting posterior distributions to characterize the impact of model risk on fermentation output variability. The harvesting problem is formulated as a Markov decision process model with knowledge states that summarize the posterior distributions and hence incorporate the model risk in decision-making. The resulting model is solved by using a reinforcement learning algorithm based on Bayesian sparse sampling. We provide analytical results on the structure of the optimal policy and its objective function, and explicitly study the impact of model risk on harvesting decisions. Our case studies at MSD Animal Health demonstrate that the proposed model and solution approach improve the harvesting decisions in real life by achieving substantially higher average output from a fermentation batch along with lower batch-to-batch variability.

Keywords Biomanufacturing, fermentation, limited data, process control, model-based reinforcement learning, threshold-type policies

1 Introduction

The biomanufacturing industry has developed several innovative treatments for cancer, adult blindness, and COVID-19 among many other diseases. Despite its increasing success, biomanufacturing is a challenging production environment. Different from classical pharmaceutical manufacturing, biomanufacturing methods use living organisms (e.g., bacteria, viruses or mammalian cells) during the production processes. These living organisms are custom-engineered to produce highly complex active ingredients for biopharmaceutical drugs. However, the use of living organisms also introduces several operational challenges related to batch-to-batch variability in the production outcomes.

The drug substance manufacturing can be broadly categorized into two main steps: fermentation and purification operations. During the fermentation process, the living organisms grow and produce the desired active ingredients. Specific characteristics of active ingredients (e.g., monoclonal antibodies, biomass, proteins, antigens, etc.) could vary across different drugs. In the remainder of this paper, we refer to the resulting target active ingredient as *protein*. After fermentation, the batch continues with a series of purification operations to comply with stringent regulatory requirements on safety and quality. Our main focus in this study is the fermentation process.

*Corresponding author: w.xie@northeastern.edu

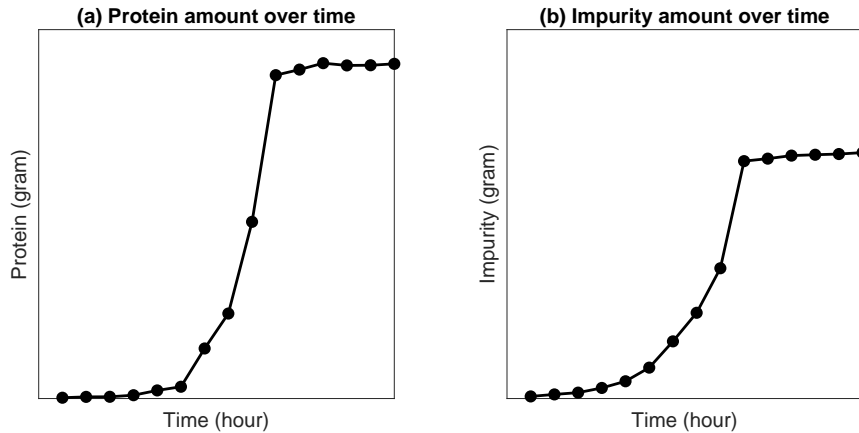


Figure 1: Illustration of fermentation dynamics using industry data from MSD

The fermentation process is typically carried out inside a stainless steel vessel called *bioreactor*. Bioreactors are equipped with advanced sensors to achieve a highly controlled environment via monitoring of critical process parameters (e.g., cell growth rate, protein accumulation, impurity accumulation, etc.). Figure 1 uses industry data to illustrate the main dynamics of a batch fermentation process. As the fermentation continues, we observe from Figure 1(a) that the amount of protein produced during fermentation increases exponentially over time. Hence, this specific phase of fermentation is known as the *exponential growth* phase. However, the exponential growth phase continues only for a finite period of time (e.g., several hours or days depending on the application) because of the inherent limitations of biological processes (e.g., limitations in media, cell viability, and growth). After the exponential growth phase, the fermentation enters a *stationary phase* in which the protein production stops and the batch needs to be harvested. In addition, we observe from Figure 1(b) that unwanted *impurities* accumulate inside the bioreactor along with the desired proteins. The specific nature of impurities varies across applications but impurities often represent unwanted byproducts, such as ammonia, dead cells, etc. These impurities are subsequently filtered and eliminated through a series of purification operations.

1.1 The Harvesting Problem: Trade-offs and Challenges

The simultaneous growth of desired proteins and unwanted impurities, as shown in Figure 1, is often known as the *purity–yield trade-off* in fermentation processes. From a practical perspective, the purity–yield trade-off presents a critical challenge in fermentation harvesting (stopping) decisions. Waiting too long to harvest the fermentation, in anticipation of a higher amount of protein production, may result in a higher amount of impurities. In turn, this could increase the cost (difficulty) of subsequent purification operations. This purity–yield trade-off motivates our main research question: (1) *What is an optimal harvesting policy (i.e., when should we stop the fermentation) to maximize the expected profit obtained from a batch?*

In addition to the purity–yield trade-off, process “uncertainty” imposes another critical challenge on harvesting decisions. In particular, two types of process uncertainty are commonly encountered in biomanufacturing practice: (i) *inherent stochasticity* and (ii) *model risk*. In our problem setting, *inherent stochasticity* represents the uncertainty in the amounts of protein and impurity produced throughout fermentation, and it is often caused by the inherent complexity of biological systems. Because living organisms are used during fermentation, the rate at which proteins and impurities accumulate is random (although fermentation is carried out under identical conditions). Therefore, the inherent stochasticity of biological processes motivates our second research question: (2) *How can we develop an analytical model to learn the inherent stochasticity of fermentation processes and incorporate it into optimal harvesting decisions?*

Most often, the inherent stochasticity can not be controlled but can be predicted through historical process data. However, building a reliable prediction model is challenging in practice because most biomanufacturing applications involve only a limited amount of historical process data. We refer to the resulting uncertainty in the prediction model itself as the *model risk*. The problem of decision-making under limited data (i.e., under model risk) is a critical concern for both research and development (R&D) projects and industry-scale applications. In biopharmaceutical R&D projects, each protein is unique such that the scientists re-engineer and manufacture it for the first time. This implies that harvesting decisions are typically made under limited R&D data. In industry-scale applications, the problem of limited data

becomes relevant every time a change occurs in equipment or raw materials. For example, the supplier of raw materials (i.e., medium or seed cells) might change their formulations, the management might purchase a new bioreactor, etc. Such changes have a substantial impact on the output of fermentation which often makes the historical process data obsolete or unreliable. Thus, it is of practical importance to have a harvesting strategy that accounts for the model risk. It is possible that ignoring the model risk might lead to sub-optimal decisions. From a practical perspective, decision-making under limited data leads to a natural “learning-by-doing” mechanism where the biomanufacturer sequentially collects real-world data (by implementing a policy) under model risk. This motivates our third and fourth research questions: (3) *Given a limited amount of historical data, how can we develop a learning mechanism to simultaneously account for inherent stochasticity and model risk while making harvesting decisions?* (4) *What are the structural characteristics of optimal harvesting policies? How do their performance compare to the alternative harvesting policies used in practice?*

1.2 Contributions

To address the aforementioned research questions, we build a solution framework based on a reinforcement learning model using the theory of Bayesian statistics and Markov decision processes. A key aspect of our work is that we build analytical models that combine the knowledge from life sciences and operations research (OR) to support biomanufacturing decisions under limited historical data and the inherent stochasticity of biological systems. In life sciences research, there are well-known mechanistic models to predict the evolution of fermentation [1]. However, existing models do not mathematically capture both aspects of limited process data and the inherent stochasticity of fermentation. Our study is a first attempt to apply operations research concepts to fermentation decisions under limited data, and combines the knowledge from life sciences and stochastic modeling to derive guidelines that improve industry practices.

In addition, we characterize the structural properties of optimal harvesting decisions, and show that the optimal policy has a control-limit structure with respect to the impurity amount under some practically-relevant sufficient conditions. As a benchmark for the optimal policy, we investigate a simpler class of policies (so-called myopic policy), which makes the harvesting decisions by looking only one period ahead. We established the optimality of myopic policy under the perfect-information setting (i.e., when the true distribution of the growth rates is known). We also study how the posterior predictive distributions of the growth rates affect the harvesting decisions under the myopic policy when there is a model risk. Our framework enables decision makers to do a rigorous assessment of the impact of limited data on operating decisions, and provides managerial insights on the value of collecting additional data. At a given knowledge state, we also analytically characterize the contributions of the inherent stochasticity and the model risk to the overall uncertainty faced by the decision maker. To the best of our knowledge, these two sources of uncertainty have been a critical challenge for practitioners but their impact on optimal costs and harvesting decisions has not been fully understood. In summary, our model formalizes our understanding of fermentation decisions under limited historical data, and our results inform practitioners on the impact of adopting a learning-by-doing framework on current practice.

This research is an outcome of a multi-year collaboration with MSD Animal Health in Boxmeer, Netherlands.¹ The facility in Boxmeer is a leading biomanufacturing hub in Europe that conducts both biopharmaceutical R&D and large-scale production. Since September 2019, the developed framework has been used in daily operations to support harvesting decisions. The implementation has resulted in around 50% improvement in batch yield on average. This project is part of a long-term university-industry collaboration as described in [2]. Due to its scalability and potential impact, the project has been internationally recognized in several platforms [3, 4, 5, 6, 7]. Moreover, the research outcomes have been recognized as a finalist of 2022 INFORMS Franz Edelman Prize for achievement in the practice of operations research and management science [8, 9].

The remainder of the paper is organized as follows. We review the related literature in Section 2. We develop a stochastic optimization model in Section 3, and analyze its structural characteristics in Section 4. We elaborate on the implementation process and impact in Section 5 and present a case study in Section 6. We provide the concluding remarks in Section 7.

2 Literature Review

Our work is closely related to two main streams of research: (1) modeling and control of fermentation based on a *known* model that describes the dynamics of the fermentation process, and (2) reinforcement learning approaches to predict and control fermentation processes. We restrict our scope to studies related to biomanufacturing applications, and refer to [10] for a survey of analytical models for biopharmaceutical operations and supply chains.

A vast body of life sciences literature focuses on modeling the biological dynamics of fermentation processes. In particular, predictive models are built to estimate the evolution of fermentation, and then these models are used to guide the search for optimal control strategies. In this context, most studies develop deterministic or stochastic models to predict and control fermentation. Deterministic models typically build kinetic process models (i.e., differential equations) on cell growth and product formation [11, 1, 12]. These kinetic models are also integrated with optimization models. For example, [13] constructed a dynamic flux balance model for a fermentation process. They developed a closed-loop control for feed rate and dissolved oxygen concentration profiles to maximize yield production.

Data-driven stochastic optimization is relatively understudied to predict and control fermentation processes. Existing studies typically focus on the inherent stochasticity of fermentation. For example, [14] used approximate dynamic programming to maximize yield and minimize process time in fed-batch fermentation. [15] adopted a Markov chain Monte Carlo approach to optimize the kinetics of a fermentation process. More recently, [16] and [17] developed a Markov decision processes (MDP) model to optimize fermentation operating decisions. However, their optimization models are built based on sufficiently large historical data, and hence are not equipped to capture the impact of model risk (limited historical data) on biomanufacturing decisions. [18] developed a portfolio of decision support tools to improve production planning and reduce biomanufacturing costs. However, they omitted the model risk and did not characterize optimal harvesting policies. When decisions are made under limited data, ignoring the model risk would lead to a bias in decision-making. To the best of our knowledge, this paper is the first to simultaneously capture the inherent stochasticity of biological systems and model risk to optimize harvesting decisions in biomanufacturing systems.

Reinforcement learning approaches have been recently developed for bioprocess control. For example, [19] and [20] developed model-free deep-Q-network-based reinforcement learning approaches to maintain the cells at target populations by controlling the feeding profiles and maximize the yield by controlling the flow rate. [21] constructed a model-based reinforcement learning for biomanufacturing control, with a predictive distribution of system response. After that, they proposed a simulation-assisted policy gradient algorithm that can efficiently reuse the previous process outputs to facilitate the learning and the search for the optimal policy. Our paper is different from [21] in the following ways: (1) We study the harvesting problem in fermentation, while [21] focus on a chromatography problem in purification operations, (2) we explicitly incorporate the posterior distributions of unknown fermentation-process parameters as knowledge states of the MDP model; and (3) their focus is developing a solution algorithm, while we focus on analytical properties of the optimal harvesting policy and practical implementation in real life.

In reinforcement learning literature, the model-based Bayesian Reinforcement learning, or the Bayes-Adaptive Markov decision process (BAMDP), explicitly maintain a posterior over the model parameters as knowledge states to select actions, which can automatically balance both exploration and exploitation. A comprehensive review of Bayesian reinforcement learning methodologies can be found in [22]. Notice an equivalent representation is considering the parameters as unobservable states of the system, which can be formulated as a partially observable Markov decision process (POMDP) [23]. Since solving the original model-based Bayesian reinforcement learning is notoriously complex due to potentially huge state space, various approximation algorithms have been developed, including offline value approximation and computing the policy a priori through POMDP planning [24]; online near-myopic value and tree search approximation that focus on realized knowledge states in planning [25, 26, 27]; and exploration bonus based methods where an agent acts according to an optimistic model of MDP under uncertainty [28, 29, 30]. Motivated by those studies, in this paper, we develop a model-based Bayesian reinforcement learning approach, which can account for model risk in guiding fermentation harvesting decisions. In addition, we provide structural and sensitivity analyses to study how the model risk impacts the value function and optimal policies.

3 Model

Section 3.1 introduces a stochastic model to represent the protein and impurity accumulation in the fermentation process. Section 3.2 presents a Bayesian approach to capture the uncertainty in the unknown parameters of this model, and describes how this uncertainty can be updated with new protein and impurity observations collected during the fermentation process. Finally, Section 3.3 presents an MDP model formulation, accounting for both inherent stochasticity and model risk, to optimize the harvesting decision in the fermentation process.

3.1 Fermentation Process Modeling

The accumulation of protein and impurity amount in the exponential-growth phase of a fermentation process is commonly modeled with the so-called *cell-growth kinetics* mechanism [1]. The cell-growth kinetics mechanism is often represented as an ordinary differential equation. To be specific, the protein amount at time t , denoted by p_t , is given by

the functional form $\frac{dp_t}{dt} = \phi p_t$, where ϕ is referred to as the *specific growth rate* of protein. Therefore, it is common to assume that the protein amount at time t follows the functional form $p_t = p_0 e^{\phi t}$, where p_0 is the starting amount of protein (seed). Similarly, the impurity amount at time t follows the functional form $i_t = i_0 e^{\psi t}$, where ψ is the specific growth rate of impurity and i_0 is the starting amount of impurity. In our model, we consider that measurements are performed at discrete time points $\mathcal{T} = \{t : 0, 1, \dots, T\}$, where T denotes the time point at which the fermentation process is harvested. The time between two measurements is fixed and it can be a day or longer, depending on the process characteristics. This leads to a recursive representation $p_{t+1} = p_t e^{\phi}$ for the protein amount and $i_{t+1} = i_t e^{\psi}$ for the impurity amount for $t \in \{0, 1, \dots, T-1\}$.

Because living biological systems (e.g., cells) are used in the fermentation process, their specific growth rates are random; see for example [31] and [32]. We let Φ_t and Ψ_t denote the independent random variables that represent the specific growth rates of protein and impurity, respectively, in the time interval from time t to $t+1$. The independence of the protein and impurity growth rates is a reasonable assumption given that there are so many biological and chemical factors that randomly influence the “production speed” for impurity and protein, i.e., the rate of generating metabolic wastes and antibody proteins [33, 15]. Moreover, we shall assume that the random variables $\Phi_t, t \in \{0, 1, \dots, T-1\}$, are independent and normally distributed. Let $\mu_c^{(p)}$ and $\sigma_c^{(p)2}$ denote the true (unknown) mean and the variance of Φ_t . Similarly, the random variables $\Psi_t, t \in \{0, 1, \dots, T-1\}$, are independent and normally distributed with true mean $\mu_c^{(i)}$ and variance $\sigma_c^{(i)2}$. The modeling of growth rates as normally distributed random variables leads to the recursive representations of the protein and impurity amount given by

$$\begin{aligned} p_{t+1} &= p_t \cdot e^{\Phi_t}, & \Phi_t &\sim \mathcal{N}(\mu_c^{(p)}, \sigma_c^{(p)2}) \\ i_{t+1} &= i_t \cdot e^{\Psi_t}, & \Psi_t &\sim \mathcal{N}(\mu_c^{(i)}, \sigma_c^{(i)2}) \end{aligned} \quad (1)$$

for $t \in \{0, 1, \dots, T-1\}$, accounting for the *inherent stochasticity* in the accumulation of protein and impurity in a fermentation process. In (1), we use the notation \sim to mean “distributed as” and $\mathcal{N}(a, b)$ to represent a normal distribution with mean a and variance b .

The independent and normally distributed growth rates are commonly used in the literature to model their random variations over time [34, 35, 36]. We also validated this assumption using historical data in our case study, as described in Section 6.1. The stationarity assumption for the growth rate distributions is linked to the fact that the fermentation process has a well-controlled cell culture condition, where the so-called metabolic quasi-steady state is achieved. Thus, the metabolic flux (and hence the corresponding distribution of the protein and impurity growth rates during the exponential growth phase) does not change over time. This assumption is also validated in our case study (Section 6.1).

3.2 Bayesian Learning for the Fermentation Process

The true parameters of the underlying stochastic model for the protein and impurity growth rates, denoted by $\theta^c = \{\mu_c^{(p)}, \sigma_c^{(p)2}, \mu_c^{(i)}, \sigma_c^{(i)2}\}$, are unknown and often need to be estimated from a very limited amount of real-world data (especially for new products that are not yet in production). In this work, we adopt a Bayesian approach and model the mean and variance of the protein and impurity growth rates as random variables, denoted by $\theta = \{\mu^{(p)}, \sigma^{(p)2}, \mu^{(i)}, \sigma^{(i)2}\}$. By representing the model risk in this way, we are able to quantify the model risk by using a posterior distribution which can be efficiently updated with the collection of more data points. In the remainder of this section, we describe how we specify the prior distribution for θ , obtain its posterior distribution by updating the prior with new data on protein and impurity accumulation, and characterize the posterior predictive distributions for the protein and impurity growth rates.

Specification of prior distribution. For the protein growth rate, we build the joint *prior* distribution of $(\mu^{(p)}, \sigma^{(p)2})$ in the following way. First, the marginal distribution of variance $\sigma^{(p)2}$ is chosen as an inverse-gamma distribution with prior parameters $\lambda_0^{(p)}$ and $\beta_0^{(p)}$, denoted as $\sigma^{(p)2} \sim \text{Inv}\Gamma(\lambda_0^{(p)}, \beta_0^{(p)})$. Next, given the value of $\sigma^{(p)2}$, the conditional distribution of mean $\mu^{(p)}$ is assumed to be $\mathcal{N}(\alpha_0^{(p)}, \sigma^{(p)2}/\nu_0^{(p)})$, where $\alpha_0^{(p)}$ and $\nu_0^{(p)}$ are also prior parameters. It then follows that the joint prior distribution of $(\mu^{(p)}, \sigma^{(p)2})$ has a normal-inverse-gamma distribution [37], i.e.,

$$(\mu^{(p)}, \sigma^{(p)2}) \sim \mathcal{N}(\alpha_0^{(p)}, \sigma^{(p)2}/\nu_0^{(p)}) \cdot \text{Inv}\Gamma(\lambda_0^{(p)}, \beta_0^{(p)}). \quad (2)$$

For the impurity growth rate, we obtain the joint prior distribution of $(\mu^{(i)}, \sigma^{(i)2})$ in a similar way by using the prior parameters $\alpha_0^{(i)}, \nu_0^{(i)}, \lambda_0^{(i)}$ and $\beta_0^{(i)}$; i.e.,

$$(\mu^{(i)}, \sigma^{(i)2}) \sim \mathcal{N}(\alpha_0^{(i)}, \sigma^{(i)2}/\nu_0^{(i)}) \cdot \text{Inv}\Gamma(\lambda_0^{(i)}, \beta_0^{(i)}). \quad (3)$$

It is well known that normal-inverse-gamma distribution is conjugate when combined with normally distributed observations [37, 38]. This enables us to efficiently update the prior distributions with the arrival of new data to obtain the posterior distributions.

Characterization of the posterior distribution. Suppose that $(\alpha_t^{(p)}, \nu_t^{(p)}, \lambda_t^{(p)}, \beta_t^{(p)})$ represent our belief on the distribution of protein growth rate at time point t , and we make an observation of the protein amount p_{t+1} at time point $t + 1$. That is, we make an observation $\phi_t = \ln(p_{t+1}/p_t)$, which is a *random* realization of the normally distributed protein growth rate Φ_t . Then, the posterior distribution of $(\mu^{(p)}, \sigma^{(p)2})$ follows a normal-inverse-gamma distribution, i.e.,

$$\left(\mu^{(p)}, \sigma^{(p)2}\right) \sim \mathcal{N}(\alpha_{t+1}^{(p)}, \sigma^{(p)2}/\nu_{t+1}^{(p)}) \cdot \text{Inv}\Gamma(\lambda_{t+1}^{(p)}, \beta_{t+1}^{(p)}) \quad (4)$$

with updated parameters

$$\alpha_{t+1}^{(p)} = \alpha_t^{(p)} + \frac{\phi_t - \alpha_t^{(p)}}{\nu_{t+1}^{(p)}}, \quad \nu_{t+1}^{(p)} = \nu_t^{(p)} + 1, \quad \lambda_{t+1}^{(p)} = \lambda_t^{(p)} + \frac{1}{2}, \quad \beta_{t+1}^{(p)} = \beta_t^{(p)} + \frac{\nu_t^{(p)}(\phi_t - \alpha_t^{(p)})^2}{2\nu_{t+1}^{(p)}}. \quad (5)$$

Given our belief $(\alpha_t^{(i)}, \nu_t^{(i)}, \lambda_t^{(i)}, \beta_t^{(i)})$ about the distribution of impurity growth rate at time point t , since the observation $\psi_t = \ln(i_{t+1}/i_t)$ is a *random* realization of the normally distributed impurity growth rate Ψ_t , the posterior distribution of $(\mu^{(i)}, \sigma^{(i)2})$ is also a normal-inverse-gamma; i.e.,

$$\left(\mu^{(i)}, \sigma^{(i)2}\right) \sim \mathcal{N}(\alpha_{t+1}^{(i)}, \sigma^{(i)2}/\nu_{t+1}^{(i)}) \cdot \text{Inv}\Gamma(\lambda_{t+1}^{(i)}, \beta_{t+1}^{(i)}), \quad (6)$$

with the updated parameters

$$\alpha_{t+1}^{(i)} = \alpha_t^{(i)} + \frac{\psi_t - \alpha_t^{(i)}}{\nu_{t+1}^{(i)}}, \quad \nu_{t+1}^{(i)} = \nu_t^{(i)} + 1, \quad \lambda_{t+1}^{(i)} = \lambda_t^{(i)} + \frac{1}{2}, \quad \beta_{t+1}^{(i)} = \beta_t^{(i)} + \frac{\nu_t^{(i)}(\psi_t - \alpha_t^{(i)})^2}{2\nu_{t+1}^{(i)}}. \quad (7)$$

For further details on the Bayesian update procedure, we refer the reader to [37]².

Posterior predictive distribution of the growth rates. Given the Bayesian model described above, the density of the protein growth rate at time t , conditional on the historical protein data (i.e., summarized by the belief parameters $(\alpha_t^{(p)}, \nu_t^{(p)}, \lambda_t^{(p)}, \beta_t^{(p)})$), is given by

$$\mathbf{p}\left(\phi_t | \alpha_t^{(p)}, \nu_t^{(p)}, \lambda_t^{(p)}, \beta_t^{(p)}\right) = \int \int \mathbf{p}\left(\phi_t | \mu^{(p)}, \sigma^{(p)2}\right) \mathbf{p}\left(\mu^{(p)}, \sigma^{(p)2} | \alpha_t^{(p)}, \nu_t^{(p)}, \lambda_t^{(p)}, \beta_t^{(p)}\right) d\mu^{(p)} d\sigma^{(p)2}, \quad (8)$$

where $\mathbf{p}\left(\phi_t | \mu^{(p)}, \sigma^{(p)2}\right)$ is the density of the normally distributed protein growth rate Φ_t and $\mathbf{p}\left(\mu^{(p)}, \sigma^{(p)2} | \alpha_t^{(p)}, \nu_t^{(p)}, \lambda_t^{(p)}, \beta_t^{(p)}\right)$ is the joint posterior density of the normal-inverse-gamma distributed $(\mu^{(p)}, \sigma^{(p)2})$. In (8), the integral marginalizes out the variables $\mu^{(p)}$ and $\sigma^{(p)2}$, leading to the predictive density of the future observation of the protein growth rate given the current belief parameters on the underlying protein growth model. We let $\tilde{\Phi}_t$ denote the predictive protein growth-rate random variable at time point t , and it has the density given in (8), accounting for both the model risk and the inherent stochasticity in the protein accumulation. It can be shown that the random variable $\tilde{\Phi}_t$ follows a generalized t-distribution [39], i.e.,

$$\tilde{\Phi}_t \sim t_{2\lambda_t^{(p)}}\left(\alpha_t^{(p)}, \frac{\beta_t^{(p)}(1 + \nu_t^{(p)})}{\nu_t^{(p)}\lambda_t^{(p)}}\right), \quad (9)$$

where $\tilde{\Phi}_t \sim t_v(a, b)$ means that $(\tilde{\Phi}_t - a)/\sqrt{b}$ follows a standard t-distribution with v degrees of freedom. We refer to the term $\beta_t^{(p)}(1 + \nu_t^{(p)})/(\nu_t^{(p)}\lambda_t^{(p)})$ in (9) as the predictive variance of the protein growth rate, and denote it with $\tilde{\sigma}_t^{(p)2}$.

The same result holds for the predictive impurity growth-rate $\tilde{\Psi}_t$ at time point t :

$$\tilde{\Psi}_t \sim t_{2\lambda_t^{(i)}}\left(\alpha_t^{(i)}, \frac{\beta_t^{(i)}(1 + \nu_t^{(i)})}{\nu_t^{(i)}\lambda_t^{(i)}}\right), \quad (10)$$

where we refer to the term $\beta_t^{(i)}(1 + \nu_t^{(i)})/(\nu_t^{(i)}\lambda_t^{(i)})$ in (10) as the predictive variance of the impurity growth rate and denote it with $\tilde{\sigma}_t^{(i)2}$. In the remainder of the paper, we use $f_t^{(p)}(\cdot)$ and $f_t^{(i)}(\cdot)$ to denote the posterior predictive density functions of the random variables $\tilde{\Phi}_t$ and $\tilde{\Psi}_t$, respectively.

3.3 Markov Decision Process Model

It is of practical importance to optimize when to harvest the fermentation process under limited historical data. We will formulate this problem as a Markov Decision Processes (MDP) model with Bayesian updates on the parameters of the protein and impurity growth-rate distributions.

Decision Epochs. We consider a finite-horizon discrete-time model with decision epochs $\mathcal{T} = \{t : 0, 1, \dots, \bar{T}\}$, representing the time points at which the protein and impurity amounts are measured. The parameter \bar{T} denotes the time point at which the fermentation must be harvested, if not done yet. We consider an upper bound on the time of harvest because it is often known when the growth stops (i.e., there are no incentives for continuing the fermentation beyond that point). Also, it gives some level of certainty in the planning of the bioreactor. Note that $T \in \mathcal{T}$, i.e., the time point at which the fermentation is harvested must be a decision epoch and it is at most \bar{T} .

Physical States. The levels of protein and impurity during the fermentation process constitute the physical states. In practice, there is an upper limit on the cell density that can be accommodated by a bioreactor with a certain volume. Thus, it is undesired to continue fermentation beyond a certain level of protein accumulation. We let \bar{P} represent this upper limit on the accumulated protein level at which the fermentation must be harvested. On the other hand, we let \bar{I} denote the maximum impurity value at which the batch is considered as failed. If the accumulated impurity level reaches \bar{I} , a predefined value in accordance with regulatory standards on batch quality, the fermentation process must be terminated. At decision epoch t , the physical state \mathcal{S}_t is specified by the current protein amount $p_t \in [0, \bar{P}]$ and the current impurity amount $i_t \in [0, \bar{I}]$ in the fermentation process, i.e., $\mathcal{S}_t = (p_t, i_t)$.

Action Space. At a decision epoch before reaching the stationary phase, we can either continue the fermentation process one more time period (denoted by action C) or terminate the fermentation process by harvesting it (denoted by action H). The harvest action is the only possible action if: (1) the current protein amount reaches the harvesting limit \bar{P} ; (2) there is a batch failure, caused by the impurity level reaching the threshold level \bar{I} ; or (3) the fermentation process reaches the decision epoch \bar{T} . The action space can be formalized as $\{H\}$ if $p_t = \bar{P}$ or $i_t = \bar{I}$ or $t = \bar{T}$. On the other hand, the action space is given by $\{C, H\}$ if $p_t < \bar{P}$, $i_t < \bar{I}$, and $t < \bar{T}$.

Knowledge State. Since the true parameters θ^c of the underlying model are unknown and estimated from real-world data, we use the *knowledge state*, specified by the parameters of the posterior distribution of θ , to quantify our current belief about θ^c . That is, we specify the posterior-distribution parameters (from Section 3.2) as the knowledge state at decision epoch t , denoted by $\mathcal{I}_t = \{\alpha_t^{(p)}, \nu_t^{(p)}, \lambda_t^{(p)}, \beta_t^{(p)}, \alpha_t^{(i)}, \nu_t^{(i)}, \lambda_t^{(i)}, \beta_t^{(i)}\}$.

Hyper States & Hyper State Transition: We introduce the *hyper states* $\mathcal{H}_t \equiv (\mathcal{S}_t, \mathcal{I}_t)$, including both physical state $\mathcal{S}_t = (p_t, i_t)$ and knowledge state \mathcal{I}_t . If the action at decision epoch t is to continue the fermentation, i.e., $a_t = C$, the hyper state transition probability can be specified as

$$\Pr(\mathcal{S}_{t+1}, \mathcal{I}_{t+1} | \mathcal{S}_t, \mathcal{I}_t; C) = \Pr(\mathcal{S}_{t+1} | \mathcal{S}_t, \mathcal{I}_t) \Pr(\mathcal{I}_{t+1} | \mathcal{S}_{t+1}, \mathcal{S}_t, \mathcal{I}_t) \quad (11)$$

where $\Pr(\mathcal{S}_{t+1} | \mathcal{S}_t, \mathcal{I}_t)$ represents the probability that the physical state transits to \mathcal{S}_{t+1} (i.e., conditioned on the current physical state and knowledge state), and $\Pr(\mathcal{I}_{t+1} | \mathcal{S}_{t+1}, \mathcal{S}_t, \mathcal{I}_t, C)$ represents the probability that the knowledge state transits to \mathcal{I}_{t+1} given the realization of \mathcal{S}_{t+1} (i.e., conditioned on the current knowledge state as well as the realized physical-state transition).

In (11), the first term $\Pr(\mathcal{S}_{t+1} | \mathcal{S}_t, \mathcal{I}_t)$ can be determined by the protein and impurity transition equations $p_{t+1} = p_t e^{\tilde{\phi}_t}$ and $i_{t+1} = i_t e^{\tilde{\psi}_t}$, where $\tilde{\phi}_t$ and $\tilde{\psi}_t$ are the realizations of the random variables $\tilde{\Phi}_t$ and $\tilde{\Psi}_t$ with distributions specified in (9) and (10), respectively. The second term $\Pr(\mathcal{I}_{t+1} | \mathcal{S}_{t+1}, \mathcal{S}_t, \mathcal{I}_t)$ follows the Bayesian updates for the knowledge states as specified in (5) and (7) given the realization of the physical states (p_{t+1}, i_{t+1}) or equivalently the growth rate samples $(\tilde{\phi}_t, \tilde{\psi}_t) = (\ln(p_{t+1}/p_t), \ln(i_{t+1}/i_t))$.

At any decision epoch t with physical states (p_t, i_t) , if the action is to harvest (i.e., $a_t = H$), the fermentation process ends. We model this situation by assuming that, if the harvest action is taken, the state of the MDP makes a transition to an *absorbing stopping state* Δ . Thus, the counterpart of (11) for the harvest action can be written as $\Pr(\Delta | \mathcal{S}_t, \mathcal{I}_t; H) = 1$.

Reward: At any decision epoch t , if the decision is to continue, the immediate cost c_u is charged. The cost c_u represents the cost of resources allocated to continue the fermentation process one more time step (e.g., a fixed energy cost for the bioreactor, operator cost, clean room charges). Since the time periods are of equal length, it is natural to assume a constant operating cost c_u per time unit (regardless of how much protein or impurity accumulated inside the bioreactor). On the other hand, if the decision is to harvest, the fermentation is terminated and a reward is collected. The reward of the harvest decision depends on the current physical state. Specifically, if the harvest decision is taken because of a failure (i.e., if $i_t = \bar{I}$), then the failure penalty r_f is charged as the cost of losing the batch due to the failure. On the

other hand, if there is no failure at the harvesting moment (i.e., if $i_t < \bar{I}$), the harvest reward

$$r_h(p_t, i_t) = c_0 + c_1 p_t - c_2 i_t \quad (12)$$

is collected as an immediate reward. In (12), $c_0 > 0$ represents the lump-sum reward collected per fermentation batch, while $c_1 > 0$ and $c_2 > 0$ represent the marginal reward collected per unit of protein and the marginal cost encountered per unit of impurity, respectively. Furthermore, the term $c_2 i_t$ allows us to account for the impact of fermentation harvesting decisions on the downstream purification costs. In our problem setting, higher impurity levels obtained from fermentation imply a higher workload in downstream purification operations (e.g., a higher number of chromatography cycles, leading to a higher cost of raw materials and labor to eliminate the impurities). The cost of purification mainly consists of the material costs (e.g., cost of resins, media and buffers) and labor cost needed for the chromatography and filtration processes [40, 41]. We shall assume that $r_f > c_2 \bar{I}$, reflecting the fact that a failure is costlier than even the worst harvesting outcome. To summarize, given the physical states (p_t, i_t) and the action a_t , the reward $R(p_t, i_t; a_t)$ at decision epoch t can be written as,

$$R(p_t, i_t; a_t) = \begin{cases} -c_u, & a_t = C, i_t < \bar{I} \\ r_h(p_t, i_t), & a_t = H, i_t < \bar{I} \\ -r_f, & a_t = H, i_t = \bar{I} \end{cases} \quad (13)$$

Policy: Let π denote a nonstationary policy $\{\pi_t(\cdot); t = 0, 1, \dots, \bar{T}\}$, which is a mapping from any hyper state \mathcal{H}_t to an action a_t , i.e., $a_t = \pi_t(\mathcal{H}_t)$. Given the policy π , the expected total discounted reward is

$$\rho(\pi) = \mathbb{E} \left[\sum_{t=0}^T \gamma^t R(p_t, i_t; \pi_t(\mathcal{H}_t)) \middle| \mathcal{H}_0, \pi \right], \quad (14)$$

where $\gamma \in (0, 1]$ is the discount factor. Notice that (14) represents the expected total discounted reward under the policy π from time point 0 until the termination of the fermentation process. The stopping time T in (14) is the decision epoch at which the harvest action is taken; i.e., if $\pi_t(\mathcal{H}_t) = H$, then $T = t$. Our objective is to find the optimal policy π^* that maximizes the expected total discounted reward, i.e., $\pi^* = \arg \max_{\pi} \rho(\pi)$.

Value Function: The value function $V_t(\mathcal{H}_t)$ is defined as the expected total discounted reward starting from the decision epoch t with hyper state \mathcal{H}_t under the optimal policy π^* , i.e.,

$$V_t(\mathcal{H}_t) = \mathbb{E} \left[\sum_{\ell=t}^T \gamma^\ell R(p_\ell, i_\ell; \pi_\ell^*(\mathcal{H}_\ell)) \middle| \mathcal{H}_t \right].$$

The value function $V_t(\mathcal{H}_t)$, or equivalently $V_t(p_t, i_t, \mathcal{I}_t)$, represents the maximum expected total discounted reward starting from decision epoch t with physical state (p_t, i_t) and knowledge state \mathcal{I}_t , and it can be recursively written as

$$V_t(p_t, i_t, \mathcal{I}_t) = \begin{cases} \max \{r_h(p_t, i_t), -c_u + \gamma \mathbb{E}[V_{t+1}(p_{t+1}, i_{t+1}, \mathcal{I}_{t+1})]\} & \text{if } p_t < \bar{P} \text{ and } i_t < \bar{I} \\ r_h(p_t, i_t) & \text{if } p_t = \bar{P} \text{ and } i_t < \bar{I} \\ -r_f & \text{if } i_t = \bar{I} \end{cases} \quad (15)$$

for $t = 0, 1, \dots, \bar{T} - 1$.

At the decision epoch \bar{T} (i.e., if the stationary phase is reached in the fermentation process), the value function is equal to

$$V_{\bar{T}}(p_{\bar{T}}, i_{\bar{T}}, \mathcal{I}_{\bar{T}}) = \begin{cases} r_h(p_{\bar{T}}, i_{\bar{T}}), & \text{if } i_{\bar{T}} < \bar{I} \\ -r_f, & \text{if } i_{\bar{T}} = \bar{I}. \end{cases} \quad (16)$$

because the only feasible action is to harvest if the time point \bar{T} is reached, and either the harvesting reward or the failure cost is charged depending on the impurity amount at decision epoch \bar{T} . Recall that the hyper state transits to the absorbing stopping state Δ after the harvest action, and the value function is equal to zero for a process already at the stopping state, i.e., $V_t(\mathcal{H}_t) = 0$ if $\mathcal{H}_t = \Delta$ at any t . So, the transition to the stopping state Δ is omitted in (29) and (30). Consistent with the implementation at MSD, our objective is to maximize the expected total reward obtained from a *single* batch. In Appendix A, we provide a model extension with *multiple* batches and fermentation campaigns (i.e., multiple batches with setup times are produced over a finite planning horizon).

4 Analysis

Section 4.1 presents a characterization of the variability in the posterior predictive distribution of the growth rates. Section 4.2 provides some analytical properties of the optimal policy. We note that the MDP model introduced in Section 3.3 is a variant of the classical optimal stopping problem [42]. A well-known class of policies for optimal-stopping problems is look-ahead policies. Motivated by its simplicity for applying in practice, we consider the *one-step look-ahead policy* (referred to as myopic policy) in Section 4.3. Finally, Section 4.4 discusses our solution approach to obtain the optimal policy. All the proofs and the algorithm procedure are provided in the Appendix.

4.1 Growth-Rate Variability under Model Risk

Recall that the uncertainty in the protein and impurity growth rates comes from two sources: the inherent stochasticity of the fermentation and the model risk. Conditional on the historical data collected until the decision epoch t , the predictive protein growth rate $\tilde{\Phi}_t$ and the predictive impurity growth rate $\tilde{\Psi}_t$ are the random variables that the decision maker uses to model the growth rates, and these random variables account for both sources of uncertainty (see Section 3.2). The objective of this section is to quantify the contribution of each source of uncertainty to the predictive variance of the random variables $\tilde{\Phi}_t$ and $\tilde{\Psi}_t$, denoted with $\tilde{\sigma}_t^{(p)2}$ and $\tilde{\sigma}_t^{(i)2}$, respectively.

Let $\mathcal{D}_t = \{(\phi^{(0)}, \psi^{(0)}), (\phi^{(1)}, \psi^{(1)}), \dots, (\phi^{(J_t)}, \psi^{(J_t)})\}$ denote the historical data on past realizations of the growth rates available at the t -th decision epoch of the fermentation process. It is possible that the data size J_t can be greater than t as the historical data \mathcal{D}_t may also include the growth-rate realizations from the previous fermentation processes. Recall from Section 3.2 that the knowledge states can be recursively written as a function of the historical data \mathcal{D}_t ; see equations (5) and (7). By applying the commonly used improper prior that assumes the initial belief states $\alpha_0^{(p)}, \nu_0^{(p)}, \lambda_0^{(p)}, \beta_0^{(p)}, \alpha_0^{(i)}, \nu_0^{(i)}, \lambda_0^{(i)}, \beta_0^{(i)}$ are all equal to 0, the knowledge states can be obtained as

$$\alpha_t^{(p)} = \bar{\phi}, \nu_t^{(p)} = J_t, \lambda_t^{(p)} = \frac{J_t}{2}, \beta_t^{(p)} = \frac{1}{2} \sum_{j=1}^{J_t} (\phi^{(j)} - \bar{\phi})^2,$$

$$\alpha_t^{(i)} = \bar{\psi}, \nu_t^{(i)} = J_t, \lambda_t^{(i)} = \frac{J_t}{2}, \beta_t^{(i)} = \frac{1}{2} \sum_{j=1}^{J_t} (\psi^{(j)} - \bar{\psi})^2,$$

where $\bar{\phi} = \sum_{j=1}^{J_t} \phi^{(j)} / J_t$ and $\bar{\psi} = \sum_{j=1}^{J_t} \psi^{(j)} / J_t$. The posterior predictive variances are then given by

$$\tilde{\sigma}_t^{(p)2} = \frac{J_t + 1}{(J_t - 2)J_t} \sum_{j=1}^{J_t} (\phi^{(j)} - \bar{\phi})^2, \quad \tilde{\sigma}_t^{(i)2} = \frac{J_t + 1}{(J_t - 2)J_t} \sum_{j=1}^{J_t} (\psi^{(j)} - \bar{\psi})^2 \quad (17)$$

for $J_t > 2$. Next, by considering the randomness in the historical data \mathcal{D}_t , Proposition 1(i) establishes the expectation and variance of $\tilde{\sigma}_t^{(p)2}$ (i.e., similar to the characterization of the expectation and variance for the sample variance of a set of realizations from a specific population). For a particular realization of the historical data set \mathcal{D}_t , Proposition 1(ii) characterizes the predictive variance $\tilde{\sigma}_t^{(p)2}$ as the sum of two closed-form terms that represent the variability in the growth rate due to the inherent stochasticity of the fermentation process and the model risk, respectively.

Proposition 1. (i) $E[\tilde{\sigma}_t^{(p)2}] = \sigma_c^{(p)2} + \frac{(2J_t - 1)\sigma_c^{(p)2}}{(J_t^2 - 2J_t)}$ and $\text{Var}[\tilde{\sigma}_t^{(p)2}] = \frac{2(J_t^3 + J_t^2 - J_t - 1)\sigma_c^{(p)4}}{J_t^4 - 4J_t^3 + 4J_t^2}$.

(ii) Conditional on the historical data \mathcal{D}_t , the predictive variance $\tilde{\sigma}_t^{(p)2}$ for the protein growth rate can be decomposed into two components $\hat{\sigma}_t^{(p)2} = \frac{\beta_t^{(p)}}{\lambda_t^{(p)} - 1}$ and $\check{\sigma}_t^{(p)2} = \frac{\beta_t^{(p)}}{(\lambda_t^{(p)} - 1)\nu_t^{(p)}}$, representing the variability of the protein growth rate due to inherent stochasticity and the model risk, respectively; i.e., $\tilde{\sigma}_t^{(p)2} = \hat{\sigma}_t^{(p)2} + \check{\sigma}_t^{(p)2}$ with $\hat{\sigma}_t^{(p)2} = \frac{\sum_{j=1}^{J_t} (\phi^{(j)} - \bar{\phi})^2}{J_t - 2}$ and $\check{\sigma}_t^{(p)2} = \frac{\sum_{j=1}^{J_t} (\phi^{(j)} - \bar{\phi})^2}{J_t^2 - 2J_t}$.

We notice from Proposition 1(i) that the bias $E[\tilde{\sigma}_t^{(p)2} - \sigma_c^{(p)2}] = \frac{(2J_t - 1)\sigma_c^{(p)2}}{J_t^2 - 2J_t} > 0$ for $J_t > 2$. Therefore, under model risk, on average the predictive variance $\tilde{\sigma}_t^{(p)2}$ will be greater than the true variance $\sigma_c^{(p)2}$. Furthermore, as the

amount of historical data J_t increases, $\text{Var} \left[\tilde{\sigma}_t^{(p)2} \right]$ converges to zero, and the predictive variance $\tilde{\sigma}_t^{(p)2}$ will converge to $\sigma_c^{(p)2}$, which represents the protein growth-rate variance under perfect information. Given a particular realization of the historical data set \mathcal{D}_t , Proposition 1(ii) is useful in practice as it allows making a judgment on how the overall uncertainty in the protein growth rate is affected from the inherent stochasticity of the fermentation process and from the model risk. Notice that the ratio of model risk to the inherent stochasticity, i.e., $\tilde{\sigma}_t^{(p)2} / \hat{\sigma}_t^{(p)2} = 1/\nu_t^{(p)}$, only depends on the shape parameter $\nu_t^{(p)}$ which is equal to J_t . This intuitively shows that the model risk becomes smaller (relative to the inherent stochasticity of the process) as the size of the historical data increases.

Notice that the results in Proposition 1 also apply to the impurity growth model. To be specific, the same results and discussion hold for the predictive variance $\tilde{\sigma}_t^{(i)2}$ of the impurity growth rate, as the functional form and the underlying modeling assumptions are the same as in the protein growth model. For brevity, we do not repeat those results in the paper.

4.2 Analytical Properties of the Optimal Policy

We start our analysis by first showing the monotonicity of the value function, and then present sufficient conditions for the existence of a *control-limit policy* with respect to the impurity level.

Theorem 1. *Given the knowledge state \mathcal{I}_t , the value function $V_t(p_t, i_t, \mathcal{I}_t)$ is a non-increasing function of the impurity level i_t and a non-decreasing function of the protein level p_t .*

Based on the monotonicity properties presented in Theorem 1, we can derive sufficient conditions for the existence of a control-limit policy as follows.

Theorem 2. *At any decision epoch t with a given protein level and knowledge state, there exists a critical threshold i_t^* such that the optimal decision is to harvest for the impurity level $i_t \geq i_t^*$ if the following condition holds for all $i_t^+ > i_t^- \geq 0$:*

$$c_2(i_t^+ - i_t^-) \leq \gamma r_f [\Pr(i_{t+1} \leq \bar{I}|i_t^-) - \Pr(i_{t+1} \leq \bar{I}|i_t^+)] - \gamma c_1 \bar{P} \Pr(i_{t+1} \leq \bar{I}|i_t^-) \quad (18)$$

where $\Pr(i_{t+1} < \bar{I}|i_t) = \Pr(i_t e^{\tilde{\Psi}_t} < \bar{I}) = \int_{-\infty}^{\ln \bar{I} - \ln i_t} f_t^{(i)}(\psi_t) d\psi_t$ is the probability that the process failure doesn't occur in the time period that starts with the impurity level i_t at decision epoch t .

Theorem 2 presents the existence of a critical threshold i_t^* with respect to the impurity level: given the same protein and knowledge states, if we harvest at a certain impurity level, we will also harvest at any higher level of impurity. That is, the physical-state space can be split into a harvest zone and a continue zone indicating the optimal action at a particular physical state. The notations i_t^+ and i_t^- in Theorem 2 represent any two distinct values of the impurity state that must satisfy the sufficient condition (18) to assure the optimality of a control-limit policy with respect to the impurity level. Given a fixed protein level and knowledge state, if it is optimal to harvest at a certain impurity level i_t^- , then it is also optimal at any higher impurity level i_t^+ . If condition (18) is satisfied for all $i_t^+ > i_t^- \geq 0$, the optimal policy is guaranteed to be a control-limit policy with a critical threshold on the impurity level. We note that condition (18) holds for the realistic cases we studied. In particular, this condition is more likely to be satisfied as the relative value of the failure penalty r_f increases compared to c_1 and c_2 . In practice, it is common that r_f is much larger compared to c_1 and c_2 , reflecting the fact that failures are undesired because of strict safety concerns, loss of reputation, and extra rework.

Next, we focus on understanding how the value function $V_t(p_t, i_t, \mathcal{I}_t)$ is affected by the posterior predictive distribution of the growth rates. Note that these distributions are updated every decision epoch based on the collected data, and they are represented by the knowledge state \mathcal{I}_t . Theorem 3 formally shows the monotonicity of $V_t(p_t, i_t, \mathcal{I}_t)$ with respect to the expected value of the posterior predictive distribution of each growth rate.

Theorem 3. *Given the physical state (p_t, i_t) , the value function $V_t(p_t, i_t, \mathcal{I}_t)$ is a non-decreasing function of the expected protein growth rate (i.e., $E[\tilde{\Phi}_t]$) and a non-increasing function of the expected impurity growth rate (i.e., $E[\tilde{\Psi}_t]$) at decision epoch t .*

The result in Theorem 3 is intuitive considering the effect of protein and impurity levels on the harvest reward. If the expected growth rate of the protein becomes larger, more protein tends to be accumulated over time, leading to a higher reward. On the other hand, if the expected growth rate of the impurity increases, more impurity would be accumulated, leading to a lower reward.

4.3 Myopic Policy

A well-known class of policies for optimal-stopping problems is look-ahead policies. In this section, we consider the one-step look-ahead policy. We refer to it as the myopic policy because it makes the harvesting decisions by only comparing the reward of harvesting at the current decision epoch with the expected reward of harvesting at the next decision epoch.

4.3.1 Myopic Policy under Perfect Information.

Here we suppose that the true parameters of the underlying stochastic model are known, referred to as the *perfect-information* case. That is, the parameters $\mu_c^{(p)}$ and $\sigma_c^{(p)2}$ for the protein growth rate and the parameters $\mu_c^{(i)}$ and $\sigma_c^{(i)2}$ for the impurity growth rate are known by the decision maker. The analysis in this section assumes that the probability of a negative growth rate is negligible (i.e., the realizations of the growth rate random variables Φ_t and Ψ_t are always non-negative), which is often the case in practice with a standard deviation of the normally distributed growth rates expected to be much smaller than their mean values.

In the perfect-information setting, we define the myopic policy as the policy which decides to harvest the fermentation process at the first decision epoch t in which $(p_t, i_t) \in A$, where

$$A = \{(p, i) : r_h(p, i) \geq -c_u + \gamma E[R(p', i'; H)|p, i]\}. \quad (19)$$

The expectation in (19) is with respect to the underlying true growth model (1), and (p', i') denotes the protein and impurity levels of the next decision epoch after the continue action is taken in the current decision epoch at state (p, i) . The set A represents the subset of physical-state space at which harvesting is at least as good as continuing for exactly one more time period and then harvesting. Our objective is to establish when the myopic policy is optimal in the perfect-information setting. Theorem 4 establishes a sufficient condition for the optimality of the myopic policy.

Theorem 4. *The optimal policy under perfect information is the myopic policy, which takes the harvest decision if and only if the state variables $(p, i) \in A$, given the following conditions hold:*

- (i) if $(p, i) \in A$, then $(p^+, i) \in A$ for any $p^+ > p$; and
- (ii) if $(p, i) \in A$, then $(p, i^+) \in A$ for any $i^+ > i$.

It is important to know when the conditions stated in Theorem 4 hold so that we can understand when the myopic policy is optimal. Condition (i) assures that if the myopic policy harvests at a given protein level p , it also harvests at a higher protein level p^+ . Lemma 1 establishes this result.

Lemma 1. *Condition (i) in Theorem 4 holds if $p \in [\underline{p}, \bar{P}]$, where*

$$\underline{p} = \exp \left\{ \ln \bar{P} - \mu_c^{(p)} - \sigma_c^{(p)2} - \sigma_c^{(p)} \Phi^{-1} \left[\frac{e^{-\mu_c^{(p)} - \sigma_c^{(p)2}/2}}{\gamma \Phi \left(\frac{\ln \bar{I} - \ln i_0 - \mu_c^{(i)}}{\sigma_c^{(i)}} \right)} \right] \right\}. \quad (20)$$

According to Lemma 1, when the protein level is sufficiently large, if myopic policy decides to harvest at a certain protein level, it also harvests at a higher protein level. Intuitively, this can be explained by the fact that, if greater than \underline{p} , the protein amount is large enough, making it unnecessary to consider the continue action in the future periods given the failure risk.

On the other hand, condition (ii) in Theorem (4) means that if the myopic policy harvests at a given impurity level i , it also harvests at a higher impurity level i^+ . In Lemma 2, we introduce a sufficient condition that assures this result.

Lemma 2. *Condition (ii) in Theorem 4 holds if*

$$\begin{aligned} \frac{c_2}{\gamma} (i^+ - i) \leq r_f \left[\Phi \left(\frac{\ln \bar{I} - \ln i - \mu_c^{(i)}}{\sigma_c^{(i)}} \right) - \Phi \left(\frac{\ln \bar{I} - \ln i^+ - \mu_c^{(i)}}{\sigma_c^{(i)}} \right) \right] \\ - c_2 \bar{I} e^{\mu_c^{(i)} + \sigma_c^{(i)2}/2} \left[\Phi \left(\frac{\ln \bar{I} - \ln i - \mu_c^{(i)} - \sigma_c^{(i)2}}{\sigma_c^{(i)}} \right) - \Phi \left(\frac{\ln \bar{I} - \ln i^+ - \mu_c^{(i)} - \sigma_c^{(i)2}}{\sigma_c^{(i)}} \right) \right] \end{aligned} \quad (21)$$

for all $i, i^+ \in [i_0, \bar{I}]$ with $i < i^+$.

We note that the inequality in (21) is not immediately intuitive. To make it easier to interpret, we simplify this condition by applying a Taylor series approximation as indicated in Corollary 5.

Corollary 5. *By applying first-order Taylor series approximation of the nonlinear terms on both sides of inequality (21), it can be approximated as*

$$r_f \geq c_2 \bar{I} \left[\frac{\sqrt{2\pi}\sigma_c^{(i)}}{\gamma} + e^{\mu_c^{(i)} + \sigma_c^{(i)2}/2} \right]. \quad (22)$$

The inequality (22) provides an intuitive interpretation of the sufficient condition (21) which assures that the myopic policy that harvests at a given impurity level also harvests at a higher impurity level. Note that (22) is more likely to hold as the failure cost r_f increases or the maximum purification cost $c_2 \bar{I}$ decreases. Corollary 6 summarizes our main takeaways regarding the optimality of the myopic policy in the perfect-information setting:

Corollary 6. *Given that the condition (21) holds and the current protein level p is greater than the threshold p characterized in (20), the myopic policy is optimal. In particular, the optimal action is to harvest for the states in set \bar{A} that is characterized by (19).*

4.3.2 Myopic Policy under Model Risk.

In this section, the true parameters of the underlying stochastic model of the growth rates are not known. That is, in contrast to the case with perfect information, there is a model risk. Our objective is to investigate how the model risk affects the harvesting decisions of the myopic policy.

Recall that the myopic policy decides whether to harvest or not by comparing the reward of harvesting at the current decision epoch with the expected reward of harvesting at the next decision epoch. When there is model risk, the expected reward of harvesting at the next decision epoch is calculated by using the posterior predictive distributions of the growth rates (i.e., the distributions characterized in (9) and (10)). Let $E[R(p', i'; H)|p, i, \alpha^{(p)}, \tilde{\sigma}^{(p)}, \alpha^{(i)}, \tilde{\sigma}^{(i)}]$ denote this expectation, given that the posterior predictive distributions have the mean $\alpha^{(p)}$ and $\alpha^{(i)}$ and standard deviation $\tilde{\sigma}^{(p)}$ and $\tilde{\sigma}^{(i)}$ for the protein and impurity growth rates, respectively. In the remainder of this section, we use the normal approximations of these posterior predictive distributions.³ Note that the myopic policy takes the harvest action if $\tilde{h}(\alpha^{(p)}, \tilde{\sigma}^{(p)}, \alpha^{(i)}, \tilde{\sigma}^{(i)}; p, i) \geq 0$ and continues the fermentation if $\tilde{h}(\alpha^{(p)}, \tilde{\sigma}^{(p)}, \alpha^{(i)}, \tilde{\sigma}^{(i)}; p, i) < 0$, where

$$\tilde{h}(\alpha^{(p)}, \tilde{\sigma}^{(p)}, \alpha^{(i)}, \tilde{\sigma}^{(i)}; p, i) = r_h(p, i) + c_u - \gamma E[R(p', i'; H)|p, i, \alpha^{(p)}, \tilde{\sigma}^{(p)}, \alpha^{(i)}, \tilde{\sigma}^{(i)}]. \quad (23)$$

We will study the effect of model risk on the harvesting decisions of the myopic policy by investigating how the so-called *harvest boundary*, which is given by

$$\{(p, i) : \tilde{h}(\alpha^{(p)}, \tilde{\sigma}^{(p)}, \alpha^{(i)}, \tilde{\sigma}^{(i)}; p, i) = 0\},$$

is influenced by the parameters of the posterior predictive distributions. For this purpose, Figure 2 plots the harvest boundary for various levels of model risk. To be specific, Figure 2 considers a scaling factor k that links each parameter to its true counterpart, and plots the harvest boundaries for some relevant values of k . For example, $k = 1$ represents the case where each predictive-distribution parameter reduces to its true counterpart (e.g., $\alpha_t^{(p)}$, the mean of the predictive distribution of the protein growth rate, becomes equal to $\mu_c^{(p)}$, the true mean of the protein growth rate), and thus, the resulting decision boundary becomes equivalent to the decision boundary of the myopic policy under perfect information. Recall from Corollary 6 that the myopic policy is optimal under perfect information when certain conditions hold. In Figure 2, we know condition (21) is satisfied and p from (20) is equal to 17.34. Thus, for protein levels greater than 17.34, Figure 2 already gives an insight into how close the myopic policy is to the optimal policy under model risk.

Figure 2 (top, left) shows that as the predictive mean of protein $\alpha_t^{(p)}$ increases, the harvest boundary moves up, indicating that it becomes less beneficial to harvest immediately when the potential future gain in protein amount is high. Also, the difference on the left part (with a small amount of protein p_t) is larger than on the right (with a large amount of protein p_t), since as protein approaches the harvesting limit, an increase in $\alpha_t^{(p)}$ becomes less influential on the harvesting decision. Figure 2 (top, right) shows that as the predictive mean of impurity $\alpha_t^{(i)}$ increases, the harvest boundary moves down. This is intuitive because a higher $\alpha_t^{(i)}$ implies a stronger belief on the impurity growth rate (and hence a higher probability of a fermentation failure), so a smaller amount of current impurity level is sufficient to trigger a harvest action. According to Figure 2 (bottom, left), as the parameter $\tilde{\sigma}_t^{(p)}$ increases, the decision boundary shifts to the left. That is, with higher uncertainty of protein growth, we tend to harvest with a smaller amount of protein especially when it is close to the maximum protein level. On the other hand, as the parameter $\tilde{\sigma}_t^{(i)}$ increases, Figure 2 (bottom, right)

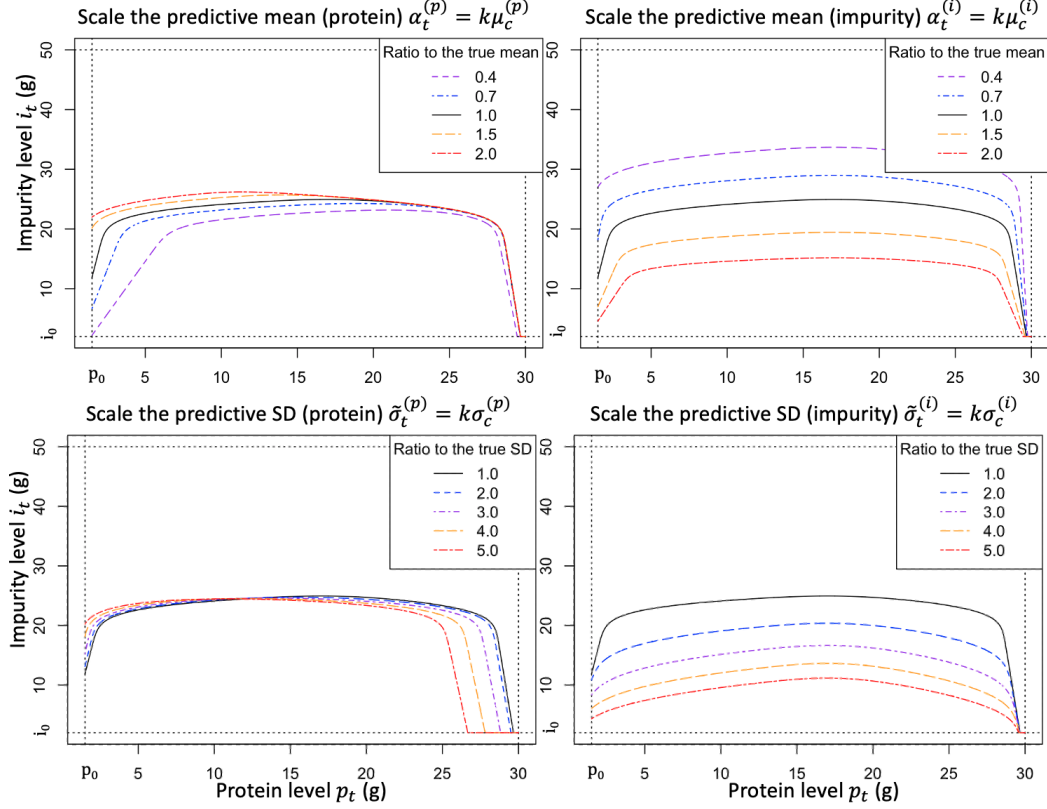


Figure 2: Illustration of how the harvest boundary is affected by the model risk (based on the case study parameters presented in Section 6.1).

shows that the decision boundary moves down. A larger $\tilde{\sigma}_t^{(i)}$ implies higher uncertainty in the impurity growth rate, and we tend to harvest with a smaller amount of impurity to avoid a batch failure.

Theorem 7 formalizes our analysis by establishing the monotonicity of the function $\tilde{h}(\alpha^{(p)}, \tilde{\sigma}^{(p)}, \alpha^{(i)}, \tilde{\sigma}^{(i)}; p, i)$ with respect to the parameters of the predictive growth-rate distributions.

Theorem 7. *The function $\tilde{h}(\alpha^{(p)}, \tilde{\sigma}^{(p)}, \alpha^{(i)}, \tilde{\sigma}^{(i)}; p, i)$ is monotonically:*

- (i) increasing in $\alpha^{(i)}$;
- (ii) decreasing in $\alpha^{(p)}$;
- (iii) increasing in $\tilde{\sigma}^{(i)}$, if $\ln \bar{I} - \ln i > \alpha^{(i)}$ and

$$\tilde{\sigma}^{(i)} \Phi \left(\frac{\ln \bar{I} - \ln i - \alpha^{(i)} - \tilde{\sigma}^{(i)2}}{\tilde{\sigma}^{(i)}} \right) - \phi \left(\frac{\ln \bar{I} - \ln i - \alpha^{(i)} - \tilde{\sigma}^{(i)2}}{\tilde{\sigma}^{(i)}} \right) > 0; \quad (24)$$

- (iv) decreasing in $\tilde{\sigma}^{(p)}$, if and only if

$$\tilde{\sigma}^{(p)} \Phi \left(\frac{\ln \bar{P} - \ln p - \alpha^{(p)} - \tilde{\sigma}^{(p)2}}{\tilde{\sigma}^{(p)}} \right) - \phi \left(\frac{\ln \bar{P} - \ln p - \alpha^{(p)} - \tilde{\sigma}^{(p)2}}{\tilde{\sigma}^{(p)}} \right) > 0. \quad (25)$$

Theorem 7 can be useful in understanding how the model risk would influence the harvest boundary of the myopic policy. For example, if the predictive mean $\alpha^{(i)}$ of the impurity growth rate increases, since $\tilde{h}(\alpha^{(p)}, \tilde{\sigma}^{(p)}, \alpha^{(i)}, \tilde{\sigma}^{(i)}; p, i)$ is increasing by Theorem 7(i), the harvest zone of the physical-state space, denoted by $\{(p, i) : \tilde{h}(\alpha^{(p)}, \tilde{\sigma}^{(p)}, \alpha^{(i)}, \tilde{\sigma}^{(i)}; p, i) \geq 0\}$, will enlarge, while the continue zone $\{(p, i) : \tilde{h}(\alpha^{(p)}, \tilde{\sigma}^{(p)}, \alpha^{(i)}, \tilde{\sigma}^{(i)}; p, i) < 0\}$ will shrink. In other words, the decision maker tends to be more willing to take

the harvest decisions for larger $\alpha^{(i)}$. Similar insights can be derived for all other predictive parameters. Notice that the harvest boundary can behave differently as a function of the predictive standard deviations (i.e., $\tilde{\sigma}^{(i)}$ and $\tilde{\sigma}^{(p)}$) at different parts of the physical-state space, since the monotonicity properties with respect to $\tilde{\sigma}^{(i)}$ and $\tilde{\sigma}^{(p)}$ depend on whether the conditions (24) and (25) hold for particular values of (p, i) in the physical-state space.

Theorem 8. *As the size of the historical data \mathcal{D}_t approaches infinity (i.e., as $J_t \rightarrow \infty$), the myopic policy under model risk becomes equivalent to the myopic policy under perfect information.*

The proof of Theorem 8 follows from the convergence of the parameters of the predictive growth-rate distributions to the corresponding parameters of the true growth-rate distributions. Intuitively, this represents the situation with a sufficient amount of historical data such that the underlying fermentation process is already learned accurately and the use of future data is no longer necessary.

4.4 Solution Approach for the Optimal Policy

We use a Bayesian reinforcement-learning algorithm to solve for the optimal policy that minimizes the objective function in (14). Different from the approximate policy in Section 4.3.2, the optimal policy takes the model risk into account by incorporating the effect of learning from future data on harvesting decisions (in a forward-looking manner). We emphasize that the harvest action at physical states (p_t, i_t) ends the fermentation with a deterministic (known) reward. Therefore, it is only needed to estimate the total reward associated with the continue action and following the optimal policy thereafter, denoted by the corresponding Q-function

$$Q_t(p_t, i_t, \mathcal{I}_t; C) \triangleq -c_u + \gamma \mathbb{E} \left[\max_{a_{t+1} \in \mathcal{A}} Q_{t+1}(p_{t+1}, i_{t+1}, \mathcal{I}_{t+1}; a_{t+1}) \right] \quad (26)$$

for $t = 0, 1, \dots, \bar{T} - 1$. On the other hand, the Q-function associated with the harvest action is denoted with

$$Q_t(p_t, i_t, \mathcal{I}_t; H) \triangleq \begin{cases} r_h(p_t, i_t), & \text{if } i_t \leq \bar{I} \\ -r_f, & \text{if } i_t > \bar{I} \end{cases} \quad (27)$$

for $t = 0, 1, \dots, \bar{T}$. Recall that harvesting is the only feasible action for $i_t > \bar{I}$, $p_t > \bar{P}$, or $t = \bar{T}$, and the harvest action takes the state of the system to a cost-free absorbing state. For a fermentation process that has not yet been harvested at decision epoch t , the value function is given by $V_t(p_t, i_t, \mathcal{I}_t) = \max_{a_t} Q_t(p_t, i_t, \mathcal{I}_t; a_t)$. Theoretically, the optimal policy that maps *any* possible hyper state to an action can be obtained through backward dynamic programming (this is also referred to as offline planning).

However, solving this dynamic program is notoriously difficult and also not necessary in practice, given that the optimal policy is only needed starting from a specific physical state (which evolves by visiting certain states more likely than others) in the real-life execution of the fermentation process. Therefore, we adopt a solution approach that executes the policy in an *online* manner, which means that we focus on estimating the Q-function in (26) at a particular current state $(p_t, i_t, \mathcal{I}_t)$, and decide to continue or harvest the fermentation process by comparing it with the harvesting reward in (27). After the selected action is executed in real life, the next decision epoch starts with a new hyper-state at which the entire procedure is repeated. We present this optimization solution procedure as Reinforcement Learning under Model Risk (RL with MR) in the online appendix B.

5 Implementation at MSD

We quantify the real-world impact obtained at MSD’s daily operations in Section 5.1 and elaborate on the implementation process in Section 5.2.

5.1 Impact

The developed optimization framework has been used in daily operations at MSD since 2019. The project has been implemented at multiple products produced in Boxmeer and directly affected the business metrics: *On average, the project resulted in a 50% increase in batch yield and around 20% reduction in batch variability.* Figure 3 presents the implementation results for one product (i.e., a veterinary vaccine). The x-axis in Figure 3 denotes time, and the y-axis shows the batch yield. The axis values are not disclosed for confidentiality. In this setting, we define the measure “batch yield” as $p - i$, i.e., the total amount of protein minus impurity present in the batch at the time of harvest. The black dots in Figure 3 show the batch yield before implementation, whereas the red ones represent post-implementation. Figure 3 shows that the mean yield has significantly increased and the batch-to-batch variability reduced after implementation.

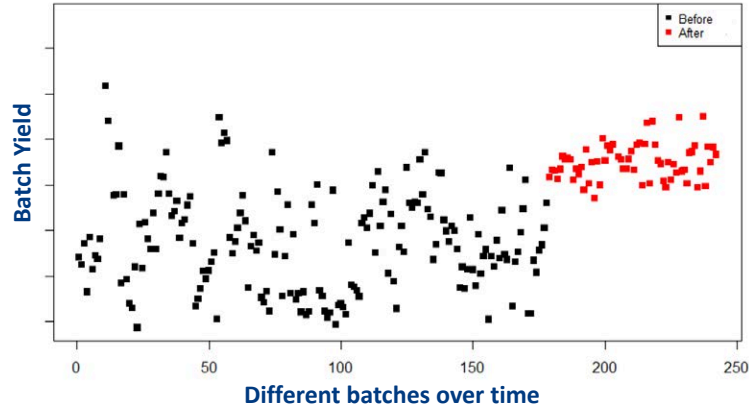


Figure 3: (Color online) Performance of different batches of the same product produced over time: before (black) and after implementation (red) of the optimal harvest policy from the proposed framework.

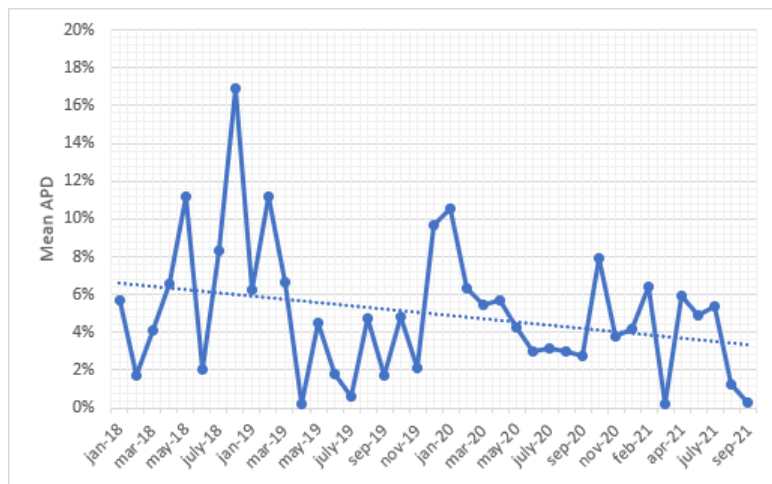


Figure 4: Impact of the learning-by-doing framework across all products considered in the implementation process.

Considering all products in which the implementation was carried out, the project realized up to a 3X increase in batch yield. We believe that both the reduction in variability and increase in mean yield are attributed to the learning-by-doing framework, i.e., we made better use of our limited data, dynamically optimized our operating decisions based on data, and achieved a better standardization of operating policies.

Prior to implementation, harvesting decisions were made based on domain knowledge and experience. For example, it was a common practice to follow simple and intuitive rules of thumb (e.g., so-called *fixed-threshold approach* which harvests the fermentation when the amount of protein and/or impurity exceeds a certain predetermined value). However, these common rules of thumb do not systematically exploit the potential value of limited historical data. The implementation of an OR-based decision-making framework encouraged the best use of limited data and helped bioreactor operators adjust decisions in real-time (see Section 6 for a performance comparison of optimal policies and current practice).

Recall that Figure 3 illustrates the results obtained for one particular product. We now present insights based on all products within the scope of the implementation during 2019-2021. In this setting, our objective is to quantify the impact of the learning-by-doing framework. For this purpose, we first collected information on the “expected” batch yield (ex-ante) and the “actual” batch yield (ex-post) obtained for each batch produced in 2019-2021. The expected batch yield represents our predicted value of the batch yield under a certain harvesting policy used for that batch; whereas the actual batch yield denotes the realized batch yield at the time of harvest. Then, we calculated the *absolute percentage difference (APD)* between expected and actual values for each batch (where the denominator captures the expected yield). We defined the measure APD to understand how our prediction capability changed over time as a result of the learning-by-doing framework. For ease of exposition, Figure 4 plots the mean APD values on a monthly basis

(i.e., the average of APD values across all batches produced in a certain month). In this figure, the implementation started around January 2019. We observe from Figure 4 that there is a clear downward trend over time, which indicates that our prediction capability has significantly improved as a result of the implementation of the learning-by-doing framework.

In this section, we quantified the impact in terms of batch yield (not cost) because we found that this approach was more intuitive and easier to explain with existing data. In particular, we had batch data associated with (at least) one year prior to and after the implementation process. In addition, the project realized several other benefits, including higher flexibility (i.e., we freed up bioreactor capacity by increasing batch yield without additional resources) and the adoption of an OR-driven mindset [18]. The concept of decision-making under model risk was new but the practitioners embraced it.

5.2 Overview of the Implementation Process

The team and project timeline. The research project has been conducted in close collaboration with a university team and a team of practitioners from MSD in the Netherlands. The university team brought in expertise on operations research, whereas the MSD team provided expertise in life sciences. A multi-disciplinary team from MSD (e.g., bioreactor operators, chemical and biological engineers, and middle/upper management) contributed to the project.

The project went through three major phases: model development, validation, and implementation. The project started in early 2018 with data collection and the development of the optimization framework. Prior to the implementation, the optimization model and the corresponding policies were validated based on (i) discussions with practitioners, and (ii) small-scale test runs. The discussions with practitioners mostly focused on computational experiments and sensitivity analysis as described in Section 6. In these discussions, we elaborated on the underlying intuition of optimal policies and trends (i.e., how optimal policies change in response to the information state, costs, inherent uncertainty, etc.). The control-limit structure of optimal policies facilitated these discussions, as these policies were “explainable” and their intuition aligned with the current practice. Following these discussions, small-scale test runs were performed during the Christmas holidays (i.e., when there was a lower workload in the production facility). The results obtained from both computational experiments and real-world test runs established the required foundation and trust to proceed with industry-scale implementation in 2019.

Scope and aspects related to data. The implementation focused on industry-scale production orders with limited historical process data. As a common characteristic, these products were typically high-mix, low-volume batches produced only a few times a year. Moreover, we encountered challenges with limited data when new equipment or raw materials were used.

Our data consisted of two main data sets for each batch: (i) fermentation information (e.g., the initial amount of protein and impurity, information on growth rates, etc.), and (ii) physicochemical parameters monitored during fermentation (e.g., temperature, pH, oxygen levels, etc.). Using standard bioreactor models, the physicochemical parameters were used to determine the duration of the exponential growth phase [1]. To summarize, we had the following data for each batch: the amount of protein and impurity, the duration of the exponential growth phase, and the realized protein and impurity growth rates over time.

Available data typically involved around 10 batches at the beginning of the decision-making process. However, some products had as little as one or two data sets (i.e., fermentation data on two batches). In some cases, we had *no* data to build the prior distribution because of a change in raw materials or equipment. All batches exhibited inherent stochasticity and model risk.

The decision-support tool. To facilitate the implementation process, the team developed a user-friendly decision-support tool for daily use. This decision-support tool reports a look-up table for optimal decisions (harvest or continue) as a function of the system’s state. The user interface of the tool is developed in MS Excel. This user interface is linked to an optimization module developed in Python. The implementation process was facilitated by Master’s students who were actively engaged in the development of the decision-support tool. Several test runs were performed prior to the real-world implementation. In particular, the user interface was modified and enhanced based on the feedback of the end users. The student assistants also prepared a short documentation and a video to support the daily use of the tool (for internal use only). The end-users at MSD found the decision-support tool user-friendly and were very satisfied with the project outcomes.

Implementation challenges. The major challenge in this project was related to data collection. In some cases, data was not available in a digital format and needed to be extracted from the memory of machines. In other cases, historical data was stored in handwritten notebooks. We also encountered a few special cases when we did not have any information to build a prior distribution (e.g., no historical data and no information in the literature). In such cases, we referred to

similar products (e.g., batches using a similar seed culture or sharing some biological characteristics) and also relied on the domain knowledge of bioreactor operators.

One of the strengths of the project is its multi-disciplinary approach which combines life sciences and operations research. However, multi-disciplinary projects have their own challenges. For example, the concept of Markov decision processes may be difficult for scientists who have no background in operations research. To assist the scientists and facilitate real-world implementation, decision support tools were developed as described above. Similarly, developing a thorough understanding of the fermentation processes was challenging for the university team (with no background in biological and chemical engineering). Therefore, both the university and MSD teams had regular meetings to learn from each other and co-design the model.

It is also important to facilitate the knowledge transfer from Boxmeer to other facilities. When the scope of the implementation expands to other facilities in the future, it can be challenging to identify the right products (and facilities) that would obtain the highest benefit from the optimization framework. For this purpose, MSD developed a dashboard that collects information from all batches produced globally. This dashboard reports the APD values of selected batches (as illustrated in Figure 4) from their global network, thereby identifying opportunities for future implementations.

6 Numerical Analysis

To have a systematic assessment of the proposed framework, we present a case study motivated by the implementation at MSD Animal Health. This case study is generated based on a veterinary drug produced using a bacterial cell culture. To protect the confidentiality, we disguised MSD’s original data and used representative values. We first present the problem setting (Section 6.1), and then analyze the impact of model risk on the value function (Section 6.2) and optimal policies (Section 6.3).

6.1 Experiment Setting and Analysis Overview

The starting protein and impurity for each batch are $p_0 = 1.5, i_0 = 2.0$ grams. The harvesting limit on protein is $\bar{P} = 30$ grams, the batch failure impurity threshold is $\bar{I} = 50$ grams, and the maximum time for a batch to reach the stationary phase is $\bar{T} = 8$ hours. To represent common industry practice, we considered the following cost and reward structures: harvest reward $r_h(p, i) = 10p - i$, the one-step operation cost $c_u = 2$, and the batch failure penalty $r_f = 880$ with no discounting. These cost structures are identified based on input received from our industry partners (see Appendix C for a sensitivity analysis on costs). Based on historical production data, we consider the following protein and impurity growth parameters $\mu_c^{(p)} = 0.488, \sigma_c^{(p)} = 0.144, \mu_c^{(i)} = 0.488, \sigma_c^{(i)} = 0.144$ as underlying truth. The realized values of growth rates ranged between 0.2 and 0.6 in our production data. The protein and impurity generation model in (1) was validated by using real-world fermentation data with a sample size of 24. We conducted the Kolmogorov–Smirnov normality test and obtained p-value 0.6416, which supports the normality assumption on the growth rate. We also conducted the ANOVA test on the constant mean assumption and the Levene’s test on the constant variance assumption over time with p-values 0.251 and 0.5035, respectively.

Analysis overview. We use the case study to generate insights for practitioners. For this purpose, we consider various practically-relevant harvesting strategies and compare their performance:⁴

- (1) **Perfect information MDP (PI-MDP).** To establish a benchmark, we consider the setting where the decision-maker has perfect information on the underlying true model characterizing fermentation dynamics. This setting represents the best possible performance that can be achieved. In this setting, the MDP model is solved as described in Section 4.4 by considering that the true parameters $\mu_c^{(p)}, \mu_c^{(i)}, \sigma_c^{(p)}$ and $\sigma_c^{(i)}$ are known.
- (2) **Current practice (CP).** In common practice, fermentation is typically harvested based on a “fixed-threshold” approach, i.e., harvest when the impurity amount i_t exceeds 60% of the maximum amount permitted \bar{I} (i.e., harvest when $i_t \geq 0.6\bar{I}$) or when the protein amount p_t reaches the limit \bar{P} or when the fermentation process transitions to the stationary phase. These fixed thresholds represent simple rules of thumb and are typically prespecified based on experience.
- (3) **Reinforcement learning ignoring model risk (RL ignoring MR).** This strategy represents the case when the decision-maker considers the inherent stochasticity of fermentation processes but ignores the model risk. To estimate state transitions, the decision-maker derives the point estimates from limited historical data (by using maximum likelihood estimation), and uses these point estimates as the true parameters $\mu_c^{(p)}, \mu_c^{(i)}, \sigma_c^{(p)}$ and $\sigma_c^{(i)}$ of the MDP model. Then, the MDP model is solved to guide harvesting decisions. Note that, for

normally distributed data, maximum likelihood estimation is equivalent to using the sample mean and the unadjusted sample variance, which is a convenient way of obtaining point estimates in practice.

- (4) **Myopic policy.** The decision-maker considers both the inherent stochasticity and the model risk. However, the harvesting decision is made by only comparing the harvesting reward at the current decision epoch with the expected reward of harvesting in the next decision epoch.
- (5) **Reinforcement learning with model risk (RL with MR).** The decision-maker considers both the inherent stochasticity of fermentation processes and the model risk caused by limited historical data. Optimal harvesting policy is obtained as described in Section B.

Performance metrics. We adopt the following approach to evaluate the performance of each strategy. For any policy π obtained by the strategies listed above, we evaluate the policy π through the expected total reward achieved for the underlying *true* process, as defined in Section 3.1,

$$\rho^c(\pi) = \mathbb{E}_{\tau^c} \left[\sum_{t=0}^T R(\mathcal{S}_t, a_t) \middle| \mathcal{S}_0, \pi \right],$$

where the expectation is taken with respect to the stochastic trajectory $\tau^c \equiv (\mathcal{S}_0, a_0, \mathcal{S}_1, a_1, \dots, \mathcal{S}_{T-1}, a_{T-1}, \mathcal{S}_T)$ with stopping time T , following the underlying physical state transition $\Pr(\mathcal{S}_{t+1} | \mathcal{S}_t, a_t; \theta^c)$ and decision policy $a_t = \pi_t(\mathcal{S}_t)$. Based on the given policy π , we can generate trajectory realizations $\tau_n^c \equiv (\mathcal{S}_0^{(n)}, a_0^{(n)}, \mathcal{S}_1^{(n)}, a_1^{(n)}, \dots, \mathcal{S}_{T_n-1}^{(n)}, a_{T_n-1}^{(n)}, \mathcal{S}_{T_n}^{(n)})$ with $n = 1, 2, \dots, N$ from the underlying model, and the expected total reward can be estimated by,

$$\widehat{\rho}^c(\pi) = \frac{1}{N} \sum_{n=1}^N \sum_{t=0}^{T_n} R(\mathcal{S}_t^{(n)}, \pi_t(\mathcal{S}_t^{(n)})),$$

where T_n denotes the stopping time in the trajectory realization n . Further, to assess the process stability, we measure the batch-to-batch variations under a given policy through the standard deviation (SD) of the total reward,

$$\text{SD}^c(\pi) = \text{SD}_{\tau^c} \left[\sum_{t=0}^T R(\mathcal{S}_t, a_t) \middle| \mathcal{S}_0, \pi \right],$$

which is estimated by sample SD from N replications of simulation experiments, i.e.,

$$\widehat{\text{SD}}^c(\pi) = \sqrt{\frac{1}{N-1} \sum_{n=1}^N \left[\sum_{t=0}^{T_n} R(\mathcal{S}_t^{(n)}, \pi_t(\mathcal{S}_t^{(n)})) - \widehat{\rho}^c(\pi) \right]^2}.$$

For each strategy, we run $N = 100$ replications to compare the mean and the standard deviation of the expected total reward.

6.2 Performance Comparison

We now evaluate the performance of various practically-relevant strategies. In particular, we focus on the performance metrics, such as, the expected total reward $\widehat{\rho}^c(\pi)$, and the standard deviation $\widehat{\text{SD}}^c(\pi)$ under different sizes of historical data (i.e., $J_0 = 3, 10, 20$) and harvest policy π , as described in Section 6.1. Table 1 reports the performance of the considered strategies at the starting state $p_0 = 1.5$ and $i_0 = 2$. Recall that harvesting policies π under both PI-MDP and CP are independent of data size J_0 . The column labeled “% of PI-MDP” in Table 1 uses the perfect information setting (PI-MDP) as a benchmark to assess the performance of the considered strategies.

We observe from Tables 1 that the strategy RL-with-MR provides substantial benefits (in terms of the performance metrics $\widehat{\rho}^c$ and $\widehat{\text{SD}}^c$) compared to all other strategies. In addition, we notice that the average reward of all strategies increases while variability decreases as the number of historical data increases. In this specific case study, we also observe that CP does not perform well compared to PI-MDP. For practitioners, these results emphasize the business value (and the potential impact) of accounting for the model risk in harvesting decisions. In addition, we observe that the strategy RL-with-MR results in a lower standard deviation $\widehat{\text{SD}}^c$ compared to current practice CP, even when the amount of historical data is small ($J_0 = 3$). This observation is interesting because the objective of the optimization model is to maximize the expected total reward (not to minimize variability). Recall that we obtained a similar result from the implementation at MSD (i.e., variability reduced after the implementation, as discussed in Section 5.1). Lastly, we refer the reader to Appendix D for additional experiments on costs and rewards. Our analysis shows that the potential impact of model risk is more prominent when the unit revenue and/or failure cost are higher.

Table 1: The mean and standard deviation of the total reward achieved by different strategies.

	$\widehat{\rho}^c(\pi)$	% of PI-MDP	$\widehat{SD}^c(\pi)$	% of PI-MDP
PI-MDP	177.23	100.0%	125.86	100.0%
CP	97.40	55.0%	318.19	252.8%
$J_0 = 3$				
RL ignoring MR	132.00	74.5%	221.68	176.1%
Myopic Policy	151.22	85.3%	166.14	132.0%
RL with MR	159.16	89.8%	128.76	102.3%
$J_0 = 10$				
RL ignoring MR	143.47	81.0%	196.39	156.0%
Myopic Policy	168.21	94.9%	166.31	132.1%
RL with MR	171.63	96.8%	126.68	100.7%
$J_0 = 20$				
RL ignoring MR	153.98	86.9%	165.79	131.7%
Myopic Policy	175.34	98.9%	127.74	101.5%
RL with MR	176.30	99.5%	126.26	100.3%

6.3 Impact of Limited Historical Data on Harvesting Decisions

We illustrate the impact of model risk on harvesting decisions. For this purpose, our analysis considers two different sizes of historical data, $J_0 = 3, 20$. We use the strategy PI-MDP as a benchmark to represent the case with perfect information. Figure 5 represents the optimal harvesting policy under the strategy PI-MDP (black line) for the physical states $p_t \in [1.5, 30]$ and $i_t \in [2.0, 50]$. Moreover, Figure 5 shows the fixed-threshold based CP (purple dashed line), and the mean harvesting threshold under the strategy RL with MR (red line) with its corresponding 95% confidence band (blue dashed line).

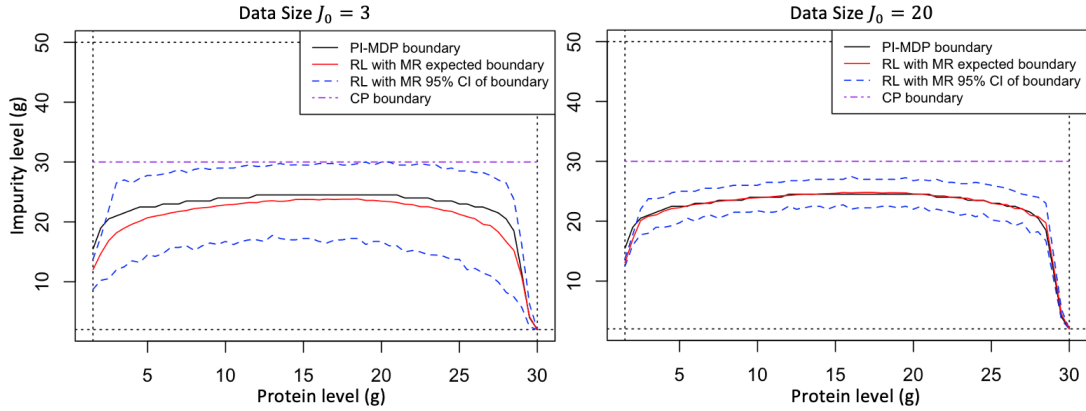


Figure 5: Optimal harvesting thresholds (above curve denotes harvest region) with $J_0 \in \{3, 20\}$ under the strategies PI-MDP, RL with MR, and CP.

Figure 5 shows how the optimal harvesting threshold moves as the number of historical data J_0 increases from 3 to 20. As the number of historical data increases, we see that the 95% confidence band of the harvest boundary shrinks and becomes closer to the one under the optimal harvest policy with perfect information.

7 Conclusions

Limitations in historical process data (model risk) are often perceived as a common industry challenge in biomanufacturing. Yet the implications of model risk on optimal costs and harvesting decisions have not been fully understood. Our work provides one of the first attempts at modeling and optimization of fermentation systems under model risk (caused by limited historical data) and inherent stochasticity (caused by the uncertain nature of biological systems).

We developed an MDP model to guide fermentation harvesting decisions under a learning-by-doing framework. In particular, we used a Bayesian approach where the decision-maker sequentially collects real-world data on fermentation

dynamics and updates the beliefs on state transitions. As a salient feature, the MDP model combines the knowledge from life sciences and operations research, and is equipped to capture the complex dynamics of fermentation processes under limited data. We studied the structural properties of the value function and optimal policies, and characterized the impact of model risk on biomanufacturing harvesting decisions. To illustrate the use of the optimization model, we present a case study from MSD Animal Health. The implementation at MSD has shown that linking operations research with life sciences drives substantial productivity improvements. We hope that our results will inspire the global biomanufacturing industry and stimulate new research at the intersection of operations research and life sciences.

The developed optimization framework is generic and addresses common industry challenges. Therefore, it can be easily implemented at other production lines and facilities. For example, MSD is currently in the process of implementing this decision-making framework on other production lines in the Boxmeer facility. The long-term vision is to encourage the worldwide use of such optimization models at other facilities. As another future work, it will be interesting to explore the potential applications in other industries. For example, the food industry encounters similar challenges related to fermentation trade-offs and process uncertainties, and may benefit from the developed optimization model. Moreover, the scope of this paper can be expanded to incorporate production scheduling aspects.

Endnotes

1. The company is known as “Merck” in the United States and Canada, and “MSD” elsewhere.
2. Our Bayesian learning framework could be generalized to also learn the correlation between the growth rates of the protein and impurity. For this purpose, the conjugacy of the normal-inverse-Wishart distribution can be used to efficiently update the parameters of the posterior distribution of the growth-rate means and covariance. Our solution approach can still be used for the extended MDP model that would have the same physical states but a larger knowledge-state space to include the posterior parameters of the normal-inverse-Wishart distribution.
3. A t-distribution with 30 or more degrees of freedom is known to be well approximated with a normal distribution. We numerically investigated the effect of normal approximation for smaller data sizes and showed that the impact of this approximation on the performance of the policies introduced in this paper is negligible.
4. We defined these strategies based on the feedback we received from practitioners.
5. Numerical results for the strategy “RL with MR” are generated by the Bayesian sparse sampling described in Section B. The analysis starts with the non-informative prior that $\alpha_0^{(p)} = \nu_0^{(p)} = \lambda_0^{(p)} = \beta_0^{(p)} = \alpha_0^{(i)} = \nu_0^{(i)} = \lambda_0^{(i)} = \beta_0^{(i)} = 0$. For each case (i.e., $J_0 = 3, 10, 20$), we performed 100 macro-replications to assess the performance of the proposed reinforcement learning framework. In each macro-replication, we generated J_0 number of process data \mathcal{D}_0 from the underlying true distribution of the protein and impurity growth rates, and then updated the knowledge states. After that, with the updated knowledge state, we estimated the Q-function for the continue action over the physical state space $(p_t, i_t) \in [1.5, 30] \times [2.0, 50]$ at time t , based on Bayesian sparse sampling in Algorithm 2. We obtained the *mean* decision boundary and the corresponding 95% confidence band based on 100 macro-replications.

Acknowledgment

This research was funded by the Dutch Science Foundation (NWO-VENI Scheme). We would like to thank the Master’s students Thijs Diessen and Len Hermsen for their assistance during the project. We also thank Oscar Repping from MSD Animal Health for his continuous support during the collaboration.

References

- [1] Pauline M. Doran. *Bioprocess Engineering Principles*. Academic Press, 2nd edition, 2013.
- [2] T. Martagan, Adan I., M. Baaijens, C. Dirckx, O. Repping, B. Ravenstein, and P Yegneswaran. Merck animal health uses operations research methods to transform biomanufacturing productivity for lifesaving medicines. *Franz Edelman Special Issue of INFORMS Journal on Applied Analytics.*, 2022. Forthcoming.
- [3] IFORS News. Innovative applications of operations research: Reducing costs and lead times in biomanufacturing, 2020.
- [4] IMPACT. Operational research improves biomanufacturing efficiency, 2020.

- [5] European Commission. The research project was one of the three finalists of 2020 MSCA2020.HR Awards. The competition was among all disciplines to acknowledge the most influential projects under Horizon 2020 program of European Commission, 2020.
- [6] INFORMS. The research project was awarded with second prize in INFORMS Innovative Applications in Analytics Award., 2021.
- [7] Genetic Engineering & Biotechnology News. Avoiding errors by thoroughly understanding bioprocess mechanisms, 2022.
- [8] MSD. Operations research improves biomanufacturing efficiency, 2021. Date accessed June 25, 2022.
- [9] INFORMS. 2022 Franz Edelman Competition: Merck Animal Health, 2022.
- [10] Philip Kaminsky and Yang Wang. Analytical models for biopharmaceutical operations and supply chain management: a survey of research literature. *Pharmaceutical Bioprocessing*, 3(1):61–73, 2015.
- [11] B. McNeil and L. M. Harvey. *Practical Fermentation Technology*. 2008. John Wiley & Sons, New York.
- [12] Meilana Dharma Putra and Ahmed E. Abasaed. A more generalized kinetic model for binary substrates fermentations. *Process Biochemistry*, 75:31 – 38, 2018.
- [13] Liang Chang, Xinggao Liu, and Michael A Henson. Nonlinear model predictive control of fed-batch fermentations using dynamic flux balance models. *Journal of Process Control*, 42:137–149, 2016.
- [14] C. V. Peroni, N. S. Kaisare, and J. H. Lee. Optimal control of fed-batch bioreactor using simulation based approximate dynamic programming. *IEEE Transactions*, 13:786–790, 2005.
- [15] Zizhuo Xing, Nikki Bishop, Kirk Leister, and Zheng Jian Li. Modeling kinetics of a large-scale fed-batch cho cell culture by markov chain monte carlo method. *Biotechnology progress*, 26(1):208–219, 2010.
- [16] Tugce Martagan, Ananth Krishnamurthy, and Christos T Maravelias. Optimal condition-based harvesting policies for biomanufacturing operations with failure risks. *IIE Transactions*, 48(5):440–461, 2016.
- [17] T.G Martagan, A. Krishnamurthy, and P. Leland. Managing trade-offs in protein manufacturing: How much to waste? *Manufacturing & Service Operations Management*, 22(2):223–428, 2020.
- [18] Tugce Martagan, Yesim Koca, Ivo Adan, Bram van Ravenstein, Marc Baaijens, and Oscar Repping. Operations research improves biomanufacturing efficiency at MSD animal health. *INFORMS Journal on Applied Analytics*, 51(2):150–163, 2021.
- [19] Neythen J Treloar, Alex JH Fedorec, Brian Ingalls, and Chris P Barnes. Deep reinforcement learning for the control of microbial co-cultures in bioreactors. *PLOS Computational Biology*, 16(4):e1007783, 2020.
- [20] Saxena Nikita, Anamika Tiwari, Deepak Sonawat, Hariprasad Kodamana, and Anurag S. Rathore. Reinforcement learning based optimization of process chromatography for continuous processing of biopharmaceuticals. *Chemical Engineering Science*, 230:116171, 2021.
- [21] Hua Zheng, Wei Xie, and M. Ben Feng. Green simulation assisted reinforcement learning with model risk for biomanufacturing learning and control. In *Proceedings of the 2020 Winter Simulation Conference*, page 337–348, 2020.
- [22] Mohammad Ghavamzadeh, Shie Mannor, Joelle Pineau, and Aviv Tamar. Bayesian reinforcement learning: A survey. *arXiv preprint arXiv:1609.04436*, 2016.
- [23] Michael O Duff. *Optimal learning: Computational procedures for Bayes-adaptive Markov decision processes*. PhD thesis, University of Massachusetts Amherst, 2002.
- [24] Pascal Poupart, Nikos Vlassis, Jesse Hoey, and Kevin Regan. An analytic solution to discrete bayesian reinforcement learning. In *Proceedings of the 23rd international conference on Machine learning*, pages 697–704, 2006.
- [25] Stephane Ross, Brahim Chaib-draa, and Joelle Pineau. Bayesian reinforcement learning in continuous pomdps with application to robot navigation. In *2008 IEEE International Conference on Robotics and Automation*, pages 2845–2851. IEEE, 2008.
- [26] Ian Osband, Daniel Russo, and Benjamin Van Roy. (more) efficient reinforcement learning via posterior sampling. In *Advances in Neural Information Processing Systems*, pages 3003–3011, 2013.
- [27] Raphael Fonteneau, Lucian Buşoniu, and Rémi Munos. Optimistic planning for belief-augmented markov decision processes. In *2013 IEEE Symposium on Adaptive Dynamic Programming and Reinforcement Learning (ADPRL)*, pages 77–84. IEEE, 2013.

- [28] J Zico Kolter and Andrew Y Ng. Near-bayesian exploration in polynomial time. In *Proceedings of the 26th annual international conference on machine learning*, pages 513–520, 2009.
- [29] John Asmuth and Michael L Littman. Approaching bayes-optimality using monte-carlo tree search. In *Proc. 21st Int. Conf. Automat. Plan. Sched., Freiburg, Germany*, 2011.
- [30] John Asmuth, Lihong Li, Michael L Littman, Ali Nouri, and David Wingate. A bayesian sampling approach to exploration in reinforcement learning. *arXiv preprint arXiv:1205.2664*, 2012.
- [31] Neil Templeton, Jason Dean, Pranhitha Reddy, and Jamey D Young. Peak antibody production is associated with increased oxidative metabolism in an industrially relevant fed-batch cho cell culture. *Biotechnology and bioengineering*, 110(7):2013–2024, 2013.
- [32] Daniel C Odenwelder, Xiaoming Lu, and Sarah W Harcum. Induced pluripotent stem cells can utilize lactate as a metabolic substrate to support proliferation. *Biotechnology Progress*, 37(2):e3090, 2021.
- [33] Y-S Tsao, AG Cardoso, RGG Condon, M Voloch, P Lio, JC Lagos, BG Kearns, and Z Liu. Monitoring chinese hamster ovary cell culture by the analysis of glucose and lactate metabolism. *Journal of biotechnology*, 118(3):316–327, 2005.
- [34] Patrick Wechselberger, Patrick Sagmeister, and Christoph Herwig. Model-based analysis on the extractability of information from data in dynamic fed-batch experiments. *Biotechnology progress*, 29(1):285–296, 2013.
- [35] Linas Mockus, John J Peterson, Jose Miguel Lainez, and Gintaras V Reklaitis. Batch-to-batch variation: a key component for modeling chemical manufacturing processes. *Organic Process Research & Development*, 19(8):908–914, 2015.
- [36] Johannes Möller, Tanja Hernández Rodríguez, Jan Müller, Lukas Arndt, Kim B Kuchemüller, Björn Frahm, Regine Eibl, Dieter Eibl, and Ralf Pörtner. Model uncertainty-based evaluation of process strategies during scale-up of biopharmaceutical processes. *Computers & Chemical Engineering*, 134:106693, 2020.
- [37] A. Gelman, J. B. Carlin, H. S. Stern, and D. B. Rubin. *Bayesian Data Analysis*. Taylor and Francis Group, LLC, New York, 2nd edition, 2004.
- [38] Warren B Powell and Ilya O Ryzhov. *Optimal learning*, volume 841. John Wiley & Sons, 2012.
- [39] Kevin P Murphy. Conjugate bayesian analysis of the gaussian distribution. Technical report, University of British Columbia, 2007.
- [40] M Franzeb, E Muller, and J Vajda. Cost estimation for protein a chromatography: an in silico approach to mab purification strategy. *BioProcess International*, 12(9):44–52, 2014.
- [41] Valdemir M Cardoso, Gilson Campani, Maurício P Santos, Gabriel G Silva, Manuella C Pires, Viviane M Gonçalves, Roberto de C Giordano, Cíntia R Sargo, Antônio CL Horta, and Teresa C Zangirolami. Cost analysis based on bioreactor cultivation conditions: Production of a soluble recombinant protein using escherichia coli b121 (de3). *Biotechnology reports*, 26:e00441, 2020.
- [42] Thomas S. Ferguson. Optimal stopping and applications, 2000. [Online; accessed 10-Apr-2022].
- [43] Michael Kearns, Yishay Mansour, and Andrew Y Ng. A sparse sampling algorithm for near-optimal planning in large markov decision processes. *Machine learning*, 49(2-3):193–208, 2002.
- [44] Tao Wang, Daniel Lizotte, Michael Bowling, and Dale Schuurmans. Bayesian sparse sampling for on-line reward optimization. In *Proceedings of the 22nd international conference on Machine learning*, pages 956–963, 2005.
- [45] Stéphane Ross and Joelle Pineau. Model-based bayesian reinforcement learning in large structured domains. In *Proceedings of the Twenty-Fourth Conference on Uncertainty in Artificial Intelligence*, page 476–483, Arlington, Virginia, USA, 2008. AUAI Press.

A Model Extension with Multiple Batches and Fermentation Campaigns

We extend the single-batch harvesting model introduced in Section 3 to a situation where multiple batches (of the same product) are produced in a fixed time horizon. We refer to this fixed amount of time as the *campaign length*, and assume that it is equal to L periods. There must be a setup between two subsequent batches (due to, for example, cleaning and sterilization of the bioreactor, and changing the catalysts and reagents). The setup time S is a discrete random variable with sample space $\{1, 2, \dots, \mathcal{S}\}$, and p_s denotes the probability that $S = s$. The setup cost c_s is charged per each time period the setup continues. Once a batch is harvested, the bioreactor is cleaned and sterilized (setup) and a new batch is started. The problem is to decide when to end an ongoing batch (and hence start a new batch) given the time left in the campaign length. The objective is to find a harvesting policy that maximizes the expected total discounted reward obtained in the finite time horizon equal to the campaign length. In this section, we will focus on the differences between the extended model for multiple batches and the original model for a single batch, and emphasize the additional elements needed in the MDP model to capture the dynamics of this new problem.

Decision Epochs. The decision epochs are now given by $\mathcal{T} = \{t : 0, 1, \dots, L\}$, representing the equidistant time points at which the protein and impurity amounts are measured during the production campaign. Once the end of the time horizon is reached, the ongoing batch must be terminated regardless of the status of the process.

Physical States. At decision epoch t , in addition to the protein level p_t and the impurity level i_t of the current fermentation process, there are two new physical states δ_t and τ_t . The first new state variable δ_t is a binary variable that indicates whether a fermentation activity or a setup activity is undergoing at decision epoch t , i.e., $\delta_t = 1$ indicates there is an ongoing setup process at the decision epoch t (it is known the setup process must continue at least one more time period), while $\delta_t = 0$ indicates that there is no ongoing setup process (setup may have just been completed or there is an ongoing fermentation process). The second new state variable $\tau_t \in \{0, 1, 2, \dots, \max\{\mathcal{S}, \bar{T}\}\}$ is a time counter, tracking the duration of the ongoing activity (a setup or a fermentation process). For example, the state pair $(\delta_t, \tau_t) = (0, 3)$ means that, at the current decision epoch t , there is a fermentation process that started 3 periods ago; and $(\delta_t, \tau_t) = (1, 2)$ means that at the current decision epoch t , there is a setup process that started 2 periods ago and will continue at least one more period. Hence, the physical states of the MDP model are extended to $\mathcal{S}_t = (p_t, i_t, \delta_t, \tau_t)$.

Action Space. Recall that there are situations where the harvest action is the only possible action in the original model. These remain the same in the extended model. At a decision epoch before the end of the time horizon (i.e., $t < L$), the action space depends on whether the ongoing activity is a fermentation or a setup. For $\delta_t = 1$ (i.e., the ongoing activity is a fermentation), the action space is $\{H\}$ if $p_t = \bar{P}$ or $i_t = \bar{I}$ or $\tau_t = \bar{T}$, and the action space is given by $\{C, H\}$, otherwise. For $\delta_t = 0$ (i.e., the ongoing activity is a setup), the action space is $\{C\}$, meaning that the setup process must continue at least one more period. Notice that the feasible actions depend on the physical states p_t, i_t and δ_t at decision epoch t ; for brevity, we denote the corresponding action space with $\mathcal{A}(p_t, i_t, \delta_t)$. Finally, when the end of the production campaign is reached (i.e., $t = L$), the process must be terminated regardless of the status of the process. If there is an ongoing batch at $t = L$, it must be harvested.

Knowledge State. The parameters of the posterior distribution of θ denote the knowledge state at decision epoch t , $\mathcal{I}_t = \{\alpha_t^{(p)}, \nu_t^{(p)}, \lambda_t^{(p)}, \beta_t^{(p)}, \alpha_t^{(i)}, \nu_t^{(i)}, \lambda_t^{(i)}, \beta_t^{(i)}\}$, as in the original model.

Hyper States & Hyper State Transition: The hyper states $\mathcal{H}_t \equiv (\mathcal{S}_t, \mathcal{I}_t)$ include both physical state $\mathcal{S}_t = (p_t, i_t, \delta_t, \tau_t)$ and knowledge state \mathcal{I}_t . We distinguish two possible types of state transitions after taking an action at decision epochs $t \in \{0, 1, \dots, L-1\}$, depending on whether a setup process is ongoing or not at decision epoch t :

Case I ($\delta_t = 0$): This is the case when no setup is ongoing at decision epoch t (i.e., there is a fermentation process just started or there is one already started earlier). Suppose that continue action is taken at decision epoch t , denoted by $a_t = C$. Then, physical states are updated as $p_{t+1} = p_t e^{\tilde{\phi}_t}$ and $i_{t+1} = p_t e^{\tilde{\psi}_t}$, where $\tilde{\phi}_t$ and $\tilde{\psi}_t$ are the realizations of the random variables $\tilde{\Phi}_t$ and $\tilde{\Psi}_t$ with distributions specified in (9) and (10), respectively. Furthermore, it follows that $\delta_{t+1} = 0$ and $\tau_{t+1} = \tau_t + 1$. Similar to the original model, the knowledge state \mathcal{I}_{t+1} follows from the Bayesian updates specified in (5) and (7) given the realization of the physical states (p_{t+1}, i_{t+1}) (or equivalently the growth rate samples $(\phi_t, \psi_t) = (\ln(p_{t+1}/p_t), \ln(i_{t+1}/i_t))$).

On the other hand, suppose that harvest action is taken at decision epoch t , denoted by $a_t = H$. Different from the original model, the harvest action triggers the setup activity of the next batch. At the next decision epoch, this information is captured with the updated state variables $\delta_{t+1} = 1$ and $\tau_{t+1} = 1$. There is no protein and impurity amount during a setup process, and this is denoted by $p_{t+1} = \emptyset$ and $i_{t+1} = \emptyset$. Because no new information is collected on the growth rates, the knowledge state remains the same, i.e., $\mathcal{I}_{t+1} = \mathcal{I}_t$.

Case II ($\delta_t = 1$): This means there is a setup process at decision epoch t and it will take at least one more period. In this case, the setup process must continue one more period, i.e., $a_t = C$. There are two possibilities:

(i) The setup process ends by the next decision epoch. The probability of this event is given by $\mathbb{P}(S = \tau_t + 1 | S > \tau_t) = p_{\tau_t+1} / \sum_{i=\tau_t+1}^S p_i$. With this probability, the updated state variables becomes $\delta_{t+1} = 0$ and $\tau_{t+1} = 0$ at the next decision epoch. At that moment (as soon as the setup ends), the next batch starts with the pre-specified initial protein and impurity amounts, denoted by $p_{t+1} = p_0$ and $i_{t+1} = i_0$. The knowledge state remains the same as there is no new information collected on the growth rates, i.e., $\mathcal{I}_{t+1} = \mathcal{I}_t$.

(ii) The setup process does not end by the next decision epoch (i.e., it must continue at least one more time unit after the next decision epoch). The probability of this event is given by $\mathbb{P}(S > \tau_t + 1 | S > \tau_t) = (1 - \sum_{i=1}^{\tau_t+1} p_i) / \sum_{i=\tau_t+1}^S p_i$. In this case, the state variables are updated as $\delta_{t+1} = 1$ and $\tau_{t+1} = \tau_t + 1$. Since there is no protein and impurity amount during a setup process, and no new information collected on the growth rates, the states remain the same: $p_{t+1} = \emptyset$, $i_{t+1} = \emptyset$, and $\mathcal{I}_{t+1} = \mathcal{I}_t$.

Reward: The only difference from the original model with a single batch is the presence of setup cost that is charged every time period the setup process continues. Accordingly, the reward function at decision epoch t is given by

$$R(p_t, i_t, \delta_t; a_t) = \begin{cases} -c_u, & \delta_t = 0, a_t = C \\ -c_s, & \delta_t = 1, a_t = C \\ -r_f, & i_t = \bar{I}, a_t = H \\ r_h(p_t, i_t), & i_t < \bar{I}, a_t = H. \end{cases}$$

Policy: We now let π denote a nonstationary policy $\{\pi_t(\cdot); t = 0, 1, \dots, L\}$, which is a mapping from any hyper state \mathcal{H}_t to an action a_t , i.e., $a_t = \pi_t(\mathcal{H}_t)$. Given the policy π , the expected total discounted reward becomes

$$\rho(\pi) = \mathbb{E} \left[\sum_{t=0}^L \gamma^t R(p_t, i_t, \delta_t; \pi_t(\mathcal{H}_t)) \middle| \mathcal{H}_0, \pi \right]. \quad (28)$$

The objective is to find the optimal policy π^* that maximizes the expected total discounted reward, i.e., $\pi^* = \arg \max_{\pi} \rho(\pi)$.

Value Function: The value function $V_t(\mathcal{H}_t)$ is defined as the expected total discounted reward starting from the decision epoch t with hyper state \mathcal{H}_t under the optimal policy π^* , i.e.,

$$V_t(\mathcal{H}_t) = \mathbb{E} \left[\sum_{\ell=t}^L \gamma^\ell R(p_\ell, i_\ell, \delta_\ell; \pi_\ell^*(\mathcal{H}_\ell)) \middle| \mathcal{H}_t \right].$$

The value function $V_t(\mathcal{H}_t)$, or equivalently $V_t(p_t, i_t, \delta_t, \tau_t, \mathcal{I}_t)$, can be recursively written as

$$V_t(p_t, i_t, \delta_t, \tau_t, \mathcal{I}_t) = \max_{a_t \in \mathcal{A}(p_t, i_t, \delta_t)} \{R(p_t, i_t, \delta_t; a_t) + \gamma \mathbb{E}[V_{t+1}(p_{t+1}, i_{t+1}, \delta_{t+1}, \tau_{t+1}, \mathcal{I}_{t+1})]\} \quad (29)$$

for $t \in \{0, 1, \dots, L-1\}$. At the decision epoch L (i.e., when the end of the production campaign is reached), the value function is equal to

$$V_L(p_L, i_L, \delta_L, \tau_L, \mathcal{I}_L) = \begin{cases} r_h(p_L, i_L), & \text{if } \delta_L = 1, i_{\bar{T}} < \bar{I} \\ -r_f, & \text{if } \delta_L = 1, i_{\bar{T}} = \bar{I} \\ 0, & \text{if } \delta_L = 0. \end{cases} \quad (30)$$

B Solution Approach

The procedure of Reinforcement Learning under Model Risk (RL with MR) is provided in Algorithm 1. We initialize in Step (1). In Step (2), the Q-function needs to be estimated. For this purpose, we apply the sparse sampling idea of [43], which generates future trajectories (i.e., state-action pairs over time) for modeling the uncertainty in the hyper state evolution and chooses the optimal action by constructing a look-ahead tree with these trajectories. Similar to [44] and [25], we generate the future states by using the Bayesian updated posterior predictive distributions. To be specific, given the current hyper state $\mathcal{H}_t = (\mathcal{S}_t, \mathcal{I}_t)$ with $\mathcal{S}_t = (p_t, i_t)$, the samples of next hyper state can be generated through the transition probability $\Pr(\mathcal{S}_{t+1}, \mathcal{I}_{t+1} | \mathcal{S}_t, \mathcal{I}_t, a_t) = \Pr(\mathcal{S}_{t+1} | \mathcal{S}_t, \mathcal{I}_t, a_t) \Pr(\mathcal{I}_{t+1} | \mathcal{S}_{t+1}, \mathcal{S}_t, \mathcal{I}_t, a_t)$ in two steps. First, we generate the K scenarios of physical states (p_{t+1}, i_{t+1}) by sampling the protein growth rates $\tilde{\phi}_t^{(k)}$ and $\tilde{\psi}_t^{(k)}$ from the posterior predictive distributions in (9) and (10), and then using the equations $p_{t+1}^{(k)} = p_t \cdot e^{\tilde{\phi}_t^{(k)}}$ and $i_{t+1}^{(k)} = i_t \cdot e^{\tilde{\psi}_t^{(k)}}$

ALGORITHM 1: Reinforcement Learning under Model Risk (RL with MR)

Input: Initial physical states $\mathcal{S}_0 = (p_0, i_0)$ and the initial knowledge states \mathcal{I}_0 .

Output: The stopping time T and total reward $Total.R$.

 (1) Set the total reward $Total.R = 0$.

for $t = 0, 1, \dots, T$ **do**

 if $p_t < \bar{P}$ and $i_t < \bar{I}$ and $t < \bar{T}$ **then**

 (2) Estimate the Q-function in (26) by calling $\hat{Q}_t(p_t, i_t, \mathcal{I}_t; C) = \text{Qfunction}(p_t, i_t, \mathcal{I}_t, C)$;

 (3) Choose the ‘harvest’ action if $Q_t(p_t, i_t, \mathcal{I}_t; H) \geq \hat{Q}_t(p_t, i_t, \mathcal{I}_t, C)$, and ‘continue’ otherwise;

 else

(4) Choose the ‘harvest’ action;

if ‘continue’ action is chosen **then**

 (5) Continue the fermentation process one more period, $Total.R = Total.R - c_u$, and observe the realized physical states (p_{t+1}, i_{t+1}) in real life;

 (6) Obtain the updated knowledge states \mathcal{I}_{t+1} as described in Section 3.2;

 else

 (7) Terminate the fermentation process, set the stopping time $T = t$ and $Total.R = Total.R + R(p_t, i_t; H)$, break the ‘for loop’;

end

 (8) Output the total reward $Total.R$;

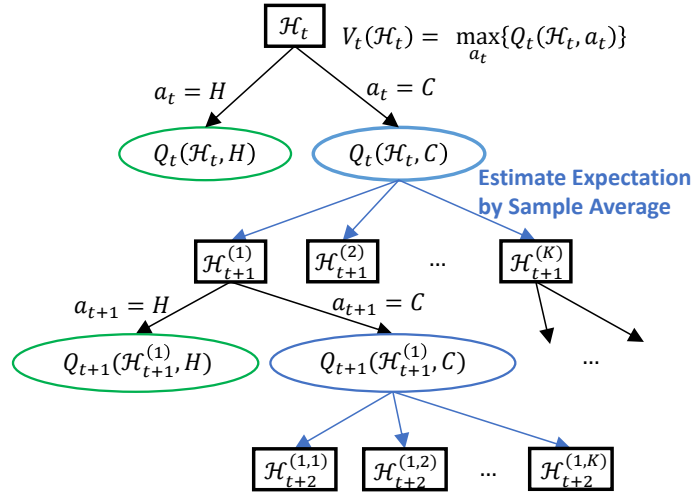


Figure 6: Illustration of the lookahead tree for Bayesian sparse sampling.

for $k = 1, 2, \dots, K$. Second, based on the collected samples of protein and impurity growth rates $\tilde{\phi}_t^{(k)}$ and $\tilde{\psi}_t^{(k)}$, the knowledge state can be updated by using (5) and (7). In Figure 6, we illustrate the main idea of Bayesian sparse sampling.

Bayesian sparse sampling considers a look-ahead tree starting with the root at the current hyper state \mathcal{H}_t , followed by two potential actions: harvest or continue fermentation. The Q-function value of harvest decision is known and given by (27). For the continue action, the expected value $E[\max_{a_{t+1}} Q_{t+1}(p_{t+1}, i_{t+1}, \mathcal{I}_{t+1}; a_{t+1})]$ in (26) is estimated by using sample average approximation, which grows the tree into K following nodes that each representing a sample of the next hyper state $\mathcal{H}_{t+1}^{(k)} = (p_{t+1}^{(k)}, i_{t+1}^{(k)}, \mathcal{I}_{t+1}^{(k)})$ for $k = 1, 2, \dots, K$. The same procedure is repeated for each node until all the leaf nodes reach the end of the fermentation, i.e. the harvest decision is made. The Q-function (and the value function) estimates are computed from leaf nodes rolling-backing up to the root. The procedure is summarized in Algorithm 2.

It is known that the online sparse sampling algorithm (which is implemented by Algorithms 1 and 2 for our problem) is guaranteed to compute a near-optimal action at any state of the MDP model [43]. The theoretical results on the quality of the near-optimal action depends on the number of samples K at each node and the depth of the look-ahead tree. In our implementation of the sparse-sampling algorithm, we do not set a specific value for the depth of the look-ahead tree, but instead continue branching until all the leaves represent a harvest action (i.e., step (A3) in Algorithm 2 ends up with step (B1) for each k). Notice that the tree grows until at most decision epoch \bar{T} at which the fermentation process must be terminated (if not done yet). In our implementation, the number of samples K is the only parameter that controls the

ALGORITHM 2: Bayesian Sparse Sampling for Estimating the Q-Function

Input: The current hyper state $\mathcal{H}_t = (\mathcal{S}_t, \mathcal{I}_t)$ with physical states $\mathcal{S}_t = (p_t, i_t)$ and knowledge states \mathcal{I}_t ; the action a_t , and the number of samples K .

Output: Estimated value of the Q-function $\widehat{Q}_t(p_t, i_t, \mathcal{I}_t, a_t)$.

Function `Qfunction`($p_t, i_t, \mathcal{I}_t, a_t$):

```
if  $a_t = H$  then
  (A1) return harvest reward  $R(p_t, i_t, H)$  as in (A);
else
  (A2) Generate  $K$  samples of next hyper state  $\mathcal{H}_{t+1}^{(k)} = (p_{t+1}^{(k)}, i_{t+1}^{(k)}, \mathcal{I}_{t+1}^{(k)})$ ,  $k = 1, 2, \dots, K$  from
     $\Pr(\mathcal{S}_{t+1}, \mathcal{I}_{t+1} | \mathcal{S}_t, \mathcal{I}_t, a_t)$  as discussed in Section B;
  (A3) For each  $k$ , call  $\widehat{V}_{t+1}^{(k)}(\mathcal{H}_{t+1}^{(k)}) = \text{Valuefunction}(p_{t+1}^{(k)}, i_{t+1}^{(k)}, \mathcal{I}_{t+1}^{(k)})$  to estimate the value function of hyper state
     $\mathcal{H}_{t+1}^{(k)}$  at the next decision epoch  $t + 1$ ;
  (A4) return  $\widehat{Q}_t(\mathcal{H}_t, C) = -c_u + \frac{\gamma}{K} \sum_{k=1}^K \widehat{V}_{t+1}^{(k)}(\mathcal{H}_{t+1}^{(k)})$ ;
```

Function `Valuefunction`(p_t, i_t, \mathcal{I}_t):

```
if  $p_t \geq \bar{P}$  or  $i_t \geq \bar{I}$  or  $t = \bar{T}$  then
  (B1) return harvest reward  $R(p_t, i_t, H)$  as in (A);
else
  (B2) Generate  $K$  samples of next hyper state  $\mathcal{H}_{t+1}^{(k)} = (p_{t+1}^{(k)}, i_{t+1}^{(k)}, \mathcal{I}_{t+1}^{(k)})$ ,  $k = 1, 2, \dots, K$  from
     $\Pr(\mathcal{S}_{t+1}, \mathcal{I}_{t+1} | \mathcal{S}_t, \mathcal{I}_t, a_t)$  as discussed in Section B;
  (B3) For each  $k$ , call  $\widehat{V}_{t+1}^{(k)}(\mathcal{H}_{t+1}^{(k)}) = \text{Valuefunction}(p_{t+1}^{(k)}, i_{t+1}^{(k)}, \mathcal{I}_{t+1}^{(k)})$  to estimate the value function of hyper state
     $\mathcal{H}_{t+1}^{(k)}$  at the next decision epoch  $t + 1$ ;
  (B4) return  $\widehat{V}_t(\mathcal{H}_t) = \max \left\{ R(p_t, i_t, H), -c_u + \frac{\gamma}{K} \sum_{k=1}^K \widehat{V}_{t+1}^{(k)}(\mathcal{H}_{t+1}^{(k)}) \right\}$ ;
```

computation time and quality of the solution. In literature, it is typical to set the value of K not too large considering the branches grow exponentially; e.g., [43] and [45] set K equal to 5 in their implementation of Bayesian sparse sampling. In our numerical study, we set $K = 10$, as it is observed that the results do not change by increasing the value of K further.

C Proofs

Proof of Proposition 1

(i) Notice that $\phi_j, j = 1, \dots, J_t$, are i.i.d. samples from underlying true protein growth rate distribution $\mathcal{N}(\mu^{(p)}, \sigma^{(p)2})$. According to the properties of Gaussian sample mean and sample variance, we have $\bar{\phi} \sim \mathcal{N}(\mu^{(p)}, \frac{\sigma^{(p)2}}{J_t})$, $\frac{\sum_{j=1}^{J_t} (\phi_j - \bar{\phi})^2}{\sigma^{(p)2}} \sim \chi^2(J_t - 1)$, and they are independent of each other. Thus, $\tilde{\sigma}_t^{(p)2} = \frac{J_t + 1}{(J_t - 2)J_t} \sum_{j=1}^{J_t} (\phi^{(j)} - \bar{\phi})^2 \sim \frac{(J_t + 1)\sigma^{(p)2}}{(J_t - 2)J_t} \chi^2(J_t - 1)$. Based on the mean and variance of Chi-square distribution, we have

$$\mathbb{E} \left[\tilde{\sigma}_t^{(p)2} \right] = \frac{(J_t^2 - 1)\sigma^{(p)2}}{(J_t^2 - 2J_t)} = \sigma^{(p)2} + \frac{(2J_t - 1)\sigma^{(p)2}}{(J_t^2 - 2J_t)}, \quad \text{Var} \left[\tilde{\sigma}_t^{(p)2} \right] = \frac{2(J_t^3 + J_t^2 - J_t - 1)\sigma^{(p)4}}{J_t^4 - 4J_t^3 + 4J_t^2}.$$

(ii) Recall that the predictive growth rate $\tilde{\Phi}_t$ is a compound random variable, i.e., $\tilde{\Phi}_t \sim \mathcal{N}(\mu^{(p)}, \sigma^{(p)2})$ where $(\mu^{(p)}, \sigma^{(p)2}) \sim \mathcal{N}(\alpha_t^{(p)}, \sigma^{(p)2}/\nu_t^{(p)}) \cdot \text{Inv}\Gamma(\lambda_t^{(p)}, \beta_t^{(p)})$ at decision epoch t . For brevity, let $\theta^{(p)}$ denote the random variables $(\mu^{(p)}, \sigma^{(p)2})$. The variance of the compound random variable $\tilde{\Phi}_t$ can be decomposed as follows:

$$\tilde{\sigma}_t^{(p)2} \triangleq \text{Var} \left[\tilde{\Phi}_t \right] = \mathbb{E}_{\theta^{(p)}} \left[\text{Var} \left(\tilde{\Phi}_t \mid \theta^{(p)} \right) \right] + \text{Var}_{\theta^{(p)}} \left[\mathbb{E} \left(\tilde{\Phi}_t \mid \theta^{(p)} \right) \right] \quad (31)$$

$$\begin{aligned} &= \mathbb{E}_{\theta^{(p)}} \left[\sigma^{(p)2} \right] + \text{Var}_{\theta^{(p)}} \left[\mu^{(p)} \right] \\ &= \mathbb{E}_{\theta^{(p)}} \left[\sigma^{(p)2} \right] + \mathbb{E}_{\theta^{(p)}} \left[\text{Var} \left(\mu^{(p)} \mid \sigma^{(p)2} \right) \right] + \text{Var}_{\theta^{(p)}} \left[\mathbb{E} \left(\mu^{(p)2} \mid \sigma^{(p)2} \right) \right] \end{aligned} \quad (32)$$

$$\begin{aligned} &= \mathbb{E}_{\theta^{(p)}} \left[\sigma^{(p)2} \right] + \mathbb{E}_{\theta^{(p)}} \left[\sigma^{(p)2}/\nu_t^{(p)} \right] + \text{Var}_{\theta^{(p)}} \left[\alpha_t^{(p)} \right] \\ &= \frac{\beta_t^{(p)}}{\lambda_t^{(p)} - 1} + \frac{\beta_t^{(p)}}{(\lambda_t^{(p)} - 1)\nu_t^{(p)}}. \end{aligned} \quad (33)$$

where the equations in (31) and (32) hold by law of total variance. We note that $\text{Var}_{\theta^{(p)}} \left[\alpha_t^{(p)} \right]$ is zero because $\alpha_t^{(p)}$ is a constant. The first term in the right-hand side of (33) (i.e., $\hat{\sigma}_t^{(p)2} \triangleq \frac{\beta_t^{(p)}}{\lambda_t^{(p)} - 1}$) corresponds to $\mathbb{E}_{\theta^{(p)}} \left[\sigma^{(p)2} \right]$, measuring the expected variability of the protein growth rate due to inherent stochasticity of the fermentation. The second term (i.e., $\check{\sigma}_t^{(p)2} \triangleq \frac{\beta_t^{(p)}}{(\lambda_t^{(p)} - 1)\nu_t^{(p)}}$) corresponds to $\mathbb{E}_{\theta^{(p)}} \left[\text{Var} \left(\mu^{(p)} \mid \sigma^{(p)2} \right) \right]$ and it represents the expected variability of the protein growth rate due to model risk.

Proof of Theorem 1

Notice that, at time \bar{T} , we have

$$V_{\bar{T}}(p_{\bar{T}}, i_{\bar{T}}, \mathcal{I}_{\bar{T}}) = \begin{cases} r_h(p_{\bar{T}}, i_{\bar{T}}), & \text{if } i_{\bar{T}} < \bar{I} \\ -r_f, & \text{if } i_{\bar{T}} = \bar{I}, \end{cases}$$

which is non-increasing in $i_{\bar{T}}$ and non-decreasing in $p_{\bar{T}}$. Based on the value function given in Section 3.3, we can prove Theorem 1 through backward induction.

As the induction hypothesis, assume that $V_{t+1}(p_{t+1}, i_{t+1}, \mathcal{I}_{t+1})$ is non-increasing in i_{t+1} and non-decreasing in p_{t+1} for a given $t \in \{0, 1, \dots, \bar{T} - 1\}$. Recall from (29) that the value function at decision epoch t is given by

$$V_t(p_t, i_t, \mathcal{I}_t) = \begin{cases} \max \{ r_h(p_t, i_t), -c_u + \gamma \mathbb{E} [V_{t+1}(p_{t+1}, i_{t+1}, \mathcal{I}_{t+1})] \} & \text{if } p_t < \bar{P} \text{ and } i_t < \bar{I} \\ r_h(p_t, i_t) & \text{if } p_t = \bar{P} \text{ and } i_t < \bar{I} \\ -r_f & \text{if } i_t = \bar{I}, \end{cases}$$

where $\mathbb{E} [V_{t+1}(p_{t+1}, i_{t+1}, \mathcal{I}_{t+1})] = \mathbb{E} [V_{t+1}(p_t e^{\tilde{\Phi}_t}, i_t e^{\tilde{\Psi}_t}, \mathcal{I}_{t+1})]$. For any $i_t^+ \geq i_t$, we know that

$$\mathbb{E} [V_{t+1}(p_t e^{\tilde{\Phi}_t}, i_t e^{\tilde{\Psi}_t}, \mathcal{I}_{t+1})] = -r_f \int_{\ln \bar{I} - \ln i_t}^{\infty} f_t^{(i)}(\psi_t) d\psi_t$$

$$\begin{aligned}
& + \int_{-\infty}^{\ln \bar{I} - \ln i_t} \int_{-\infty}^{\ln \bar{P} - \ln p_t} V_{t+1}(p_t e^{\phi_t}, i_t e^{\psi_t}, \mathcal{I}_{t+1}) f_t^{(p)}(\phi_t) f_t^{(i)}(\psi_t) d\phi_t d\psi_t \\
& + \int_{-\infty}^{\ln \bar{I} - \ln i_t} \int_{\ln \bar{P} - \ln p_t}^{\infty} r_h(\bar{P}, i_t e^{\psi_t}) f_t^{(p)}(\phi_t) f_t^{(i)}(\psi_t) d\phi_t d\psi_t \\
= & -r_f \int_{\ln \bar{I} - \ln i_t}^{\infty} f_t^{(i)}(\psi_t) d\psi_t \\
& + \int_{-\infty}^{\ln \bar{I} - \ln i_t^+} \int_{-\infty}^{\ln \bar{P} - \ln p_t} V_{t+1}(p_t e^{\phi_t}, i_t e^{\psi_t}, \mathcal{I}_{t+1}) f_t^{(p)}(\phi_t) f_t^{(i)}(\psi_t) d\phi_t d\psi_t \\
& + \int_{-\infty}^{\ln \bar{I} - \ln i_t^+} \int_{\ln \bar{P} - \ln p_t}^{\infty} r_h(\bar{P}, i_t e^{\psi_t}) f_t^{(p)}(\phi_t) f_t^{(i)}(\psi_t) d\phi_t d\psi_t \\
& + \int_{\ln \bar{I} - \ln i_t^+}^{\ln \bar{I} - \ln i_t} \int_{-\infty}^{\ln \bar{P} - \ln p_t} V_{t+1}(p_t e^{\phi_t}, i_t e^{\psi_t}, \mathcal{I}_{t+1}) f_t^{(p)}(\phi_t) f_t^{(i)}(\psi_t) d\phi_t d\psi_t \\
& + \int_{\ln \bar{I} - \ln i_t^+}^{\ln \bar{I} - \ln i_t} \int_{\ln \bar{P} - \ln p_t}^{\infty} r_h(\bar{P}, i_t e^{\psi_t}) f_t^{(p)}(\phi_t) f_t^{(i)}(\psi_t) d\phi_t d\psi_t \\
\geq & -r_f \int_{\ln \bar{I} - \ln i_t}^{\infty} f_t^{(i)}(\psi_t) d\psi_t \\
& + \int_{-\infty}^{\ln \bar{I} - \ln i_t^+} \int_{-\infty}^{\ln \bar{P} - \ln p_t} V_{t+1}(p_t e^{\phi_t}, i_t e^{\psi_t}, \mathcal{I}_{t+1}) f_t^{(p)}(\phi_t) f_t^{(i)}(\psi_t) d\phi_t d\psi_t \\
& + \int_{-\infty}^{\ln \bar{I} - \ln i_t^+} \int_{\ln \bar{P} - \ln p_t}^{\infty} r_h(\bar{P}, i_t e^{\psi_t}) f_t^{(p)}(\phi_t) f_t^{(i)}(\psi_t) d\phi_t d\psi_t \\
& - r_f \int_{\ln \bar{I} - \ln i_t^+}^{\ln \bar{I} - \ln i_t} \int_{-\infty}^{\ln \bar{P} - \ln p_t} f_t^{(p)}(\phi_t) f_t^{(i)}(\psi_t) d\phi_t d\psi_t \\
& - r_f \int_{\ln \bar{I} - \ln i_t^+}^{\ln \bar{I} - \ln i_t} \int_{\ln \bar{P} - \ln p_t}^{\infty} f_t^{(p)}(\phi_t) f_t^{(i)}(\psi_t) d\phi_t d\psi_t \\
\geq & -r_f \int_{\ln \bar{I} - \ln i_t^+}^{\infty} f_t^{(i)}(\psi_t) d\psi_t + \int_{-\infty}^{\ln \bar{I} - \ln i_t^+} \int_{-\infty}^{\ln \bar{P} - \ln p_t} V_{t+1}(p_t e^{\phi_t}, i_t^+ e^{\psi_t}, \mathcal{I}_{t+1}) f_t^{(p)}(\phi_t) f_t^{(i)}(\psi_t) d\phi_t d\psi_t \\
& + \int_{-\infty}^{\ln \bar{I} - \ln i_t^+} \int_{\ln \bar{P} - \ln p_t}^{\infty} r_h(\bar{P}, i_t^+ e^{\psi_t}) f_t^{(p)}(\phi_t) f_t^{(i)}(\psi_t) d\phi_t d\psi_t \\
= & \mathbb{E}[V_{t+1}(p_t e^{\tilde{\Phi}_t}, i_t^+ e^{\tilde{\Psi}_t}, \mathcal{I}_{t+1})]
\end{aligned}$$

where the first inequality holds because $V_{t+1}(p_t e^{\phi_t}, i_t e^{\psi_t}, \mathcal{I}_{t+1}) \geq -r_f$ and $r_h(\bar{P}, i_t e^{\psi_t}) \geq -r_f$ (this follows from the assumption $r_f > c_2 \bar{I}$), and the second inequality holds because $r_h(\bar{P}, i_t e^{\psi_t}) \geq r_h(\bar{P}, i_t^+ e^{\psi_t})$ and the induction hypothesis together with $i_t^+ e^{\psi_t} \geq i_t e^{\psi_t}$ imply that $\mathbb{E}[V_{t+1}(p_t e^{\tilde{\Phi}_t}, i_t e^{\tilde{\Psi}_t}, \mathcal{I}_{t+1})] \geq \mathbb{E}[V_{t+1}(p_t e^{\tilde{\Phi}_t}, i_t^+ e^{\tilde{\Psi}_t}, \mathcal{I}_{t+1})]$. Consequently, $V_t(p_t, i_t, \mathcal{I}_t)$ is also non-increasing in i_t .

On the other hand, for any $p_t^+ \geq p_t$, we know that

$$\begin{aligned}
\mathbb{E}[V_{t+1}(p_t e^{\tilde{\Phi}_t}, i_t e^{\tilde{\Psi}_t}, \mathcal{I}_{t+1})] & = -r_f \int_{\ln \bar{I} - \ln i_t}^{\infty} f_t^{(i)}(\psi_t) d\psi_t \\
& + \int_{-\infty}^{\ln \bar{I} - \ln i_t} \int_{-\infty}^{\ln \bar{P} - \ln p_t} V_{t+1}(p_t e^{\phi_t}, i_t e^{\psi_t}, \mathcal{I}_{t+1}) f_t^{(p)}(\phi_t) f_t^{(i)}(\psi_t) d\phi_t d\psi_t \\
& + \int_{-\infty}^{\ln \bar{I} - \ln i_t} \int_{\ln \bar{P} - \ln p_t}^{\infty} r_h(\bar{P}, i_t e^{\psi_t}) f_t^{(p)}(\phi_t) f_t^{(i)}(\psi_t) d\phi_t d\psi_t \\
& = -r_f \int_{\ln \bar{I} - \ln i_t}^{\infty} f_t^{(i)}(\psi_t) d\psi_t
\end{aligned}$$

$$\begin{aligned}
& + \int_{-\infty}^{\ln \bar{I} - \ln i_t} \int_{-\infty}^{\ln \bar{P} - \ln p_t^+} V_{t+1}(p_t e^{\phi_t}, i_t e^{\psi_t}, \mathcal{I}_{t+1}) f_t^{(p)}(\phi_t) f_t^{(i)}(\psi_t) d\phi_t d\psi_t \\
& + \int_{-\infty}^{\ln \bar{I} - \ln i_t} \int_{\ln \bar{P} - \ln p_t^+}^{\ln \bar{P} - \ln p_t} V_{t+1}(p_t e^{\phi_t}, i_t e^{\psi_t}, \mathcal{I}_{t+1}) f_t^{(p)}(\phi_t) f_t^{(i)}(\psi_t) d\phi_t d\psi_t \\
& + \int_{-\infty}^{\ln \bar{I} - \ln i_t} \int_{\ln \bar{P} - \ln p_t^+}^{\infty} r_h(\bar{P}, i_t e^{\psi_t}) f_t^{(p)}(\phi_t) f_t^{(i)}(\psi_t) d\phi_t d\psi_t \\
& - \int_{-\infty}^{\ln \bar{I} - \ln i_t} \int_{\ln \bar{P} - \ln p_t^+}^{\ln \bar{P} - \ln p_t} r_h(\bar{P}, i_t e^{\psi_t}) f_t^{(p)}(\phi_t) f_t^{(i)}(\psi_t) d\phi_t d\psi_t \\
& \leq -r_f \int_{\ln \bar{I} - \ln i_t}^{\infty} f_t^{(i)}(\psi_t) d\psi_t \\
& + \int_{-\infty}^{\ln \bar{I} - \ln i_t} \int_{-\infty}^{\ln \bar{P} - \ln p_t^+} V_{t+1}(p_t e^{\phi_t}, i_t e^{\psi_t}, \mathcal{I}_{t+1}) f_t^{(p)}(\phi_t) f_t^{(i)}(\psi_t) d\phi_t d\psi_t \\
& + \int_{-\infty}^{\ln \bar{I} - \ln i_t} \int_{\ln \bar{P} - \ln p_t^+}^{\infty} r_h(\bar{P}, i_t e^{\psi_t}) f_t^{(p)}(\phi_t) f_t^{(i)}(\psi_t) d\phi_t d\psi_t \\
& \leq -r_f \int_{\ln \bar{I} - \ln i_t}^{\infty} f_t^{(i)}(\psi_t) d\psi_t \\
& + \int_{-\infty}^{\ln \bar{I} - \ln i_t} \int_{-\infty}^{\ln \bar{P} - \ln p_t^+} V_{t+1}(p_t^+ e^{\phi_t}, i_t e^{\psi_t}, \mathcal{I}_{t+1}) f_t^{(p)}(\phi_t) f_t^{(i)}(\psi_t) d\phi_t d\psi_t \\
& + \int_{-\infty}^{\ln \bar{I} - \ln i_t} \int_{\ln \bar{P} - \ln p_t^+}^{\infty} r_h(\bar{P}, i_t e^{\psi_t}) f_t^{(p)}(\phi_t) f_t^{(i)}(\psi_t) d\phi_t d\psi_t \\
& = \mathbb{E}[V_{t+1}(p_t^+ e^{\tilde{\Phi}_t}, i_t e^{\tilde{\Psi}_t}, \mathcal{I}_{t+1})] \tag{34}
\end{aligned}$$

where the first inequality holds because $r_h(\bar{P}, i_t e^{\psi_t}) \geq V_{t+1}(p_t e^{\phi_t}, i_t e^{\psi_t}, \mathcal{I}_{t+1})$ (this holds due to the fact that the value function at a fixed impurity level can never exceed the *maximum* harvesting reward achievable at that impurity level), and the second inequality holds because of the induction hypothesis and $p_t e^{\phi_t} \leq p_t^+ e^{\phi_t}$. Consequently, we have $V_t(p_t, i_t, \mathcal{I}_t)$ is also non-decreasing in p_t .

Proof of Theorem 2

According to Theorem 2, if $\pi^*(p_t, i_t^-, \mathcal{I}_t) = H$, then $\pi^*(p_t, i_t^+, \mathcal{I}_t) = H$ for any $i^+ > i^-$. Assume that $\pi^*(p_t, i_t^-, \mathcal{I}_t) = H$ but $\pi^*(p_t, i_t^+, \mathcal{I}_t) = C$ as the contradiction hypothesis. Then, it holds that

$$\begin{aligned}
r_h(p_t, i_t^-) & \geq -c_u + \gamma \mathbb{E} \left[V_{t+1}(p_t e^{\tilde{\Phi}_t}, i_t^- e^{\tilde{\Psi}_t}, \mathcal{I}_{t+1}) \right] \\
r_h(p_t, i_t^+) & \leq -c_u + \gamma \mathbb{E} \left[V_{t+1}(p_t e^{\tilde{\Phi}_t}, i_t^+ e^{\tilde{\Psi}_t}, \mathcal{I}_{t+1}) \right].
\end{aligned}$$

Thus, we have

$$\begin{aligned}
r_h(p_t, i_t^-) - r_h(p_t, i_t^+) & \geq \gamma \mathbb{E} \left[V_{t+1}(p_t e^{\tilde{\Phi}_t}, i_t^- e^{\tilde{\Psi}_t}, \mathcal{I}_{t+1}) \right] - \gamma \mathbb{E} \left[V_{t+1}(p_t e^{\tilde{\Phi}_t}, i_t^+ e^{\tilde{\Psi}_t}, \mathcal{I}_{t+1}) \right] \\
& = -\gamma r_f \int_{\ln \bar{I} - \ln i_t^-}^{\infty} f_t^{(i)}(\psi_t) d\psi_t + \gamma r_f \int_{\ln \bar{I} - \ln i_t^+}^{\infty} f_t^{(i)}(\psi_t) d\psi_t \\
& + \gamma \int_{-\infty}^{\ln \bar{I} - \ln i_t^-} \int_{-\infty}^{\ln \bar{P} - \ln p_t} V_{t+1}(p_t e^{\phi_t}, i_t^- e^{\psi_t}, \mathcal{I}_{t+1}) f_t^{(p)}(\phi_t) f_t^{(i)}(\psi_t) d\phi_t d\psi_t \\
& + \gamma \int_{-\infty}^{\ln \bar{I} - \ln i_t^-} \int_{\ln \bar{P} - \ln p_t}^{\infty} r_h(\bar{P}, i_t^- e^{\psi_t}, \mathcal{I}_{t+1}) f_t^{(p)}(\phi_t) f_t^{(i)}(\psi_t) d\phi_t d\psi_t \\
& - \gamma \int_{-\infty}^{\ln \bar{I} - \ln i_t^+} \int_{-\infty}^{\ln \bar{P} - \ln p_t} V_{t+1}(p_t e^{\phi_t}, i_t^+ e^{\psi_t}, \mathcal{I}_{t+1}) f_t^{(p)}(\phi_t) f_t^{(i)}(\psi_t) d\phi_t d\psi_t
\end{aligned}$$

$$\begin{aligned}
& - \gamma \int_{-\infty}^{\ln \bar{I} - \ln i_t^+} \int_{\ln \bar{P} - \ln p_t}^{\infty} r_h(\bar{P}, i_t^+ e^{\psi_t}, \mathcal{I}_{t+1}) f_t^{(p)}(\phi_t) f_t^{(i)}(\psi_t) d\phi_t d\psi_t \\
\geq & \gamma r_f \left[\int_{-\infty}^{\ln \bar{I} - \ln i_t^-} f_t^{(i)}(\psi_t) d\psi_t - \int_{-\infty}^{\ln \bar{I} - \ln i_t^+} f_t^{(i)}(\psi_t) d\psi_t \right] \tag{35}
\end{aligned}$$

$$\begin{aligned}
& + \gamma \int_{-\infty}^{\ln \bar{I} - \ln i_t^-} \int_{-\infty}^{\infty} r_h(0, i_t^- e^{\psi_t}) f_t^{(p)}(\phi_t) f_t^{(i)}(\psi_t) d\phi_t d\psi_t \\
& - \gamma \int_{-\infty}^{\ln \bar{I} - \ln i_t^+} \int_{-\infty}^{\infty} r_h(\bar{P}, i_t^- e^{\psi_t}) f_t^{(p)}(\phi_t) f_t^{(i)}(\psi_t) d\phi_t d\psi_t \\
\geq & \gamma r_f \left[\int_{-\infty}^{\ln \bar{I} - \ln i_t^-} f_t^{(i)}(\psi_t) d\psi_t - \int_{-\infty}^{\ln \bar{I} - \ln i_t^+} f_t^{(i)}(\psi_t) d\psi_t \right] \tag{36} \\
& + \gamma \int_{-\infty}^{\ln \bar{I} - \ln i_t^-} r_h(0, i_t^- e^{\psi_t}) f_t^{(i)}(\psi_t) d\psi_t - \gamma \int_{-\infty}^{\ln \bar{I} - \ln i_t^-} r_h(\bar{P}, i_t^- e^{\psi_t}) f_t^{(i)}(\psi_t) d\psi_t \\
= & \gamma r_f \int_{\ln \bar{I} - \ln i_t^+}^{\ln \bar{I} - \ln i_t^-} f_t^{(i)}(\psi_t) d\psi_t - \gamma c_1 \bar{P} \int_{-\infty}^{\ln \bar{I} - \ln i_t^-} f_t^{(i)}(\psi_t) d\psi_t
\end{aligned}$$

which contradicts the condition, so that we have $p^*(p_t, i_t^+) = H$. Notice that, inequality (35) holds because: (i) $V_{t+1}(0, i_t^- e^{\psi_t}, \mathcal{I}_{t+1}) \geq r_h(0, i_t^- e^{\psi_t})$ by the definition of the value function (i.e., at any decision epoch, the value function at a particular state can never be less than the harvesting reward at that state) and $V_{t+1}(p_t e^{\phi_t}, i_t^- e^{\psi_t}, \mathcal{I}_{t+1}) \geq V_{t+1}(0, i_t^- e^{\psi_t}, \mathcal{I}_{t+1})$ by the non-decreasing behavior of the value function in p_t for any protein growth-rate realization ϕ_t , and (ii) $V_{t+1}(p_t e^{\phi_t}, i_t^+ e^{\psi_t}, \mathcal{I}_{t+1}) \leq r_h(\bar{P}, i_t^+ e^{\psi_t}) \leq r_h(\bar{P}, i_t^- e^{\psi_t})$ as the reward function r_h is non-increasing in i_t . Finally, the inequality (36) holds because $\ln \bar{I} - \ln i_t^+ \leq \ln \bar{I} - \ln i_t^-$.

Proof of Theorem 3

Note that $E[\tilde{\Phi}_t] = \alpha_t^{(p)}$ and $E[\tilde{\Psi}_t] = \alpha_t^{(i)}$. We first consider the ‘‘non-decreasing in $\alpha_t^{(p)}$,’’ part, given the rest of the knowledge state is fixed. By using the Bellman’s equation, we can do the proof through backward induction. To start with, notice that

$$V_{\bar{T}}(p_{\bar{T}}, i_{\bar{T}}, \mathcal{I}_{\bar{T}}) = \begin{cases} r_h(p_{\bar{T}}, i_{\bar{T}}), & \text{if } i_{\bar{T}} < \bar{I} \\ -r_f, & \text{if } i_{\bar{T}} = \bar{I}, \end{cases}$$

is constant in $\alpha_{\bar{T}}^{(p)}$, and hence, non-decreasing in $\alpha_{\bar{T}}^{(p)}$. As the induction hypothesis, assume that $V_{t+1}(p_{t+1}, i_{t+1}, \mathcal{I}_{t+1})$ is non-decreasing in $\alpha_{t+1}^{(p)}$. At decision epoch $t < \bar{T}$, we have

$$V_t(p_t, i_t, \mathcal{I}_t) = \begin{cases} \max \{ r_h(p_t, i_t), -c_u + \gamma E[V_{t+1}(p_{t+1}, i_{t+1}, \mathcal{I}_{t+1})] \} & \text{if } p_t < \bar{P} \text{ and } i_t < \bar{I} \\ r_h(p_t, i_t) & \text{if } p_t = \bar{P} \text{ and } i_t < \bar{I} \\ -r_f & \text{if } i_t = \bar{I}. \end{cases}$$

Note that a change in the value of $\alpha_t^{(p)}$ affects the expectation through the predictive distribution $f_t^{(p)}(\phi_t | \alpha_t^{(p)})$; and it also affects the knowledge state variables $\alpha_{t+1}^{(p)}$ and $\beta_{t+1}^{(p)}$ through the knowledge states update, i.e., see (5). Let $\mathcal{I}_{t+1}(\alpha_t^{(p)})$ denote the updated knowledge states. Then, for any $\delta > 0$, it holds that

$$\begin{aligned}
& E[V_{t+1}(p_{t+1}, i_{t+1}, \mathcal{I}_{t+1})] = E[V_{t+1}(p_t e^{\tilde{\Phi}_t}, i_t e^{\tilde{\Psi}_t}, \mathcal{I}_{t+1}(\alpha_t^{(p)})) | \alpha_t^{(p)}] \tag{37} \\
= & -r_f \int_{\ln \bar{I} - \ln i_t}^{\infty} f_t^{(i)}(\psi_t) d\psi_t \\
& + \int_{-\infty}^{\ln \bar{I} - \ln i_t} \int_{-\infty}^{\ln \bar{P} - \ln p_t} V_{t+1}(p_t e^{\phi_t}, i_t e^{\psi_t}, \mathcal{I}_{t+1}(\alpha_t^{(p)})) f_t^{(p)}(\phi_t | \alpha_t^{(p)}) f_t^{(i)}(\psi_t) d\phi_t d\psi_t \\
& + \int_{-\infty}^{\ln \bar{I} - \ln i_t} \int_{\ln \bar{P} - \ln p_t}^{\infty} r_h(\bar{P}, i_t e^{\psi_t}) f_t^{(p)}(\phi_t | \alpha_t^{(p)}) f_t^{(i)}(\psi_t) d\phi_t d\psi_t \\
= & -r_f \int_{\ln \bar{I} - \ln i_t}^{\infty} f_t^{(i)}(\psi_t) d\psi_t
\end{aligned}$$

$$\begin{aligned}
& + \int_{-\infty}^{\ln \bar{I} - \ln i_t} \int_{-\infty}^{\ln \bar{P} - \ln p_t - \delta} V_{t+1}(p_t e^{\phi_t}, i_t e^{\psi_t}, \mathcal{I}_{t+1}(\alpha_t^{(p)})) f_t^{(p)}(\phi_t | \alpha_t^{(p)}) f_t^{(i)}(\psi_t) d\phi_t d\psi_t \\
& + \int_{-\infty}^{\ln \bar{I} - \ln i_t} \int_{\ln \bar{P} - \ln p_t - \delta}^{\ln \bar{P} - \ln p_t} V_{t+1}(p_t e^{\phi_t}, i_t e^{\psi_t}, \mathcal{I}_{t+1}(\alpha_t^{(p)})) f_t^{(p)}(\phi_t | \alpha_t^{(p)}) f_t^{(i)}(\psi_t) d\phi_t d\psi_t \\
& + \int_{-\infty}^{\ln \bar{I} - \ln i_t} \int_{\ln \bar{P} - \ln p_t}^{\infty} r_h(\bar{P}, i_t e^{\psi_t}) f_t^{(p)}(\phi_t | \alpha_t^{(p)}) f_t^{(i)}(\psi_t) d\phi_t d\psi_t \\
& \leq -r_f \int_{\ln \bar{I} - \ln i_t}^{\infty} f_t^{(i)}(\psi_t) d\psi_t \tag{38} \\
& + \int_{-\infty}^{\ln \bar{I} - \ln i_t} \int_{-\infty}^{\ln \bar{P} - \ln p_t - \delta} V_{t+1}(p_t e^{\phi_t + \delta}, i_t e^{\psi_t}, \mathcal{I}_{t+1}(\alpha_t^{(p)})) f_t^{(p)}(\phi_t | \alpha_t^{(p)}) f_t^{(i)}(\psi_t) d\phi_t d\psi_t \\
& + \int_{-\infty}^{\ln \bar{I} - \ln i_t} \int_{\ln \bar{P} - \ln p_t - \delta}^{\infty} r_h(\bar{P}, i_t e^{\psi_t}) f_t^{(p)}(\phi_t | \alpha_t^{(p)}) f_t^{(i)}(\psi_t) d\phi_t d\psi_t
\end{aligned}$$

where the inequality holds because $V_{t+1}(p, i, \mathcal{I})$ is non-decreasing function of p , and $V_{t+1}(p_t e^{\phi_t + \delta}, i_t e^{\psi_t}, \mathcal{I}_{t+1}(\alpha_t^{(p)})) \leq r_h(\bar{P}, i_t e^{\psi_t})$ for any ϕ_t and ψ_t .

Now consider a value $\alpha_t^{(p)+}$ such that $\alpha_t^{(p)+} - \alpha_t^{(p)} = \delta \geq 0$, and let $\phi'_t = \phi_t + \delta$. It holds for the predictive density that

$$\begin{aligned}
f_t^{(p)}(\phi_t | \alpha_t^{(p)}) &= \pi^{-1/2} \frac{\Gamma\left(\lambda_t^{(p)} + \frac{1}{2}\right)}{\Gamma(\lambda_t^{(p)})} \left[\frac{\nu_t^{(p)}}{2\beta_t^{(p)}(1 + \nu_t^{(p)})} \right]^{1/2} \left[1 + \frac{\nu_t^{(p)}(\phi_t - \alpha_t^{(p)})^2}{2\beta_t^{(p)}(1 + \nu_t^{(p)})} \right]^{-\lambda_t^{(p)} - 1/2} \\
&= \pi^{-1/2} \frac{\Gamma\left(\lambda_t^{(p)} + \frac{1}{2}\right)}{\Gamma(\lambda_t^{(p)})} \left[\frac{\nu_t^{(p)}}{2\beta_t^{(p)}(1 + \nu_t^{(p)})} \right]^{1/2} \left[1 + \frac{\nu_t^{(p)}(\phi'_t - \alpha_t^{(p)+})^2}{2\beta_t^{(p)}(1 + \nu_t^{(p)})} \right]^{-\lambda_t^{(p)} - 1/2} = f_t^{(p)}(\phi'_t | \alpha_t^{(p)+}).
\end{aligned}$$

Then, it holds for the RHS of (38) that

$$\begin{aligned}
\text{RHS of (38)} &\leq -r_f \int_{\ln \bar{I} - \ln i_t}^{\infty} f_t^{(i)}(\psi_t) d\psi_t \\
&+ \int_{-\infty}^{\ln \bar{I} - \ln i_t} \int_{-\infty}^{\ln \bar{P} - \ln p_t - \delta} V_{t+1}(p_t e^{\phi_t + \delta}, i_t e^{\psi_t}, \mathcal{I}_{t+1}(\alpha_t^{(p)+})) f_t^{(p)}(\phi_t | \alpha_t^{(p)}) f_t^{(i)}(\psi_t) d\phi_t d\psi_t \\
&+ \int_{-\infty}^{\ln \bar{I} - \ln i_t} \int_{\ln \bar{P} - \ln p_t - \delta}^{\infty} r_h(\bar{P}, i_t e^{\psi_t}) f_t^{(p)}(\phi_t | \alpha_t^{(p)}) f_t^{(i)}(\psi_t) d\phi_t d\psi_t \\
&= -r_f \int_{\ln \bar{I} - \ln i_t}^{\infty} f_t^{(i)}(\psi_t) d\psi_t \tag{39} \\
&+ \int_{-\infty}^{\ln \bar{I} - \ln i_t} \int_{-\infty}^{\ln \bar{P} - \ln p_t} V_{t+1}(p_t e^{\phi'_t}, i_t e^{\psi_t}, \mathcal{I}_{t+1}(\alpha_t^{(p)+})) f_t^{(p)}(\phi'_t | \alpha_t^{(p)+}) f_t^{(i)}(\psi_t) d\phi'_t d\psi_t \\
&+ \int_{-\infty}^{\ln \bar{I} - \ln i_t} \int_{\ln \bar{P} - \ln p_t}^{\infty} r_h(\bar{P}, i_t e^{\psi_t}) f_t^{(p)}(\phi'_t | \alpha_t^{(p)+}) f_t^{(i)}(\psi_t) d\phi'_t d\psi_t \\
&= \mathbb{E}[V_{t+1}(p_t e^{\tilde{\Phi}_t}, i_t e^{\tilde{\Psi}_t}, \mathcal{I}_{t+1}) | \alpha_t^{(p)+}].
\end{aligned}$$

The inequality holds by induction assumption (since $\alpha_{t+1}^{(p)+} \geq \alpha_{t+1}^{(p)}$ by the update rule (5) given that $\alpha_t^{(p)+} \geq \alpha_t^{(p)}$), and (39) holds by performing variable replacement $\phi'_t = \phi_t + \delta$. Thus, we have $V_t(p_t, i_t, \mathcal{I}_t(\alpha_t^{(p)})) \leq V_t(p_t, i_t, \mathcal{I}_t(\alpha_t^{(p)+}))$.

On the other hand, to consider the ‘‘non-increasing in $\alpha_t^{(i)}$ ’’ part, notice $V_{\bar{T}}(p_{\bar{T}}, i_{\bar{T}}, \mathcal{I}_{\bar{T}})$ is non-increasing in $\alpha_{\bar{T}}^{(i)}$. As the induction hypothesis, assume that $V_{t+1}(p_{t+1}, i_{t+1}, \mathcal{I}_{t+1})$ is non-increasing in $\alpha_{t+1}^{(i)}$. Similarly, change in the value of $\alpha_t^{(i)}$ affects the expectation through the predictive distribution $f_t^{(i)}(\psi_t | \alpha_t^{(i)})$; and it also affects the knowledge state variables $\alpha_{t+1}^{(i)}$ and $\beta_{t+1}^{(i)}$ through the knowledge states update. Let $\mathcal{I}_{t+1}(\alpha_t^{(i)})$ denote the updated knowledge states.

Then, for any $\delta > 0$,

$$\begin{aligned}
& \mathbb{E}[V_{t+1}(p_{t+1}, i_{t+1}, \mathcal{I}_{t+1})] = \mathbb{E}[V_{t+1}(p_t e^{\tilde{\Phi}_t}, i_t e^{\tilde{\Psi}_t}, \mathcal{I}_{t+1}(\alpha_t^{(i)})) | \alpha_t^{(i)}] \tag{40} \\
&= -r_f \int_{\ln \bar{I} - \ln i_t}^{\infty} f_t^{(i)}(\psi_t | \alpha_t^{(i)}) d\psi_t \\
&\quad + \int_{-\infty}^{\ln \bar{I} - \ln i_t} \int_{-\infty}^{\ln \bar{P} - \ln p_t} V_{t+1}(p_t e^{\phi_t}, i_t e^{\psi_t}, \mathcal{I}_{t+1}(\alpha_t^{(i)})) f_t^{(p)}(\phi_t) f_t^{(i)}(\psi_t | \alpha_t^{(i)}) d\phi_t d\psi_t \\
&\quad + \int_{-\infty}^{\ln \bar{I} - \ln i_t} \int_{\ln \bar{P} - \ln p_t}^{\infty} r_h(\bar{P}, i_t e^{\psi_t}) f_t^{(p)}(\phi_t) f_t^{(i)}(\psi_t | \alpha_t^{(i)}) d\phi_t d\psi_t \\
&= -r_f \int_{\ln \bar{I} - \ln i_t - \delta}^{\infty} f_t^{(i)}(\psi_t | \alpha_t^{(i)}) d\psi_t + r_f \int_{\ln \bar{I} - \ln i_t}^{\ln \bar{I} - \ln i_t} f_t^{(i)}(\psi_t | \alpha_t^{(i)}) d\psi_t \\
&\quad + \int_{-\infty}^{\ln \bar{I} - \ln i_t} \int_{-\infty}^{\ln \bar{P} - \ln p_t} V_{t+1}(p_t e^{\phi_t}, i_t e^{\psi_t}, \mathcal{I}_{t+1}(\alpha_t^{(i)})) f_t^{(p)}(\phi_t) f_t^{(i)}(\psi_t | \alpha_t^{(i)}) d\phi_t d\psi_t \\
&\quad + \int_{-\infty}^{\ln \bar{I} - \ln i_t} \int_{\ln \bar{P} - \ln p_t}^{\infty} r_h(\bar{P}, i_t e^{\psi_t}) f_t^{(p)}(\phi_t) f_t^{(i)}(\psi_t | \alpha_t^{(i)}) d\phi_t d\psi_t \\
&\geq -r_f \int_{\ln \bar{I} - \ln i_t - \delta}^{\infty} f_t^{(i)}(\psi_t | \alpha_t^{(i)}) d\psi_t \\
&\quad + \int_{-\infty}^{\ln \bar{I} - \ln i_t - \delta} \int_{-\infty}^{\ln \bar{P} - \ln p_t} V_{t+1}(p_t e^{\phi_t}, i_t e^{\psi_t}, \mathcal{I}_{t+1}(\alpha_t^{(i)})) f_t^{(p)}(\phi_t) f_t^{(i)}(\psi_t | \alpha_t^{(i)}) d\phi_t d\psi_t \\
&\quad + \int_{-\infty}^{\ln \bar{I} - \ln i_t - \delta} \int_{\ln \bar{P} - \ln p_t}^{\infty} r_h(\bar{P}, i_t e^{\psi_t}) f_t^{(p)}(\phi_t) f_t^{(i)}(\psi_t | \alpha_t^{(i)}) d\phi_t d\psi_t \\
&\geq -r_f \int_{\ln \bar{I} - \ln i_t - \delta}^{\infty} f_t^{(i)}(\psi_t | \alpha_t^{(i)}) d\psi_t \tag{41} \\
&\quad + \int_{-\infty}^{\ln \bar{I} - \ln i_t - \delta} \int_{-\infty}^{\ln \bar{P} - \ln p_t} V_{t+1}(p_t e^{\phi_t}, i_t e^{\psi_t + \delta}, \mathcal{I}_{t+1}(\alpha_t^{(i)})) f_t^{(p)}(\phi_t) f_t^{(i)}(\psi_t | \alpha_t^{(i)}) d\phi_t d\psi_t \\
&\quad + \int_{-\infty}^{\ln \bar{I} - \ln i_t - \delta} \int_{\ln \bar{P} - \ln p_t}^{\infty} r_h(\bar{P}, i_t e^{\psi_t + \delta}) f_t^{(p)}(\phi_t) f_t^{(i)}(\psi_t | \alpha_t^{(i)}) d\phi_t d\psi_t
\end{aligned}$$

where the second inequality holds because both $V_{t+1}(p, i, \mathcal{I})$ and $r_h(p, i)$ is non-increasing function of i , and the first inequality holds because

$$\begin{aligned}
& r_f \int_{\ln \bar{I} - \ln i_t}^{\ln \bar{I} - \ln i_t} f_t^{(i)}(\psi_t | \alpha_t^{(i)}) d\psi_t \\
&\quad + \int_{\ln \bar{I} - \ln i_t - \delta}^{\ln \bar{I} - \ln i_t} \int_{-\infty}^{\ln \bar{P} - \ln p_t} V_{t+1}(p_t e^{\phi_t}, i_t e^{\psi_t}, \mathcal{I}_{t+1}(\alpha_t^{(i)})) f_t^{(p)}(\phi_t) f_t^{(i)}(\psi_t | \alpha_t^{(i)}) d\phi_t d\psi_t \\
&\quad + \int_{\ln \bar{I} - \ln i_t - \delta}^{\ln \bar{I} - \ln i_t} \int_{\ln \bar{P} - \ln p_t}^{\infty} r_h(\bar{P}, i_t e^{\psi_t}) f_t^{(p)}(\phi_t) f_t^{(i)}(\psi_t | \alpha_t^{(i)}) d\phi_t d\psi_t \\
&\geq r_f \int_{\ln \bar{I} - \ln i_t - \delta}^{\ln \bar{I} - \ln i_t} f_t^{(i)}(\psi_t | \alpha_t^{(i)}) d\psi_t \\
&\quad + \int_{\ln \bar{I} - \ln i_t - \delta}^{\ln \bar{I} - \ln i_t} \int_{-\infty}^{\ln \bar{P} - \ln p_t} -r_f f_t^{(p)}(\phi_t) f_t^{(i)}(\psi_t | \alpha_t^{(i)}) d\phi_t d\psi_t \\
&\quad + \int_{\ln \bar{I} - \ln i_t - \delta}^{\ln \bar{I} - \ln i_t} \int_{\ln \bar{P} - \ln p_t}^{\infty} -r_f f_t^{(p)}(\phi_t) f_t^{(i)}(\psi_t | \alpha_t^{(i)}) d\phi_t d\psi_t \\
&= r_f \int_{\ln \bar{I} - \ln i_t - \delta}^{\ln \bar{I} - \ln i_t} f_t^{(i)}(\psi_t | \alpha_t^{(i)}) d\psi_t - r_f \int_{\ln \bar{I} - \ln i_t - \delta}^{\ln \bar{I} - \ln i_t} f_t^{(i)}(\psi_t | \alpha_t^{(i)}) d\psi_t = 0
\end{aligned}$$

since $-r_f \leq V_{t+1}(p_t e^{\phi_t}, i_t e^{\psi_t}, \mathcal{I}_{t+1}(\alpha_t^{(p)})) \leq r_h(\bar{P}, i_t e^{\psi_t})$ for any ϕ_t and ψ_t .

Consider a value $\alpha_t^{(i)+}$ such that $\alpha_t^{(i)+} - \alpha_t^{(i)} = \delta \geq 0$, and let $\psi'_t = \psi_t + \delta$. It holds for the predictive density that

$$\begin{aligned} f_t^{(i)}(\psi_t | \alpha_t^{(i)}) &= \pi^{-1/2} \frac{\Gamma\left(\lambda_t^{(i)} + \frac{1}{2}\right)}{\Gamma(\lambda_t^{(i)})} \left[\frac{\nu_t^{(i)}}{2\beta_t^{(i)}(1 + \nu_t^{(i)})} \right]^{1/2} \left[1 + \frac{\nu_t^{(i)}(\psi_t - \alpha_t^{(i)})^2}{2\beta_t^{(i)}(1 + \nu_t^{(i)})} \right]^{-\lambda_t^{(i)} - 1/2} \\ &= \pi^{-1/2} \frac{\Gamma\left(\lambda_t^{(i)} + \frac{1}{2}\right)}{\Gamma(\lambda_t^{(i)})} \left[\frac{\nu_t^{(i)}}{2\beta_t^{(i)}(1 + \nu_t^{(i)})} \right]^{1/2} \left[1 + \frac{\nu_t^{(i)}(\psi'_t - \alpha_t^{(i)+})^2}{2\beta_t^{(i)}(1 + \nu_t^{(i)})} \right]^{-\lambda_t^{(i)} - 1/2} = f_t^{(i)}(\psi'_t | \alpha_t^{(i)+}). \end{aligned}$$

Then, it holds for the RHS of (41) that

$$\begin{aligned} \text{RHS of (41)} &\geq -r_f \int_{\ln \bar{I} - \ln i_t - \delta}^{\infty} f_t^{(i)}(\psi_t | \alpha_t^{(i)}) d\psi_t \\ &\quad + \int_{-\infty}^{\ln \bar{I} - \ln i_t - \delta} \int_{-\infty}^{\ln \bar{P} - \ln p_t} V_{t+1}(p_t e^{\phi_t}, i_t e^{\psi_t + \delta}, \mathcal{I}_{t+1}(\alpha_t^{(i)+})) f_t^{(p)}(\phi_t) f_t^{(i)}(\psi_t | \alpha_t^{(i)}) d\phi_t d\psi_t \\ &\quad + \int_{-\infty}^{\ln \bar{I} - \ln i_t - \delta} \int_{\ln \bar{P} - \ln p_t}^{\infty} r_h(\bar{P}, i_t e^{\psi_t + \delta}) f_t^{(p)}(\phi_t) f_t^{(i)}(\psi_t | \alpha_t^{(i)}) d\phi_t d\psi_t \\ &= -r_f \int_{\ln \bar{I} - \ln i_t}^{\infty} f_t^{(i)}(\psi'_t | \alpha_t^{(i)+}) d\psi'_t \tag{42} \\ &\quad + \int_{-\infty}^{\ln \bar{I} - \ln i_t} \int_{-\infty}^{\ln \bar{P} - \ln p_t} V_{t+1}(p_t e^{\phi_t}, i_t e^{\psi'_t}, \mathcal{I}_{t+1}(\alpha_t^{(i)+})) f_t^{(p)}(\phi_t) f_t^{(i)}(\psi'_t | \alpha_t^{(i)+}) d\phi_t d\psi'_t \\ &\quad + \int_{-\infty}^{\ln \bar{I} - \ln i_t} \int_{\ln \bar{P} - \ln p_t}^{\infty} r_h(\bar{P}, i_t e^{\psi'_t}) f_t^{(p)}(\phi_t) f_t^{(i)}(\psi'_t | \alpha_t^{(i)+}) d\phi_t d\psi'_t \\ &= \mathbb{E}[V_{t+1}(p_t e^{\tilde{\Phi}_t}, i_t e^{\tilde{\Psi}_t}, \mathcal{I}_{t+1}) | \alpha_t^{(i)+}]. \end{aligned}$$

The inequality holds by induction assumption (since $\alpha_{t+1}^{(i)+} \geq \alpha_{t+1}^{(i)}$ by the update rule (5) given that $\alpha_t^{(p)+} \geq \alpha_t^{(p)}$), and (42) holds by performing variable replacement $\psi'_t = \psi_t + \delta$. Thus, we have $V_t(p_t, i_t, \mathcal{I}_t(\alpha_t^{(i)})) \geq V_t(p_t, i_t, \mathcal{I}_t(\alpha_t^{(i)+}))$.

Proof of Theorem 4

We prove that the myopic policy is optimal by backward induction. To start with, notice that, at time $\bar{T} - 1$, the optimal action is to harvest if and only if $(p_{\bar{T}-1}, i_{\bar{T}-1}) \in A$. Suppose the same applies at any time $t + 1$ less than $\bar{T} - 1$, i.e., the optimal action is to harvest if and only if $(p_{t+1}, i_{t+1}) \in A$. We want to show the optimal action at time t is to harvest if and only if $(p_t, i_t) \in A$.

For $(p_t, i_t) \in A$, it holds that

$$\begin{aligned} V_t(p_t, i_t) &= \max\{r_h(p_t, i_t), -c_u + \gamma V_{t+1}(p_{t+1}, i_{t+1})\} \\ &= \max\{r_h(p_t, i_t), -c_u + \gamma \mathbb{E}[R(p', i'; H) | p_t, i_t]\} \tag{43} \\ &= r_h(p_t, i_t), \tag{44} \end{aligned}$$

where (43) follows from the fact that, first, under positive growth assumption, we have $p_{t+1} \geq p_t$ and $i_{t+1} \geq i_t$, we have $(p_{t+1}, i_{t+1}) \in A$ by applying condition (i), and we have $(p_{t+1}, i_{t+1}) \in A$ by subsequently applying condition (ii), and then, by the induction hypothesis that asserts the optimal action is to harvest when $(p_{t+1}, i_{t+1}) \in A$. Furthermore, (44) holds because we know $(p_t, i_t) \in A$.

On the other hand, for $(p_t, i_t) \notin A$, the policy that continues the fermentation process one more time period and then takes the harvest decision has an expected reward of

$$-c_u + \gamma \mathbb{E}[R(p', i'; H) | p_t, i_t],$$

which is strictly greater than $r_h(p_t, i_t)$ (because $(p_t, i_t) \notin A$). Thus, we establish that $V_t(p_t, i_t) = r_h(p_t, i_t)$ for $(p_t, i_t) \in A$, and $V_t(p_t, i_t) > r_h(p_t, i_t)$ for $(p_t, i_t) \notin A$, and the result follows.

Proof of Lemma 1

Suppose the condition (i) in Theorem 4 does not hold, i.e.,

$$\begin{aligned} r_h(p, i) &\geq -c_u + \gamma \mathbf{E}[R(p', i'; H)|p, i], \\ r_h(p^+, i) &\leq -c_u + \gamma \mathbf{E}[R(p', i'; H)|p^+, i], \end{aligned}$$

implying that

$$\frac{1}{\gamma} [r_h(p^+, i) - r_h(p, i)] \leq \mathbf{E}[R(p', i'; H)|p^+, i] - \mathbf{E}[R(p', i'; H)|p, i]. \quad (45)$$

The left-hand side (LHS) of (45) is given by

$$\text{LHS} = \frac{c_1}{\gamma} (p^+ - p).$$

On the other hand, it holds for the right-hand side (RHS) of (45) that

$$\begin{aligned} \text{RHS} &= c_1 \Pr(i' < \bar{I}|i) (\mathbf{E}[p'|p^+] - \mathbf{E}[p'|p]) \\ &= c_1 \Phi \left(\frac{\ln \bar{I} - \ln i - \mu_c^{(i)}}{\sigma_c^{(i)}} \right) \left\{ p^+ e^{\mu_c^{(p)} + \sigma_c^{(p)2}/2} \Phi \left(\frac{\ln \bar{P} - \ln p^+ - \mu_c^{(p)} - \sigma_c^{(p)2}}{\sigma_c^{(p)}} \right) + \bar{P} \Phi \left(\frac{\ln \bar{P} - \ln p^+ - \mu_c^{(p)}}{\sigma_c^{(p)}} \right) \right. \\ &\quad \left. - p e^{\mu_c^{(p)} + \sigma_c^{(p)2}/2} \Phi \left(\frac{\ln \bar{P} - \ln p - \mu_c^{(p)} - \sigma_c^{(p)2}}{\sigma_c^{(p)}} \right) - \bar{P} \Phi \left(\frac{\ln \bar{P} - \ln p - \mu_c^{(p)}}{\sigma_c^{(p)}} \right) \right\} \\ &< c_1 \Phi \left(\frac{\ln \bar{I} - \ln i_0 - \mu_c^{(i)}}{\sigma_c^{(i)}} \right) \left\{ p^+ e^{\mu_c^{(p)} + \sigma_c^{(p)2}/2} \Phi \left(\frac{\ln \bar{P} - \ln p - \mu_c^{(p)} - \sigma_c^{(p)2}}{\sigma_c^{(p)}} \right) + \bar{P} \Phi \left(\frac{\ln \bar{P} - \ln p - \mu_c^{(p)}}{\sigma_c^{(p)}} \right) \right. \\ &\quad \left. - p e^{\mu_c^{(p)} + \sigma_c^{(p)2}/2} \Phi \left(\frac{\ln \bar{P} - \ln p - \mu_c^{(p)} - \sigma_c^{(p)2}}{\sigma_c^{(p)}} \right) - \bar{P} \Phi \left(\frac{\ln \bar{P} - \ln p - \mu_c^{(p)}}{\sigma_c^{(p)}} \right) \right\} \\ &= c_1 (p^+ - p) e^{\mu_c^{(p)} + \sigma_c^{(p)2}/2} \Phi \left(\frac{\ln \bar{I} - \ln i_0 - \mu_c^{(i)}}{\sigma_c^{(i)}} \right) \Phi \left(\frac{\ln \bar{P} - \ln p - \mu_c^{(p)} - \sigma_c^{(p)2}}{\sigma_c^{(p)}} \right), \end{aligned}$$

where the inequality holds because $i_0 \leq i$ and $p < p^+$. Therefore, we can simplify the inequality (45) as

$$\frac{1}{\gamma} < e^{\mu_c^{(p)} + \sigma_c^{(p)2}/2} \Phi \left(\frac{\ln \bar{I} - \ln i_0 - \mu_c^{(i)}}{\sigma_c^{(i)}} \right) \Phi \left(\frac{\ln \bar{P} - \ln p - \mu_c^{(p)} - \sigma_c^{(p)2}}{\sigma_c^{(p)}} \right).$$

However, this contradicts for $p \geq \underline{p}$ with \underline{p} given in Lemma 1. Thus, we know that Lemma 1 holds.

Proof of Lemma 2

Suppose the condition (ii) in Theorem 4 does not hold, i.e.,

$$\begin{aligned} r_h(p, i) &\geq -c_u + \gamma \mathbf{E}[R(p', i'; H)|p, i], \\ r_h(p, i^+) &\leq -c_u + \gamma \mathbf{E}[R(p', i'; H)|p, i^+], \end{aligned}$$

implying that

$$\frac{r_h(p, i) - r_h(p, i^+)}{\gamma} \geq \mathbf{E}[R(p', i'; H)|p, i] - \mathbf{E}[R(p', i'; H)|p, i^+]. \quad (46)$$

The left-hand side of (46) is

$$\text{LHS} = \frac{c_2}{\gamma} (i^+ - i).$$

On the other hand, it holds for the right-hand side of (46) that

$$\begin{aligned} \text{RHS} &= r_f [\Pr(i' \geq \bar{I}|i^+) - \Pr(i' \geq \bar{I}|i)] + (c_0 + c_1 \mathbf{E}[p'|p]) [\Pr(i' < \bar{I}|i) - \Pr(i' < \bar{I}|i^+)] \\ &\quad - c_2 \mathbf{E}[i'|i' < \bar{I}, i] \Pr(i' < \bar{I}|i) + c_2 \mathbf{E}[i'|i' < \bar{I}, i^+] \Pr(i' < \bar{I}|i^+) \\ &> r_f \left[\Phi \left(\frac{\ln \bar{I} - \ln i - \mu_c^{(i)}}{\sigma_c^{(i)}} \right) - \Phi \left(\frac{\ln \bar{I} - \ln i^+ - \mu_c^{(i)}}{\sigma_c^{(i)}} \right) \right] \\ &\quad - c_2 i e^{\mu_c^{(i)} + \sigma_c^{(i)2}/2} \Phi \left(\frac{\ln \bar{I} - \ln i - \mu_c^{(i)} - \sigma_c^{(i)2}}{\sigma_c^{(i)}} \right) + c_2 i^+ e^{\mu_c^{(i)} + \sigma_c^{(i)2}/2} \Phi \left(\frac{\ln \bar{I} - \ln i^+ - \mu_c^{(i)} - \sigma_c^{(i)2}}{\sigma_c^{(i)}} \right) \end{aligned}$$

$$\begin{aligned}
&> r_f \left[\Phi \left(\frac{\ln \bar{I} - \ln i - \mu_c^{(i)}}{\sigma_c^{(i)}} \right) - \Phi \left(\frac{\ln \bar{I} - \ln i^+ - \mu_c^{(i)}}{\sigma_c^{(i)}} \right) \right] \\
&\quad - c_2 i e^{\mu_c^{(i)} + \sigma_c^{(i)2}/2} \left[\Phi \left(\frac{\ln \bar{I} - \ln i - \mu_c^{(i)} - \sigma_c^{(i)2}}{\sigma_c^{(i)}} \right) - \Phi \left(\frac{\ln \bar{I} - \ln i^+ - \mu_c^{(i)} - \sigma_c^{(i)2}}{\sigma_c^{(i)}} \right) \right] \\
&\geq r_f \left[\Phi \left(\frac{\ln \bar{I} - \ln i - \mu_c^{(i)}}{\sigma_c^{(i)}} \right) - \Phi \left(\frac{\ln \bar{I} - \ln i^+ - \mu_c^{(i)}}{\sigma_c^{(i)}} \right) \right] \\
&\quad - c_2 \bar{I} e^{\mu_c^{(i)} + \sigma_c^{(i)2}/2} \left[\Phi \left(\frac{\ln \bar{I} - \ln i - \mu_c^{(i)} - \sigma_c^{(i)2}}{\sigma_c^{(i)}} \right) - \Phi \left(\frac{\ln \bar{I} - \ln i^+ - \mu_c^{(i)} - \sigma_c^{(i)2}}{\sigma_c^{(i)}} \right) \right],
\end{aligned}$$

where the first inequality holds because $(c_0 + c_1 E[p'|p]) [\Pr(i' \leq \bar{I}|i) - \Pr(i' \leq \bar{I}|i^+)] > 0$, the second inequality holds since $i < i^+$, and the last inequality holds since $i \leq \bar{I}$. After plugging in the expressions of LHS and RHS, we have

$$\begin{aligned}
\frac{c_2}{\gamma} (i^+ - i) &> r_f \left[\Phi \left(\frac{\ln \bar{I} - \ln i - \mu_c^{(i)}}{\sigma_c^{(i)}} \right) - \Phi \left(\frac{\ln \bar{I} - \ln i^+ - \mu_c^{(i)}}{\sigma_c^{(i)}} \right) \right] \\
&\quad - c_2 \bar{I} e^{\mu_c^{(i)} + \sigma_c^{(i)2}/2} \left[\Phi \left(\frac{\ln \bar{I} - \ln i - \mu_c^{(i)} - \sigma_c^{(i)2}}{\sigma_c^{(i)}} \right) - \Phi \left(\frac{\ln \bar{I} - \ln i^+ - \mu_c^{(i)} - \sigma_c^{(i)2}}{\sigma_c^{(i)}} \right) \right].
\end{aligned}$$

However, this contradicts with the condition given in Lemma 2. Thus, we know Lemma 2 holds.

Proof of Corollary 5

We let

$$x = \frac{\ln \bar{I} - \ln i - \mu_c^{(i)}}{\sigma_c^{(i)}}, \quad x^+ = \frac{\ln \bar{I} - \ln i^+ - \mu_c^{(i)}}{\sigma_c^{(i)}},$$

where $i^+ > i$, $x > x^+$. Then we can rewrite the inequality in (21) as

$$\frac{c_2 \bar{I}}{\gamma} (e^{-\sigma_c^{(i)} x^+ - \mu_c^{(i)}} - e^{-\sigma_c^{(i)} x - \mu_c^{(i)}}) \leq r_f [\Phi(x) - \Phi(x^+)] - c_2 \bar{I} e^{\mu_c^{(i)} + \sigma_c^{(i)2}/2} [\Phi(x - \sigma_c^{(i)}) - \Phi(x^+ - \sigma_c^{(i)})]. \quad (47)$$

We apply the first-order Taylor series expansion on each exponential term in the left-hand side and on the normal cumulative distribution functions in the right-hand side of (47), and further approximate the expansion by only taking the dominant elements, for example

$$e^{-\sigma_c^{(i)} x - \mu_c^{(i)}} = \sum_{n=0}^{\infty} \frac{(-\sigma_c^{(i)} x - \mu_c^{(i)})^n}{n!} \approx 1 - \sigma_c^{(i)} x - \mu_c^{(i)}$$

and

$$\Phi(x) = \frac{1}{\sqrt{2\pi}} \int_{-\infty}^x e^{-z^2/2} dz = \frac{1}{2} + \frac{1}{2} \operatorname{erf}\left(\frac{x}{\sqrt{2}}\right) = \frac{1}{2} + \frac{1}{2} \cdot \frac{2}{\sqrt{\pi}} \sum_{n=0}^{\infty} \frac{(-1)^n (x/\sqrt{2})^{2n+1}}{n!(2n+1)} \approx \frac{1}{2} + \frac{x}{\sqrt{2\pi}}$$

where $\operatorname{erf}(w) = \frac{2}{\sqrt{\pi}} \int_0^w e^{-z^2} dz$ is the error function. Similar approximation can be applied to $e^{-\sigma_c^{(i)} x^+ - \mu_c^{(i)}}$, $\Phi(x^+)$, $\Phi(x - \sigma_c^{(i)})$ and $\Phi(x^+ - \sigma_c^{(i)})$. Thus, we can approximate (47) as

$$\frac{c_2 \bar{I}}{\gamma} \sigma_c^{(i)} (x - x^+) \leq \frac{r_f}{\sqrt{2\pi}} (x - x^+) - \frac{c_2 \bar{I}}{\sqrt{2\pi}} e^{\mu_c^{(i)} + \sigma_c^{(i)2}/2} [(x - \sigma_c^{(i)}) - (x^+ - \sigma_c^{(i)})],$$

which leads to

$$\frac{c_2 \bar{I}}{\gamma} \sigma_c^{(i)} (x - x^+) \leq \left[\frac{r_f}{\sqrt{2\pi}} - \frac{c_2 \bar{I}}{\sqrt{2\pi}} e^{\mu_c^{(i)} + \sigma_c^{(i)2}/2} \right] (x - x^+).$$

Therefore, it follows that:

$$\frac{r_f}{\sqrt{2\pi}} \geq \frac{c_2 \bar{I}}{\gamma} \sigma_c^{(i)} + \frac{c_2 \bar{I}}{\sqrt{2\pi}} e^{\mu_c^{(i)} + \sigma_c^{(i)2}/2}$$

$$r_f \geq c_2 \bar{I} \left[\frac{\sqrt{2\pi}\sigma_c^{(i)}}{\gamma} + e^{\mu_c^{(i)} + \sigma_c^{(i)2}/2} \right].$$

Proof of Theorem 7

(i) We start with writing the function $\tilde{h}(\alpha^{(p)}, \tilde{\sigma}^{(p)}, \alpha^{(i)}, \tilde{\sigma}^{(i)}; p, i)$ explicitly:

$$\begin{aligned} \tilde{h}(\alpha^{(p)}, \tilde{\sigma}^{(p)}, \alpha^{(i)}, \tilde{\sigma}^{(i)}; p, i) &= c_0 + c_u + c_1 p - c_2 i + \gamma r_f \left[1 - \Phi \left(\frac{\ln \bar{I} - \ln i - \alpha^{(i)}}{\tilde{\sigma}^{(i)}} \right) \right] \\ &\quad - \gamma c_0 \Phi \left(\frac{\ln \bar{I} - \ln i - \alpha^{(i)}}{\tilde{\sigma}^{(i)}} \right) \\ &\quad - \gamma c_1 \bar{P} \left[1 - \Phi \left(\frac{\ln \bar{P} - \ln p - \alpha^{(p)}}{\tilde{\sigma}^{(p)}} \right) \right] \Phi \left(\frac{\ln \bar{I} - \ln i - \alpha^{(i)}}{\tilde{\sigma}^{(i)}} \right) \\ &\quad - \gamma c_1 p e^{\alpha^{(p)} + \tilde{\sigma}^{(p)2}/2} \Phi \left(\frac{\ln \bar{P} - \ln p - \alpha^{(p)} - \tilde{\sigma}^{(p)2}}{\tilde{\sigma}^{(p)}} \right) \Phi \left(\frac{\ln \bar{I} - \ln i - \alpha^{(i)}}{\tilde{\sigma}^{(i)}} \right) \\ &\quad + \gamma c_2 i e^{\alpha^{(i)} + \tilde{\sigma}^{(i)2}/2} \Phi \left(\frac{\ln \bar{I} - \ln i - \alpha^{(i)} - \tilde{\sigma}^{(i)2}}{\tilde{\sigma}^{(i)}} \right) \\ &= c_0 + c_u + c_1 p - c_2 i + \gamma r_f [1 - \Phi(x)] - \gamma c_0 \Phi(x) - \gamma c_1 \bar{P} [1 - \Phi(y)] \Phi(x) \\ &\quad - \gamma c_1 p e^{\alpha^{(p)} + \tilde{\sigma}^{(p)2}/2} \Phi(y - \tilde{\sigma}^{(p)}) \Phi(x) + \gamma c_2 i e^{\alpha^{(i)} + \tilde{\sigma}^{(i)2}/2} \Phi(x - \tilde{\sigma}^{(i)}), \end{aligned}$$

where the x and y are variable replacements defined as

$$x = \frac{\ln \bar{I} - \ln i - \alpha^{(i)}}{\tilde{\sigma}^{(i)}}, \quad y = \frac{\ln \bar{P} - \ln p - \alpha^{(p)}}{\tilde{\sigma}^{(p)}}.$$

We know that:

$$\begin{aligned} i e^{\alpha^{(i)} + \tilde{\sigma}^{(i)2}/2} \phi(x - \tilde{\sigma}^{(i)}) &= i e^{\alpha^{(i)} + \tilde{\sigma}^{(i)2}/2} \frac{e^{-(x - \tilde{\sigma}^{(i)})^2/2}}{\sqrt{2\pi}} \\ &= i e^{\alpha^{(i)} + \tilde{\sigma}^{(i)2}/2} \frac{e^{-x^2/2 + x\tilde{\sigma}^{(i)} - \tilde{\sigma}^{(i)2}/2}}{\sqrt{2\pi}} \\ &= i e^{\alpha^{(i)} + x\tilde{\sigma}^{(i)}} \frac{e^{-x^2/2}}{\sqrt{2\pi}} \\ &= i e^{\ln \bar{I} - \ln i} \phi(x) \\ &= \bar{I} \phi(x), \end{aligned} \tag{48}$$

where the equality (48) follows by plugging in $x = \frac{\ln \bar{I} - \ln i - \alpha^{(i)}}{\tilde{\sigma}^{(i)}}$. Similarly, we have

$$p e^{\alpha^{(p)} + \tilde{\sigma}^{(p)2}/2} \phi(y - \tilde{\sigma}^{(p)}) = \bar{P} \phi(y).$$

For function $\tilde{h}(\alpha^{(p)}, \tilde{\sigma}^{(p)}, \alpha^{(i)}, \tilde{\sigma}^{(i)}; p, i)$, if we only consider the parts related to $\alpha^{(i)}$, we have

$$\begin{aligned} \tilde{h}(\alpha^{(p)}, \tilde{\sigma}^{(p)}, \alpha^{(i)}, \tilde{\sigma}^{(i)}; p, i) &\propto -r_f \Phi(x) - c_0 \Phi(x) - c_1 \bar{P} [1 - \Phi(y)] \Phi(x) \\ &\quad - c_1 p e^{\alpha^{(p)} + \tilde{\sigma}^{(p)2}/2} \Phi(y - \tilde{\sigma}^{(p)}) \Phi(x) + c_2 i e^{\alpha^{(i)} + \tilde{\sigma}^{(i)2}/2} \Phi(x - \tilde{\sigma}^{(i)}), \end{aligned} \tag{49}$$

Taking derivatives with respect to $\alpha^{(i)}$ leads to:

$$\begin{aligned} \frac{\partial \tilde{h}}{\partial \alpha^{(i)}} &\propto -C \phi(x) \frac{\partial x}{\partial \alpha^{(i)}} + c_2 i e^{\alpha^{(i)} + \tilde{\sigma}^{(i)2}/2} \Phi(x - \tilde{\sigma}^{(i)}) + c_2 i e^{\alpha^{(i)} + \tilde{\sigma}^{(i)2}/2} \phi(x - \tilde{\sigma}^{(i)}) \frac{\partial x}{\partial \alpha^{(i)}} \\ &\propto C \phi(x) \frac{1}{\tilde{\sigma}^{(i)}} + c_2 i e^{\alpha^{(i)} + \tilde{\sigma}^{(i)2}/2} \Phi(x - \tilde{\sigma}^{(i)}) - c_2 \bar{I} \phi(x) \frac{1}{\tilde{\sigma}^{(i)}} \\ &\propto (C - c_2 \bar{I}) \frac{\phi(x)}{\tilde{\sigma}^{(i)}} + c_2 i e^{\alpha^{(i)} + \tilde{\sigma}^{(i)2}/2} \Phi(x - \tilde{\sigma}^{(i)}), \end{aligned}$$

where

$$C = r_f + c_0 + c_1 \bar{P}[1 - \Phi(y)] + c_1 p e^{\alpha^{(p)} + \tilde{\sigma}^{(p)2}/2} \Phi(y - \tilde{\sigma}^{(p)}).$$

Since $r_f \geq c_2 \bar{I}$, we have $C - c_2 \bar{I} > 0$, then $\frac{\partial \tilde{h}}{\partial \alpha^{(i)}} > 0$.

(ii) On the other hand, if we only consider the parts related to $\alpha^{(p)}$, we have

$$\begin{aligned} \tilde{h}(\alpha^{(p)}, \tilde{\sigma}^{(p)}, \alpha^{(i)}, \tilde{\sigma}^{(i)}; p, i) &\propto c_1 \bar{P} \Phi(y) \Phi(x) - c_1 e^{\alpha^{(p)} + \tilde{\sigma}^{(p)2}/2} \Phi(y - \tilde{\sigma}^{(p)}) \Phi(x) \\ &\propto \bar{P} \Phi(y) - p e^{\alpha^{(p)} + \tilde{\sigma}^{(p)2}/2} \Phi(y - \tilde{\sigma}^{(p)}). \end{aligned} \quad (50)$$

Taking derivatives with respect to $\alpha^{(p)}$ leads to:

$$\begin{aligned} \frac{\partial \tilde{h}}{\partial \alpha^{(i)}} &\propto \bar{P} \phi(y) \frac{\partial y}{\partial \alpha^{(p)}} - p e^{\alpha^{(p)} + \tilde{\sigma}^{(p)2}/2} \Phi(y - \tilde{\sigma}^{(p)}) - p e^{\alpha^{(p)} + \tilde{\sigma}^{(p)2}/2} \phi(y - \tilde{\sigma}^{(p)}) \frac{\partial y}{\partial \alpha^{(p)}} \\ &\propto \bar{P} \phi(y) \frac{\partial y}{\partial \alpha^{(p)}} - p e^{\alpha^{(p)} + \tilde{\sigma}^{(p)2}/2} \Phi(y - \tilde{\sigma}^{(p)}) - \bar{P} \phi(y) \frac{\partial y}{\partial \alpha^{(p)}} \\ &\propto - p e^{\alpha^{(p)} + \tilde{\sigma}^{(p)2}/2} \Phi(y - \tilde{\sigma}^{(p)}) < 0. \end{aligned}$$

(iii) If we only consider the parts related to $\tilde{\sigma}^{(i)}$, we have exactly the same formula of $\tilde{h}(\alpha^{(p)}, \tilde{\sigma}^{(p)}, \alpha^{(i)}, \tilde{\sigma}^{(i)}; p, i)$ as in (49). Taking derivatives with respect to $\tilde{\sigma}^{(i)}$, we have that

$$\begin{aligned} \frac{\partial \tilde{h}}{\partial \tilde{\sigma}^{(i)}} &\propto -C \phi(x) \frac{\partial x}{\partial \tilde{\sigma}^{(i)}} + c_2 i \tilde{\sigma}^{(i)} e^{\alpha^{(i)} + \tilde{\sigma}^{(i)2}/2} \Phi(x - \tilde{\sigma}^{(i)}) + c_2 i e^{\alpha^{(i)} + \tilde{\sigma}^{(i)2}/2} \phi(x - \tilde{\sigma}^{(i)}) \left(\frac{\partial x}{\partial \tilde{\sigma}^{(i)}} - 1 \right) \\ &\propto -C \phi(x) \frac{\partial x}{\partial \tilde{\sigma}^{(i)}} + c_2 i \tilde{\sigma}^{(i)} e^{\alpha^{(i)} + \tilde{\sigma}^{(i)2}/2} \Phi(x - \tilde{\sigma}^{(i)}) + c_2 \bar{I} \phi(x) \left(\frac{\partial x}{\partial \tilde{\sigma}^{(i)}} - 1 \right) \\ &\propto -(C - c_2 \bar{I}) \phi(x) \frac{\partial x}{\partial \tilde{\sigma}^{(i)}} + c_2 i e^{\alpha^{(i)} + \tilde{\sigma}^{(i)2}/2} \left[\tilde{\sigma}^{(i)} \Phi(x - \tilde{\sigma}^{(i)}) - \phi(x - \tilde{\sigma}^{(i)}) \right]. \end{aligned}$$

Similarly, we have $C - c_2 \bar{I} > 0$. Therefore, if the conditions in Theorem 7(iii) hold, then $\frac{\partial \tilde{h}}{\partial \tilde{\sigma}^{(i)}} < 0$, and $\tilde{\sigma}^{(i)} \Phi(x - \tilde{\sigma}^{(i)}) - \phi(x - \tilde{\sigma}^{(i)}) > 0$. Thus, $\frac{\partial \tilde{h}}{\partial \tilde{\sigma}^{(i)}} > 0$.

(iv) Further, if we only consider the parts related to $\tilde{\sigma}^{(p)}$, we will have the same formula as in (50). Taking derivatives with respect to $\tilde{\sigma}^{(p)}$, we have the following holds,

$$\begin{aligned} \frac{\partial \tilde{h}}{\partial \tilde{\sigma}^{(p)}} &\propto \bar{P} \phi(y) \frac{\partial y}{\partial \tilde{\sigma}^{(p)}} - p \tilde{\sigma}^{(p)} e^{\alpha^{(p)} + \tilde{\sigma}^{(p)2}/2} \Phi(y - \tilde{\sigma}^{(p)}) - p e^{\alpha^{(p)} + \tilde{\sigma}^{(p)2}/2} \phi(y - \tilde{\sigma}^{(p)}) \left(\frac{\partial y}{\partial \tilde{\sigma}^{(p)}} - 1 \right) \\ &\propto \bar{P} \phi(y) \frac{\partial y}{\partial \tilde{\sigma}^{(p)}} - p \tilde{\sigma}^{(p)} e^{\alpha^{(p)} + \tilde{\sigma}^{(p)2}/2} \Phi(y - \tilde{\sigma}^{(p)}) - \bar{P} \phi(y) \frac{\partial y}{\partial \tilde{\sigma}^{(p)}} + p e^{\alpha^{(p)} + \tilde{\sigma}^{(p)2}/2} \phi(y - \tilde{\sigma}^{(p)}) \\ &\propto p e^{\alpha^{(p)} + \tilde{\sigma}^{(p)2}/2} \left[\phi(y - \tilde{\sigma}^{(p)}) - \tilde{\sigma}^{(p)} \Phi(y - \tilde{\sigma}^{(p)}) \right]. \end{aligned}$$

Since $p e^{\alpha^{(p)} + \tilde{\sigma}^{(p)2}/2} > 0$, we have $\frac{\partial \tilde{h}}{\partial \tilde{\sigma}^{(p)}} < 0$ if and only if $\tilde{\sigma}^{(p)} \Phi(y - \tilde{\sigma}^{(p)}) - \phi(y - \tilde{\sigma}^{(p)}) > 0$.

Proof of Theorem 8

Define the "harvest function" of myopic policy under perfect information as following,

$$\begin{aligned} h(\mu_c^{(p)}, \sigma_c^{(p)}, \mu_c^{(i)}, \sigma_c^{(i)}; p, i) &= r_h(p, i) + c_u - \gamma \mathbb{E}[R(p', i'; H) | p, i] \\ &= r_h(p, i) + c_u - \gamma \left\{ -r_f \Pr(i' > \bar{I} | i, \mu_c^{(i)}, \sigma_c^{(i)}) \right. \\ &\quad \left. + \mathbb{E}[r_h(p', i') | i' \leq \bar{I}, p, i, \mu_c^{(p)}, \sigma_c^{(p)}, \mu_c^{(i)}, \sigma_c^{(i)}] \right\} \end{aligned}$$

then the harvest region in (19) can be written as $A = \left\{ (p, i) : h(p, i; \mu_c^{(p)}, \sigma_c^{(p)2}, \mu_c^{(i)}, \sigma_c^{(i)2}) \geq 0 \right\}$. Notice that under model risk,

$$\tilde{h}(\alpha^{(p)}, \tilde{\sigma}^{(p)}, \alpha^{(i)}, \tilde{\sigma}^{(i)}; p, i) = r_h(p, i) + c_u - \gamma \mathbb{E}[R(p', i'; H) | p, i, \alpha^{(p)}, \tilde{\sigma}^{(p)}, \alpha^{(i)}, \tilde{\sigma}^{(i)}]$$

$$r_h(p, i) + c_u - \gamma \left\{ -r_f \Pr(i' > \bar{I} | i, \alpha^{(i)}, \tilde{\sigma}^{(i)}) \right. \\ \left. + \mathbb{E}[r_h(p', i') | i' \leq \bar{I}, p, i, \alpha^{(p)}, \tilde{\sigma}^{(p)}, \alpha^{(i)}, \tilde{\sigma}^{(i)}] \right\},$$

which can be obtained by replacing the unknown parameters $\mu_c^{(i)}$ and $\sigma_c^{(i)2}$ with predictive mean $\alpha^{(i)}$ and predictive standard deviation $\tilde{\sigma}^{(i)}$ for the impurity growth rate; and similarly, by replacing $\mu_c^{(p)}$ and $\sigma_c^{(p)2}$ with $\alpha^{(p)}$ and $\tilde{\sigma}^{(p)}$ for the protein growth rate. Our objective is to show that the function $\tilde{h}(\alpha_t^{(p)}, \tilde{\sigma}_t^{(p)}, \alpha_t^{(i)}, \tilde{\sigma}_t^{(i)}; p, i)$ converges to its true counterpart $h(\mu_c^{(p)}, \sigma_c^{(p)}, \mu_c^{(i)}, \sigma_c^{(i)}; p, i)$ as the length of the historical data increases.

It is known that ϕ_j , $j = 1, 2, \dots, J_t$, are i.i.d. samples from the underlying true protein growth rate distribution $\mathcal{N}(\mu_c^{(p)}, \sigma_c^{(p)2})$. According to the properties of Gaussian sample mean and sample variance, we have

$$\bar{\phi} \sim \mathcal{N}\left(\mu_c^{(p)}, \frac{\sigma_c^{(p)2}}{J_t}\right), \frac{\sum_{j=1}^{J_t} (\phi_j - \bar{\phi})^2}{\sigma_c^{(p)2}} \sim \chi^2(J_t - 1),$$

and they are independent of each other, where $\bar{\phi} = \frac{1}{J_t} \sum_{j=1}^{J_t} \phi_j$.

According to the weak law of large numbers (WLLN), we have sample mean converge to the true mean, i.e., $\alpha_t^{(p)} \xrightarrow{p} \mu_c^{(p)}$ as $J_t \rightarrow \infty$. In addition, it is known from Proposition 1(i) that

$$\mathbb{E}[\tilde{\sigma}_t^{(p)2}] = \sigma_c^{(p)2} + \frac{(2J_t - 1)\sigma_c^{(p)2}}{(J_t^2 - 2J_t)}, \quad \text{Var}[\tilde{\sigma}_t^{(p)2}] = \frac{2(J_t^3 + J_t^2 - J_t - 1)\sigma_c^{(p)4}}{J_t^4 - 4J_t^3 + 4J_t^2}. \quad (51)$$

As $J_t \rightarrow \infty$, we will have $\mathbb{E}[\tilde{\sigma}_t^{(p)2}] \rightarrow \sigma_c^{(p)2}$ and $\text{Var}[\tilde{\sigma}_t^{(p)2}] \rightarrow 0$, so that $\tilde{\sigma}_t^{(p)2} \xrightarrow{p} \sigma_c^{(p)2}$. Similar results also apply for impurity growth rate so that we also have $\alpha_t^{(i)} \xrightarrow{p} \mu_c^{(i)}$ and $\tilde{\sigma}_t^{(i)2} \xrightarrow{p} \sigma_c^{(i)2}$. Thus, through the continuous mapping theorem, $\tilde{\sigma}_t^{(p)} \xrightarrow{p} \sigma_c^{(p)}$ and $\tilde{\sigma}_t^{(i)} \xrightarrow{p} \sigma_c^{(i)}$, and we have for any $(p_t, i_t) \in [p_0, \bar{P}] \times [i_0, \bar{I}]$ and $m = 1, 2, \dots, \bar{T} - t$, $\tilde{h}(\alpha_t^{(p)}, \tilde{\sigma}_t^{(p)}, \alpha_t^{(i)}, \tilde{\sigma}_t^{(i)}; p, i) \xrightarrow{p} h(\mu_c^{(p)}, \sigma_c^{(p)}, \mu_c^{(i)}, \sigma_c^{(i)}; p, i)$. In other words, the decision boundary under model risk will converge to the decision boundary under perfect information.

D Numerical Analysis on Costs and Rewards

We provide a sensitivity analysis with respect to (i) the unit reward obtained per protein amount, i.e., $r_h(p, i) = 5p - i$, $r_h(p, i) = 10p - i$ and $r_h(p, i) = 15p - i$; and (ii) the failure penalty cost, i.e., $r_f = 400, 880, 1000$. These different reward and cost configurations are defined to capture a wide range of practically-relevant settings. Other parameters remain the same as discussed in Section 6.1. The results are shown in Table 2.

Table 2: The mean and standard deviation of the total reward achieved by different strategies under various configurations on unit rewards and failure costs.

		Fixed Threshold		RL ignoring MR		Myopic Policy		RL with MR		Perfect Info MDP	
Protein Value	Failure Cost	$\hat{\rho}^c(\pi)$	$\widehat{SD}^c(\pi)$	$\hat{\rho}^c(\pi)$	$\widehat{SD}^c(\pi)$	$\hat{\rho}^c(\pi)$	$\widehat{SD}^c(\pi)$	$\hat{\rho}^c(\pi)$	$\widehat{SD}^c(\pi)$	$\hat{\rho}^c(\pi)$	$\widehat{SD}^c(\pi)$
5	400	29.68	142.86	66.22	58.89	67.84	59.08	71.28	33.90	72.20	34.01
10	400	140.60	184.12	155.00	135.88	175.80	122.88	181.34	110.70	185.71	87.15
15	400	251.51	226.89	298.34	140.28	285.80	173.85	299.47	123.00	314.25	105.63
5	880	-13.52	279.42	61.42	102.12	60.88	102.09	71.28	33.90	71.80	33.87
10	880	97.40	318.19	143.47	196.39	168.21	166.31	171.63	126.68	177.23	125.86
15	880	208.31	358.48	268.61	227.41	273.80	228.98	281.01	194.74	295.97	152.93
5	1000	-24.32	313.76	60.22	113.53	59.49	113.49	71.28	33.90	71.33	34.23
10	1000	86.60	352.19	139.87	215.71	165.18	181.73	170.43	137.03	176.03	136.27
15	1000	197.51	392.07	246.12	246.75	270.20	247.66	271.32	209.92	294.77	162.50

For each different revenue and cost configuration, Table 2 presents the mean $\hat{\rho}^c(\pi)$ and standard deviation $\widehat{SD}^c(\pi)$ of total reward realized by 100 batches. Each column corresponds to a harvesting strategy. We considered the size of historical data $J_0 = 10$ for Myopic, RL-ignoring-MR and RL-with-MR strategies. For each strategy, we observe from Table 2 that the average and standard deviation of the total reward increase as the unit reward of protein increases; and the average reward decreases but the standard deviation increases as the failure cost increases. This trend matches our intuition. For the cases with lower protein rewards or/and lower failure costs, we observe from Table 2 that the performance of the proposed RL-with-MR strategy (under $J_0 = 10$) is closer to that of the perfect information setting PI-MDP. For practitioners, this implies that the potential impact of model risk is higher for high-revenue (and/or cost) drugs in comparison to their low-revenue (and/or cost) counterparts.